The Dissertation Committee for Anil Tharian G. Kottam Certifies that this is the approved version of the following dissertation:

Measurement of Electrical Admittance to Study the Onset and Progression of Myocardial Ischemia

Committee:

John Pearce, Supervisor

Jonathan Valvano

Marc Feldman

Bysani Chandrasekar

Thomas Milner

Francis Bostick

Measurement of Electrical Admittance to Study the Onset and Progression of Myocardial Ischemia

by

Anil Tharian G. Kottam, B.Tech; M.S.E.

Dissertation

Presented to the Faculty of the Graduate School of

The University of Texas at Austin

in Partial Fulfillment

of the Requirements

for the Degree of

Doctor of Philosophy

The University of Texas at Austin

December, 2007

Dedication

To my parents and my sister who have been a constant source of support and encouragement in times both good and bad.

Acknowledgements

I take this opportunity to express my sincere gratitude to all those who have made a major contribution towards the completion of my dissertation.

First and foremost, I am highly indebted to my supervising professor, Dr. John Pearce for all his support and motivation throughout the duration of my graduate studies. He has been largely responsible for helping me develop an organized and professional approach towards my work and my research. I feel extremely fortunate to have had him as my supervisor and thank him wholeheartedly.

I would like to thank my co-supervisor Dr. Jon Valvano for his valuable advice, cooperation and encouragement over the past six years. He has also been largely responsible for providing me with financial support through various teaching assistantship positions.

I am grateful to Dr. Marc Feldman for his interest and support of my research. He has played a major role in helping me develop the animal study protocols and providing me with the resources to conduct animal studies in his laboratory in San Antonio. The research staff at the UTHSCSA, namely Danny Escobedo, Rudy Trevino, Sam DeLaRosa and Dr. Bysani Chandrashekar have been extremely helpful with the animal experiments and the LDH assays.

A special mention must be made of my colleagues Karthik Raghavan, John Porterfield and Erik Larson for their collective intellectual input on matters related to my project. Karthik and John have helped me immensely during the animal experiments and Erik performed numerous calibration and benchmark tests on my analog phase circuit. Moreover, Karthik's crazy antics livened up the lab; John's weekly poker nights gave us socially deprived graduate students something to look forward to and Erik sportingly resigned to being the butt of most of our jokes in the lab.

Our entire research group is also grateful to the valuable contributions made by previous graduate students who have worked on several aspects of the project and have since moved on. Chia-Ling Wei developed mouse ventricular models and improved volume equations, David Altman helped implement the first digital phase measurement system and Daniel Fernandez redesigned and build the admittance magnitude measurement system.

I must thank all my friends in the biomedical department, namely Jignesh Shah, Nachiket Kharalkar, Shalini Gupta and John Slater to name a few, for the support and encouragement they have provided me in my countless years of graduate study. I'm also grateful to my good friend and roommate Ciji Isen for having endured my eccentricities and mood swings over the last two years and also being the guinea pig for my culinary experiments.

Finally I wish to acknowledge the love and support of my parents, Mrs. Laila and Dr. George Kottam, my sister Penny and all my relatives back home in India, without whose help and encouragement none of this would have been possible.

Measurement of Electrical Admittance to Study the Onset and Progression of Myocardial Ischemia

Publication No._____

Anil Tharian G. Kottam, PhD

The University of Texas at Austin, 2007

Supervisor: John A. Pearce

The electrical admittance of myocardium can be used to distinguish between stunned, ischemic and necrotic myocardial tissue. Myocardial stunning is the reversible contractile dysfunction following a brief ischemic episode. This reversible nature is clinically significant and is in contrast to the irreversible myocardial dysfunction that occurs with necrosis. This dissertation aims at developing an instrument to measure myocardial admittance during ischemia and subsequent reperfusion and to study the underlying mechanisms governing the onset and progression of ischemia and stunning. The instrument was tested on Langendorff models of the isolated rat heart that has been subjected to varying durations of global no flow ischemia and subsequent reperfusion. The relative permittivity and conductivity of the myocardium was determined and this could be correlated to the state of the tissue.

Table of Contents

List of Tables

List of Figures

CHAPTER 1

Introduction

1.1 MOTIVATION

Ischemic heart disease is the single leading cause of death in the United States and in the developed world. Overall, there are an estimated 71.3 million people in the United States living with cardiovascular diseases (CVD), which causes over 910,000 deaths annually compared to over 554,000 cancer deaths. In 2003, it was reported that 13.2 million Americans suffered from coronary heart disease (CHD) [58] and CHD was the cause of 1 in every 5 deaths in the country. The estimated direct and indirect cost of CHD was US$142 billion in 2006.

Ischemia is a restriction in blood supply caused by constriction or blockage of the blood vessels, resulting in tissue damage or dysfunction. Insufficient blood supply causes the tissue to become hypoxic or anoxic (if no oxygen is supplied at all). This can cause tissue necrosis, usually within 10-12 hours. Ischemia of the heart muscle results in a condition called angina pectoris which could result in a myocardial infarction. This can be due to atherosclerosis, thromboembolism, tachycardia, hypotension, or other causes.

Ischemia may also be inadvertently induced during certain surgical procedures or during the storage and transport of donor hearts prior to transplantation. This has an adverse effect on the cardiac cells, which determines the further viability of the heart. Hence any parameter that can monitor the onset and progression of myocardial ischemia, such as electrical admittance, could find widespread use in medicine as a real time ischemia detector.

Myocardial ischemia is known to change electrical properties of the myocardium [6, 41, 47, 48]. Both the conductive and capacitive behavior of myocardium change in response to an ischemic event. This may enable the real time monitoring of the onset and progression of ischemia by measuring the electrical conductivity and permittivity of the cardiac muscle.

Patients undergoing vascular surgery have a high risk of suffering major post operative cardiac events. There is an increased correlation of adverse cardiac events with the presence of perioperative myocardial ischemia [25, 44]. High risk patients display an increased frequency of tachycardia and asymptomatic ischemia in the first 48 hrs post operatively, with ischemia almost uniformly preceding adverse cardiac events [35, 43, 44]. All this has indicated the need for reliable ischemia monitoring. Urban *et al.* [59] have shown that clinically available hemodynamic indicators cannot identify intraoperative myocardial ischemia.

All measures of myocardial ischemia have their limitations. The commonly used evaluation techniques involve a 12-lead electrocardiogram (ECG) and cardiac markers such as troponins. A characteristic feature of ischemia is an elevation in the ST segment of the ECG. However, variations in ECG - ST segments produced by left ventricular hypertrophy, digitalis effect, and electrolyte abnormalities can mimic the ST segment changes of ischemia [59]. Cinca *et al.* [6] have recorded ST level elevation in electrodes overlying contiguous necrotic tissue, despite there being no ischemia of viable tissue in that region. Various bio-markers that are commonly used have their own limitations as well. Lactate dehydrogenase (LDH) is not specific to cardiac tissue whereas cardiac troponins are highly specific, but often very insensitive, requiring further testing to achieve an accurate diagnosis. All this further highlights the need for innovative methods of real time ischemia detection and monitoring.

1.2 BACKGROUND

Electrical impedance measurements have been used for more than 80 years to determine passive electrical properties of several tissues, including kidneys, brain, liver and spleen [33, 47, 56, 57]. The impedance is monitored for variations shortly after death or removal of the organ from the animal. The measurement of myocardial electrical impedance thus allows an overall estimation of the passive electrical properties of cardiac tissue.

It has been widely reported that the disruption of the plasma membrane is a characteristic feature of the final stage of hypoxic and ischemic necrotic cell death [23, 24, 37, 38, 47]. Two approaches are commonly used to determine the time course of cell death in myocardial ischemia or hypoxia [47]. The first one is based on the ability of some dyes to enter or exit the cell only if sarcolemmal integrity is lost. Methods based on this approach allow the monitoring of necrotic cell death in cell preparations but not in intact myocardial tissues [15, 38]. The second approach detects the presence of large intracellular molecules (LDH and troponin) in the extracellular space [15, 41, 42, 46]. These molecules cannot leave the cell while the plasma membrane is intact. This approach cannot be used during severe ischemia when the extracellular space in inaccessible.

Considerable research has been performed on the effects of ischemia on the electrical properties of myocardial tissue. The vast majority of literature focuses on changes of myocardial resistance or resistivity, rather than separating out the real and imaginary components of the electrical properties. Jain *et al.* [27] have measured a 400% increase in baseline resistance at 1 kHz during 50 min of ischemia in isolated rat hearts. del Rio *et al.* [8] showed that the time to plateau onset in dogs was longer than in pigs and humans, but the resulting ischemic plateau values in dogs, pigs and humans were not

statistically different. Ivorra *et al.* [26] have made impedance and phase measurements on rat kidneys at 1 kHz. They have observed an impedance increase of 65% from the baseline value during 45 min of ischemia and a phase angle shift from -3.5° to -6.5° during the same period. Rodriguez-Sinovas *et al.* [46] have shown an increase in tissue resistivity from 150Ω-cm to 320Ω-cm during 45 min of ischemia in pig hearts. The resistivity returned to baseline within 15 min of reperfusion. The phase angle also shifted from -2° to -17° during the same period and returned to baseline almost immediately upon reperfusion. They made these measurements at a frequency of 7 kHz in both pig and isolated rat hearts. In rats, they report that ischemia induced a marked increase in myocardial resistivity (from 86.46±5.04 to 183.40±12.87Ω-cm at 45 min of ischemia) and a marked negative shift in phase angle (from -0.36±0.26 to -4.62±0.43 degrees). Cinca *et al.* [6] have shown that resistivity of one month old myocardial infarction at 1 kHz was significantly lower than normal myocardium (110±30 vs. 235±60Ω-cm) in pig hearts. They also show that there is a marked increase in tissue resistivity in the acute ischemic region after 60 min of proximal occlusion of the LAD and virtually no change in resistivity in the center of the necrotic scar.

1.2.1 Effects of Hypoxia on Tissue

The cell volume of virtually every human cell is regulated by a Na^+/K^+ - ATPase, commonly known as the sodium potassium pump. In order to maintain the differential cell potential, cells must keep a low concentration of sodium ions and high levels of potassium ions within the cell. In the extracellular space, there are high concentrations of sodium and low concentrations of potassium, so diffusion occurs through ion channels in the plasma membrane. In order to keep the appropriate concentrations, the sodium-potassium pump pumps sodium out and potassium in through active transport. Hypoxia

arising as a result of ischemia decreases the oxygen and hence the metabolic energy available to the cells, causing a failure of this active transport mechanism. As a result, the Na^+ equilibrium is no longer regulated and an osmotic pressure imbalance develops between the intracellular and extracellular regions. The extracellular water penetrates into the cell with a subsequent cell swelling [13] and shrinkage of the extracellular region. This is manifested as a decrease in the electrical conductivity of the tissue at low frequencies [26].

Tissue necrosis caused by hypoxia is characterized by the breakdown of the structure and function of the plasma membranes of the hypoxic cells. The breakdown of the plasma membrane permeability barrier is preceded by a short metastable state that includes bleb formation, changes in lipid fluidity, and alterations in phospholipid composition [38, 47]. During this metastable state, blebs increase rapidly in size, trapped anionic fluorophores leak from the cytosol, onset of the mitochondrial permeability transition occurs, and lysosomes disintegrate [20, 23, 37, 38, 63]. The bleb finally ruptures and there is a rapid equilibrium of intracellular and extracellular contents [38]. Various high molecular weight intracellular proteins which were previously unable to leave the cell can now escape into the extracellular space. Such proteins include creatine phosphokinase (CPK), lactate dehydrogenase (LDH) and troponin which can all be used as biomarkers for cell necrosis.

1.2.2 Myocardial Hibernation and Stunning

Myocardial hibernation and stunning are two conditions caused by ischemia of cardiac tissue. Hibernation is defined as the reversible mechanical dysfunction of the heart during severe chronic ischemia [34]. Stunning, on the other hand, is the mechanical dysfunction that persists temporarily after reperfusion despite the absence of irreversible

damage and despite restoration of normal or near normal coronary flow [2, 3]. The underlying biochemical mechanisms for stunning are still largely unknown although a number of hypotheses were proposed in the 1980s, most of which have been subsequently abandoned [3]. Presently, the two viable theories regarding the pathogenesis of myocardial stunning are the oxyradical hypothesis (generation of oxygen-derived free radicals) and the calcium hypothesis (Ca^{2+} overload and decreased responsiveness of myofilaments to calcium) [3].

The degree of myocardial dysfunction is one of the most potent predictors of future cardiovascular risk. Hence, it follows that the identification of stunned and/or hibernating myocardium can provide important information with regard to prognosis and clinical decision-making.

1.2.3 Electrical Properties of Myocardial Tissue

The major determinants of myocardial impedance are the extracellular and intracellular resistance, the gap junction conductance, and the cell membrane capacitance [6, 9, 19, 60]. Healthy myocardial tissue exhibits a marked frequency dependence in its impedance properties due to the high electrical permittivity of the cardiac muscle. Gabriel *et al.* [18] have suggested that the high permittivity most likely originates in the myocardial cellular trans-membrane charge distribution.

Myocardial electrical admittance (Y) is defined as the sinusoidal current (I) applied through the tissue divided by the voltage (V) measured across it. Due to the capacitive properties of the cell membrane, the myocardial tissue is not purely resistive. This causes a time delay between the voltage and current waves that can be determined

from the phase angle of tissue admittance. The admittance (Y) is a complex number defined by

$$Y = G + jB \quad (1)$$

$$B = 2\pi f C_m \quad (2)$$

where G is the conductance (real part), B is the susceptance (imaginary part) and C_m is the muscle capacitance. Therefore, myocardial admittance can be precisely defined by two components: tissue admittance magnitude (|Y|) and phase angle ($\theta = \tan^{-1}B/G$). If the myocardium is assumed to be a homogenous medium, an equivalent circuit model of the myocardium will comprise of the extracellular conductance in parallel with the cell membrane capacitance. The equivalent circuit is shown in Figure 1-1. G_m is the extracellular conductance and C_m is the cell membrane capacitance.

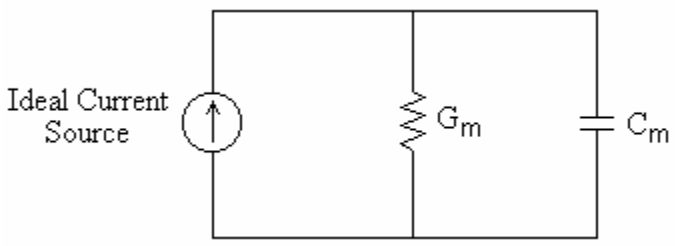

Figure 1-1: Equivalent circuit model of the myocardium (homogenous)

A more accurate approach is to model the myocardium as an inhomogeneous medium. The tissue can be considered as a combination of three main elements, namely the intracellular region, the extracellular region and the cell membranes. The intracellular and the extracellular conducting media are arranged in parallel and cell membranes act as an admittance (conductor and capacitor) connecting them. In this case, the equivalent circuit model will comprise of the extracellular conductance in parallel with a series combination of the intracellular conductance and the cell membrane capacitance.

Rodriguez-Sinovas *et al.* [47] have suggested that membrane rupture and colloid osmotic edema should reduce the total tissue resistance, considering the fact that both membrane rupture and colloid osmotic swelling have been suggested to occur almost simultaneously [38]. The equivalent circuit model for an inhomogenous medium is shown in Figure 1-2. G_i is the intracellular conductance.

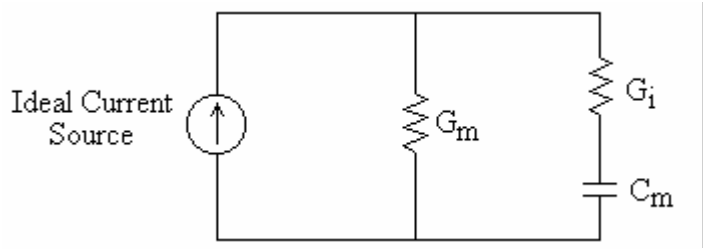

Figure 1-2: Equivalent circuit model of the myocardium (inhomogenous)

From the electromagnetic point of view, G_m and C_m are calculated from:

$$G_m = \frac{I}{V} = \frac{\iint J.dA}{-\int_L E.dl} = \frac{\iint \sigma_m E.dA}{-\int_L E.dl} \tag{3}$$

$$C_m = \frac{Q}{V} = \frac{\iint \varepsilon_m E.dA}{-\int_L E.dl} \tag{4}$$

where I is the current (A), Q is the charge (C), A is the surface enclosing the source electrode (m^2) and L is the path length for potential calculation, σ_m is the myocardial conductivity (S/m) and ε_m is the myocardial permittivity (F/m). It is assumed that both σ_m and ε_m are constants in the myocardium. Then, combining equation (3) with (4) yields the conductance capacitance analogy.

$$\frac{C_m}{G_m} = \frac{\varepsilon_m}{\sigma_m} \tag{5}$$

Accordingly the myocardial conductance can be calculated from its capacitance in a fairly straightforward manner.

Coronary occlusion causes a rise in the myocardial resistivity and this has been reported in various species [4, 5, 6, 7, 10, 28, 40]. This rise in resistivity is due to the increase in extracellular and intracellular resistance that leads to cell-to-cell electrical uncoupling [28]. Ischemia causes an accumulation of intracellular Ca^{2+} [6, 7], reduction of ATP content [6, 55] and accumulation of amphipathic lipid metabolites [6, 62] in the ischemic myocardium. All this causes an increase in gap junction resistance resulting in cellular uncoupling [6].

1.3 OBJECTIVES

Myocardial stunning is reversible contractile dysfunction following a brief ischemic episode. This reversible nature is clinically significant and is in contrast to the irreversible myocardial dysfunction that occurs with necrosis. This dissertation aims to test the following hypothesis:

Hypothesis: Measures of electrical admittance of myocardial tissue can distinguish between stunned and necrotic myocardium.

Sub Hypothesis: The permittivity of the myocardium decreases when the tissue is ischemic. This is due to the changes in cellular composition and membrane injury that occurs during ischemia. The permittivity of muscle is much higher than other types of tissue like fat, skin and bone which makes the measurement of electrical admittance a good indicator of the pathological state of the muscle.

The first objective is to build and test an analog admittance measurement system to measure myocardial admittance. This system comprises of an admittance magnitude section and a phase measurement section. The magnitude circuit was developed by graduate students in our research group and has been described in detail by Fernandez [12]. My goal is to design and build an analog phase measurement system and integrate it with the admittance magnitude system to create a Real-time Admittance Measurement System – External Sensing (RamsES I).

The second objective is to design a tetrapolar surface probe to measure myocardial admittance. The probe should have two outer electrodes delivering a constant current at a predetermined frequency and a pair of inner electrodes to measure admittance magnitude and phase angle. The electrode spacing determines the penetration depth of the electric field into the myocardium. The probe has to be sutured onto the epicardial surface and should only measure the admittance of the myocardial tissue and not blood in the left ventricle. Hence the electrical field penetration depth must not be greater than the ventricular wall thickness at diastole.

The third objective is to test the system on rat models of ischemia and stunning. The Langendorff preparation of the isolated perfused rat heart model will be used for this study. Myocardial stunning will be induced by varying durations of global no flow ischemia, followed by various methods of reperfusion. The primary goal of this section is to correlate myocardial electrical admittance with the state of the myocardium. The surface probe will be sutured on the epicardial surface to measure the magnitude and phase angle of myocardial admittance during baseline, ischemia and reperfusion of the rat heart. Based on these measurements, the muscle conductivity and relative permittivity can be calculated. The main hypothesis is that the relative permittivity of the myocardium can be used to distinguish between normal, ischemic, stunned and necrotic myocardium.

These results will be compared with actual cardiac tissue damage information obtained by measuring the levels of lactate dehydrogenase (LDH) in the coronary effluent. LDH is commonly used in medicine as a marker of tissue breakdown.

CHAPTER 2

Design and Development of a Real - Time Admittance Measurement System

2.1 ADMITTANCE MAGNITUDE MEASUREMENT SYSTEM

2.1.1 Design

The admittance magnitude measurement instrument is based on the system developed by Feldman *et al.* [11] redesigned to work at a single frequency of 30 kHz and is illustrated in Fig. 2-1. The desired excitation frequency of 30 kHz was generated using a 4 MHz crystal and a digital counter chip (CD 4040, Texas Instruments Inc., Dallas TX) to divide the crystal frequency by a factor of 128. The counter output was converted into a sinusoidal current signal that was applied to the two outer electrodes, #1 and #4 in Figure 2-1. The instantaneous voltage signal between the inner electrodes, #2 and #3 in Figure 2-1, was amplified with an instrumentation amplifier (AD 624, Analog Devices, Norwood MA). The AD624 was chosen for its high speed (f_t = 25 MHz), high common mode rejection ratio (CMRR = 85 dB) and low noise characteristics (4nV/√Hz). The signal was then actively rectified and filtered to remove the AC ripple. The constant DC voltage that is finally obtained is applied to a multiplier chip (AD 734, Analog Devices) whose output voltage is inversely proportional to the amplitude of the input signal and then scaled to $\pm$ 10V to represent the conductance signal over the range of expected values. The output resolution of the magnitude measurement is 1mV/μS.

This instrument was designed and built by Daniel Fernandez [12] as part of his Master's thesis.

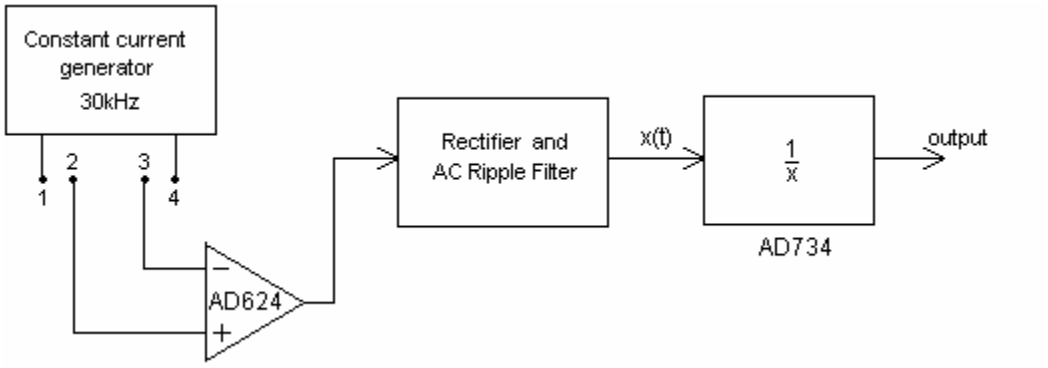

Figure 2-1: Block diagram of the admittance magnitude circuit

2.1.2 Calibration

Calibration of the conductance measurement device was accomplished with 1% metal film resistors between 200 Ω (5,000 μS) and 2.00 kΩ (500 μS). The calibration resistors were tested on an Agilent Inc. Model 4194A Impedance / Gain-Phase Analyzer to ensure that no inductive or capacitive behavior was observable in them over the frequency range of interest, 1 to 100 kHz. This curve is shown in Figure 2-2. The miniaturized tetrapolar catheter cable has substantial inter-wire capacitance: there are six inter-electrode parallel capacitances among the four lead wires [30]. The net effect of these capacitances was compensated by calibration of the catheter by immersing in a relatively large volume of saline of known electrical conductivity. The conductivity of the saline solutions was measured with a Hanna Model HI 8033 conductivity meter (Hanna Instruments, Woonsocket RI) with the temperature compensation turned off. A calibration curve was generated (for every catheter that was used) at the measurement frequency of 30 kHz to cover the range of expected effective conductivities for muscle

(2000 to 6000 µS/cm, or 0.2 to 0.6 S/m). These results are outlined in the following chapter.

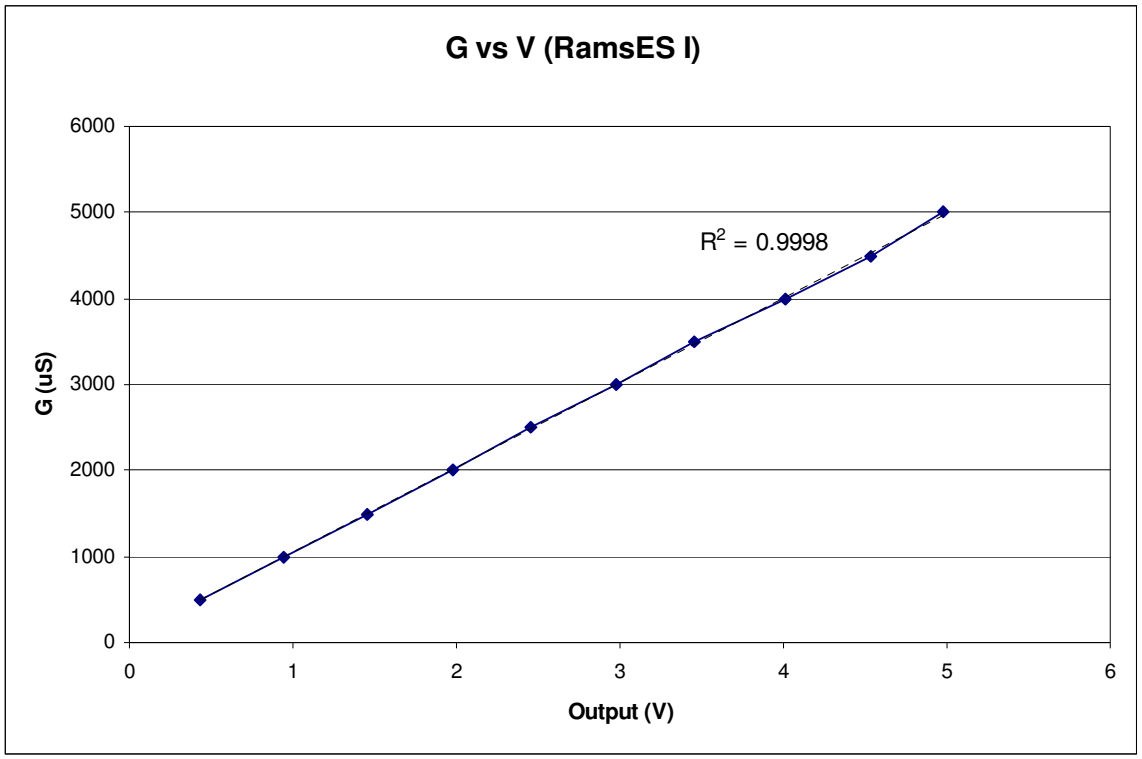

Figure 2-2: Admittance magnitude calibration curve

The conductance measurement exhibits excellent linearity for input conductance varying from 500 µS to 5000 µS as seen in Figure 2-2.

2.2 ANALOG PHASE MEASUREMENT SYSTEM

I designed and developed a phase detection system using discrete analog components that determines the phase angle between two input sinusoidal signals. The system generates an output DC voltage that is proportional to the phase difference between the input signals. The functional units in the phase detection network are illustrated in the block diagram of Figure 2-3.

2.2.1 System Overview

The high pass filters are first order filters with a cut off frequency of 33 Hz. They are used to eliminate any DC offset in the input signals. The high-speed comparators (LM 339, National Semiconductor Corp., Santa Clara CA) are used as zero crossing detectors and generate output square pulses varying from 0V to +5V with a duty cycle of 50%. These pulses are applied to the input of a NAND gate (CD 4011, Texas Instruments Inc., Dallas TX). The output of the NAND gate is a series of pulses whose duty cycle is proportional to the phase difference between the two input signals. A true RMS to DC converter chip (AD536, Analog Devices, Norwood MA) is used to obtain a DC voltage proportional to the duty cycle of the NAND gate output pulses. The low pass filter is a first order filter with a cut off frequency of 160 Hz and is used to remove any high frequency noise from the output of the true RMS chip. The gain and offset circuitry will enable the DC output of the circuit to vary from -9V to +9V for input phase angles varying from -90˚ to +90˚. The phase lag/lead circuit is essentially comprised of a D-type flip-flop whose input and clock are connected to the two comparator outputs. The output of the flop will be either 0V or +5V depending on whether the sine wave in channel 1

leads (+5V output) or lags (0V output) the wave in channel 2. This flop output is used to set the polarity of the final DC output of the system.

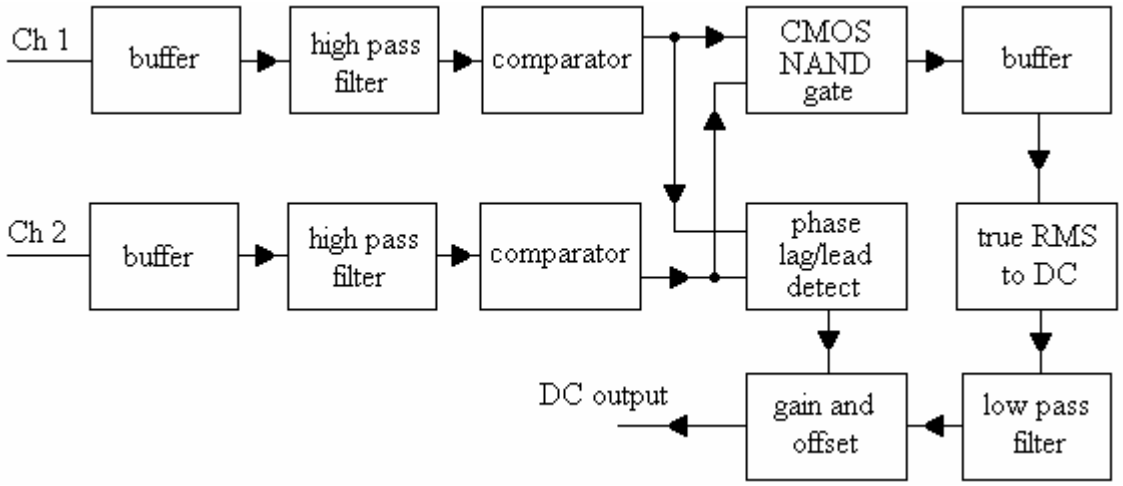

Figure 2-3: Block diagram of the analog phase system

The phase circuit has a sensitivity of 100 mV/degree. The measured phase angle is corrected to remove catheter and measurement system phase shift effects by making phase angle measurements using the same catheter in saline of known conductivity. Since the phase shift in saline has to be zero degrees, any measured phase shift is the effect of the catheter and the measurement system. For small phase angles (0 to 5˚), there is a non-linearity in the DC voltage output of the system. This does not affect the measurements since the phase from the catheter and measurement system is between 30 and 35 degrees, ensuring that the system never has to differentiate between phase angles smaller than 5 degrees.

2.2.2 Circuit Diagrams

The first stage includes high pass filters, comparators and the CMOS NAND gate, shown in Figure 2-4.

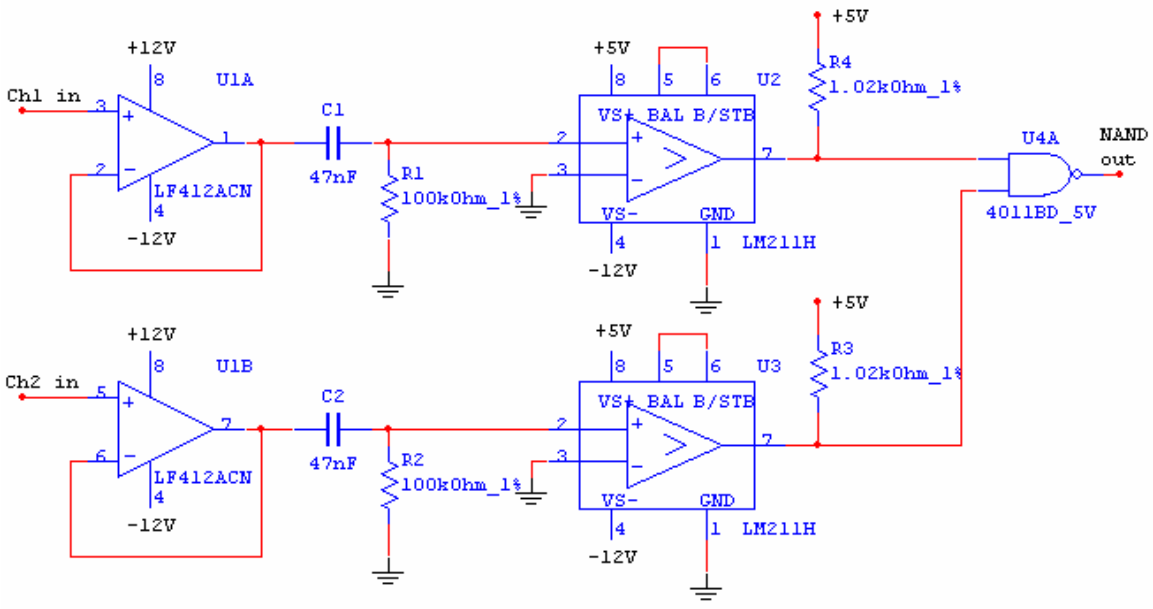

Figure 2-4: Circuit diagram of the first stage of the analog phase system

The high pass filters are passive first order filters with a cut off frequency of 33 Hz. The high speed comparators (LM211) convert the input sinusoidal signals into square waves which are applied to the two inputs of a CMOS NAND gate (CD4011). The NAND gate output is a 50% duty cycle square wave if the input signals to channels 1 and 2 are in phase. This duty cycle increases to 100% as the phase angle between the input channels increases to 180°. This is illustrated in Figures 2-5 and 2-6.

A more efficient implementation would have been to use an XOR gate instead of a NAND gate, since the square wave output duty cycle of the XOR gate would vary from 0% to 100% corresponding to input phase angles of 0° and 180° respectively. However, when the XOR gate is used in combination with the true RMS to DC chip, the output is non linear for small values of phase angle when the duty cycle has to increase from zero to one percent. Thus the NAND gate was selected over the XOR gate in the final design.

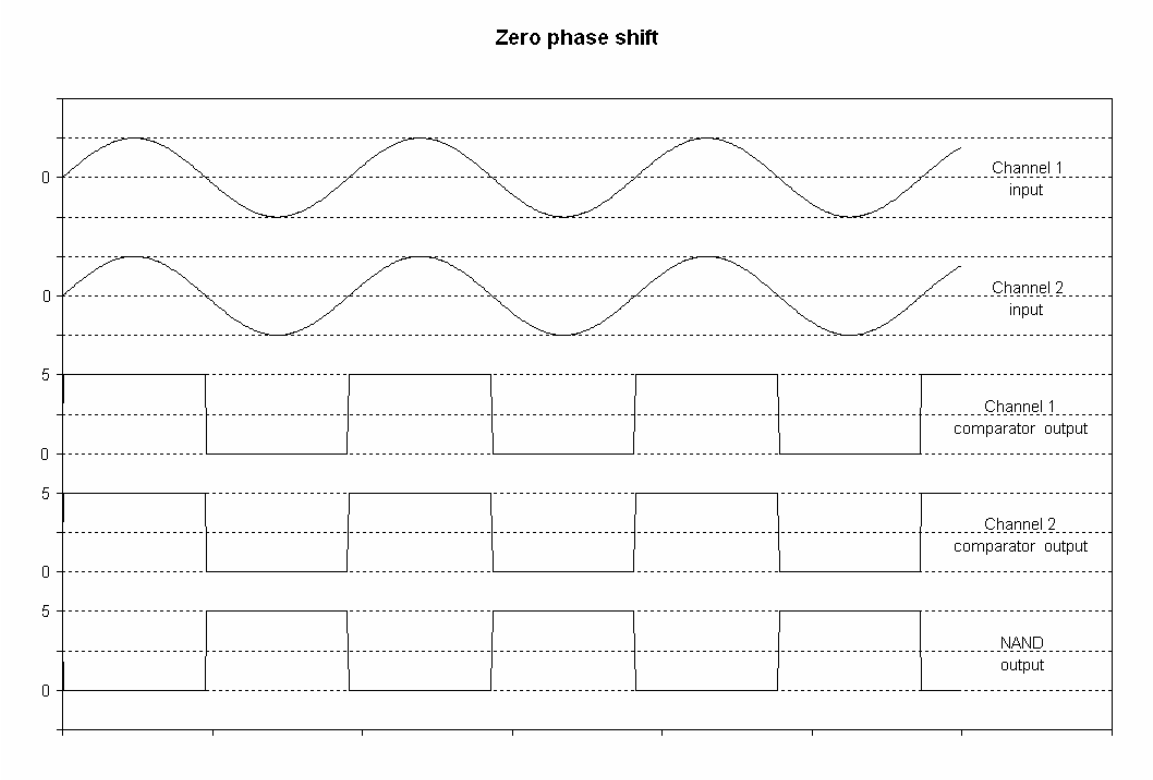

Figure 2-5: Example waveforms for zero phase shift

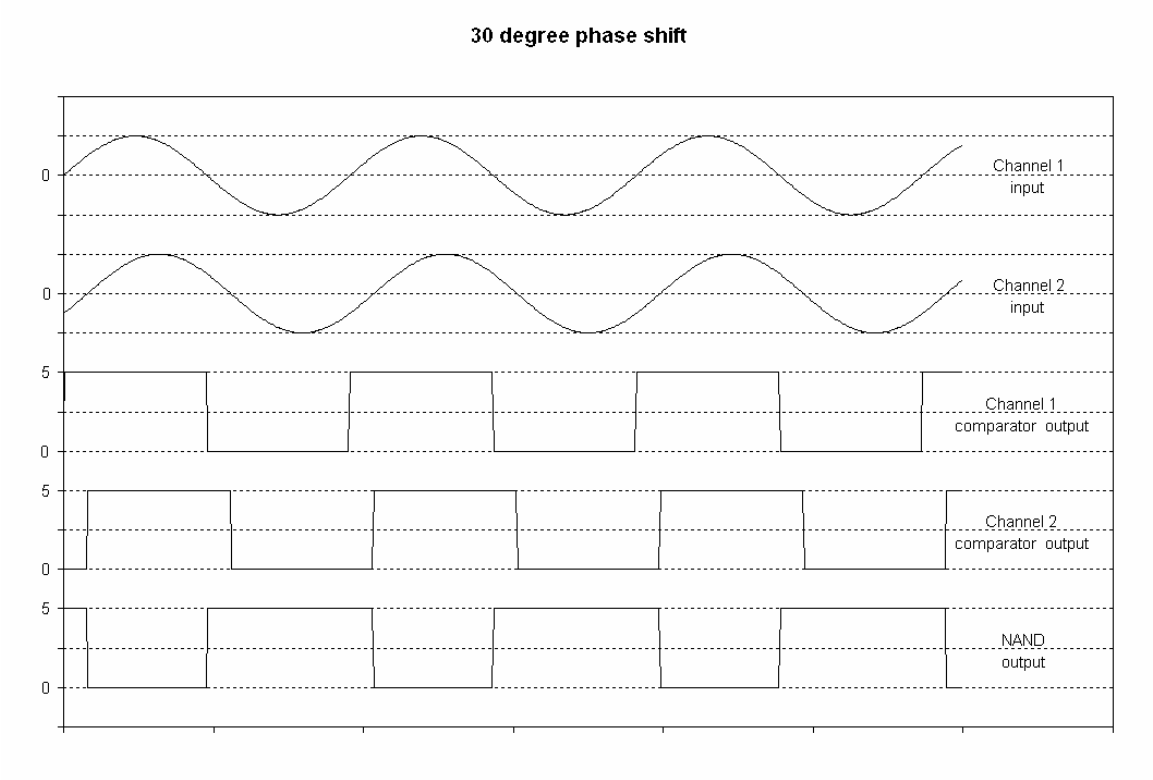

Figure 2-6: Example waveforms for 30 degree phase shift

The second stage includes the true RMS to DC conversion circuit, low pass filter and a gain and offset adjust circuit. The NAND output from the first stage is connected to the input of the true RMS to DC chip (AD536). The output of this circuit is a DC voltage level dependent on the duty cycle of the NAND output. The following low pass filter has a cut off frequency of 160 Hz to remove high frequency noise spikes from the DC output. The gain circuit consists of a summing amplifier that adds an offset voltage to the AD536 output so that a phase angle of 0° corresponds to 0V and a phase angle of 90° corresponds to +9V. The offset voltage is adjustable to calibrate out the phase effects of the instrumentation. The final output of this stage is a DC voltage ranging from 0 to +9V for phase angles varying from -90° to +90°. This stage cannot distinguish between positive and negative phase angles. This is accomplished in the third and final stage.

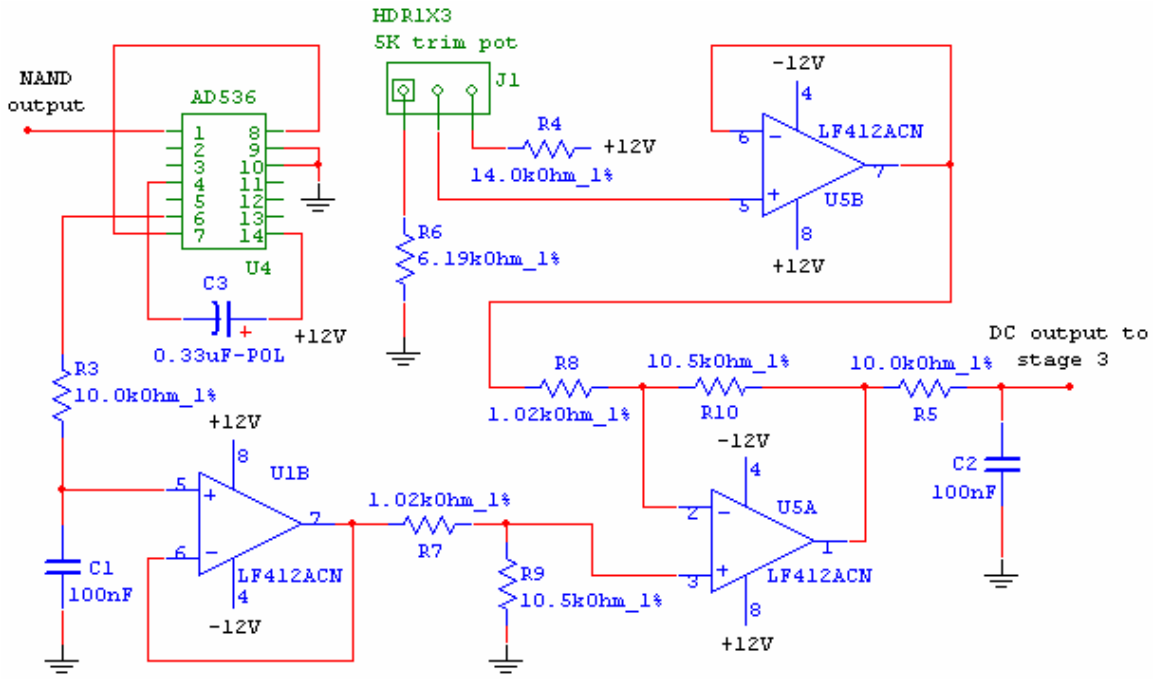

Figure 2-7: Circuit diagram of the second stage of the analog phase system

The final stage consists of the phase lag/lead detect circuit. This is accomplished using a D-type flip-flop whose input and clock are connected to the two comparator outputs. The output of the flop will be either 0V or +5V depending on whether the sine wave in channel 1 leads or lags the wave in channel 2. This flop output is used as one of the control signals of an analog switch (MAX4535) that routes the DC phase signal through either a buffer or a buffer and a unity gain inverting amplifier that inverts the polarity of the DC signal. Hence the final DC output of the system varies from -9V to +9V for phase angles varying from -90° to +90°. The final output is also scaled down by a factor of 100 and connected to an LCD panel meter to display the phase angle in degrees. The detailed circuit diagram for this stage is shown in Figure 2-8.

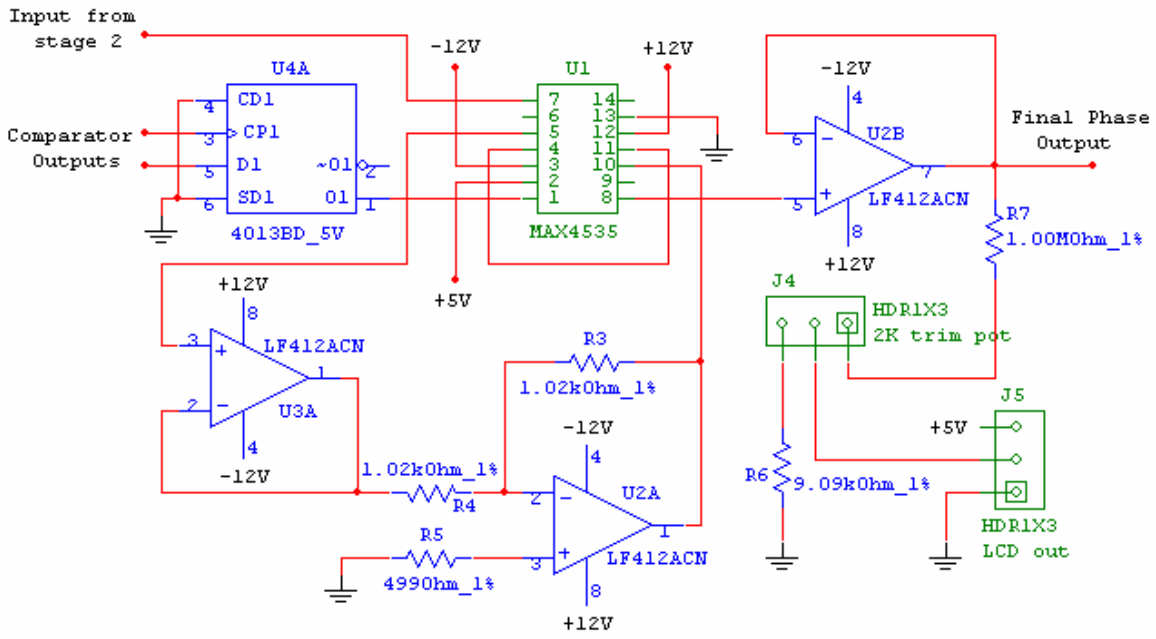

Figure 2-8: Circuit diagram of the third stage of the analog phase system

2.2.3 System Noise and Resolution

The noise analysis of the phase system was performed by taking a large number of measurements at a constant input phase difference of ten degrees. The probability density function (PDF) of approximately 3,500 output samples was acquired using an ADInstruments Powerlab data acquisition system and plotted as shown in Figure 2-9.

The noise is extremely low, ±0.05 degrees. The PDF of the distribution is very close to a Gaussian distribution and the noise has a variance of 0.006 degrees.

A simple method to estimate resolution is to measure the peak-to-peak variations resulting with a fixed input, as shown in Figure 2.9. Given this definition, the phase resolution is 0.1° because the typical variations are ±0.05°.

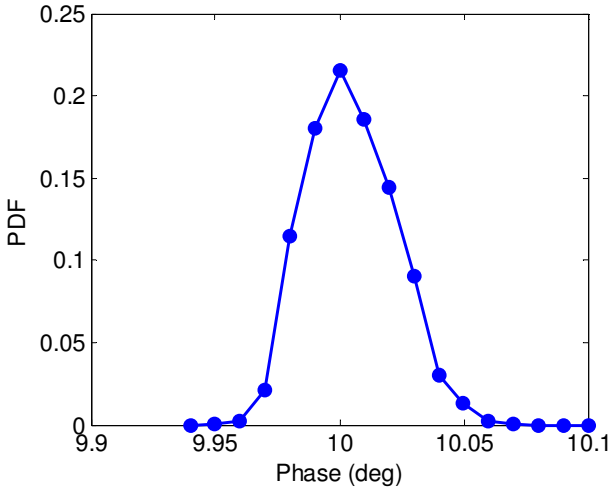

Figure 2-9: PDF with a constant input of 10 degrees

The system resolution was also determined by acquiring data for several closely spaced phase offsets. A Students-T test was performed for various numbers of samples. The PDF of several phase offsets is shown in Figure 2-10 where each PDF was calculated using approximately 3,500 samples.

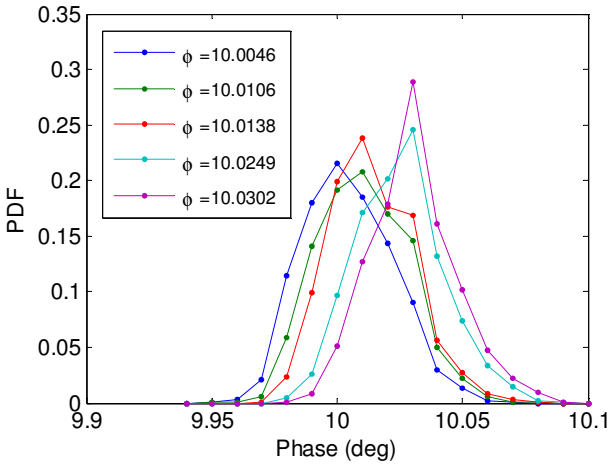

Figure 2-10: PDF for several closely spaced phase inputs

To use the *t*-statistic, one assumes the errors are normally distributed (with equal variances), and the errors are independent within each group and between the groups. Phase data is first collected for φ =10.0046°. Then, the phase is changed and phase data is collected again. The null hypothesis is that the means of two normally distributed populations are equal (meaning the instrument cannot resolve the change). For a sample size of 20, the *t*-statistic must be greater than 2.1 for a 95% confidence interval to reject the null hypothesis (meaning the instrument can resolve the change). Table 2-1 shows the calculated *t*-statistic for various numbers of samples. From the table, it is seen that the resolution for a sample size of 20 is about 0.03° (since the *t*-statistic between φ = 10.0046° and φ = 10.0304° is greater than 2.1). This value is slightly smaller than the system accuracy, which is at best 0.1°.

Samples	***t*-statistic**			
	φ=10.0106°	φ=10.0138°	φ=10.0249°	φ=10.0302°
20	0.63	2.52	0.08	4.69
100	1.80	0.40	5.76	12.25
200	3.13	1.69	9.75	17.07

Table 2-1: *t*-statistic values for various numbers of samples, taken between φ=10.0046° and the other four.

2.2.4 System Accuracy

The phase accuracy of the system was determined by applying sinusoidal signals with a known phase difference at the input and measuring the system output. The input phase difference was calculated using an oscilloscope. The measurements were made at 2 kHz and 30 kHz and the results are shown in Figures 2-11 and 2-12.

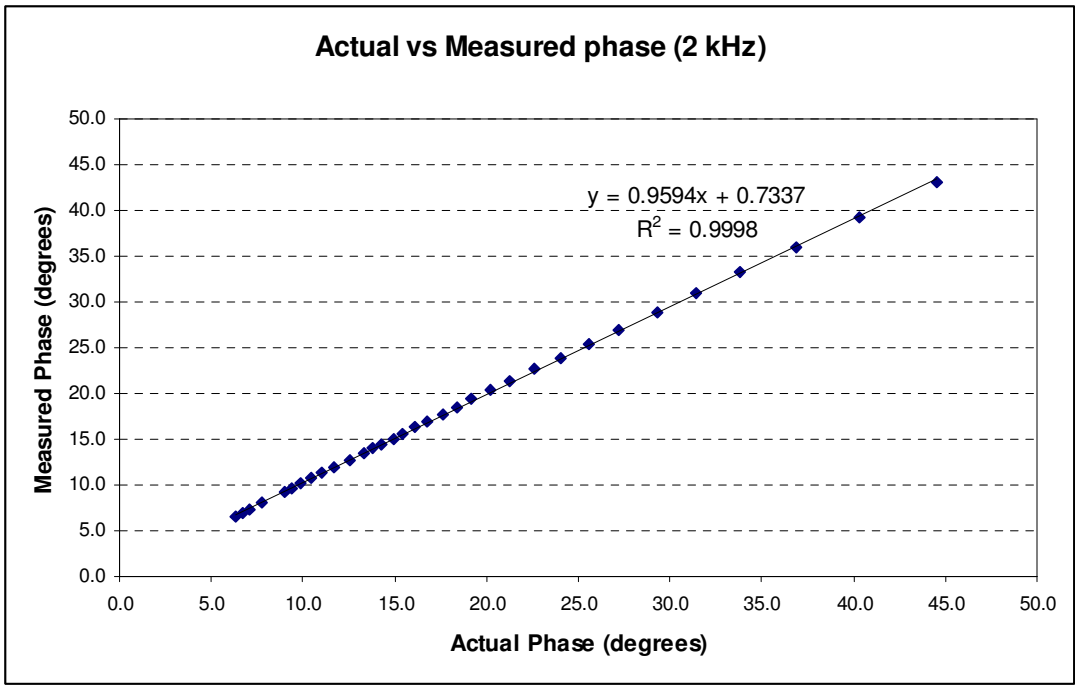

Figure 2-11: Actual phase vs. measured phase at 2 kHz

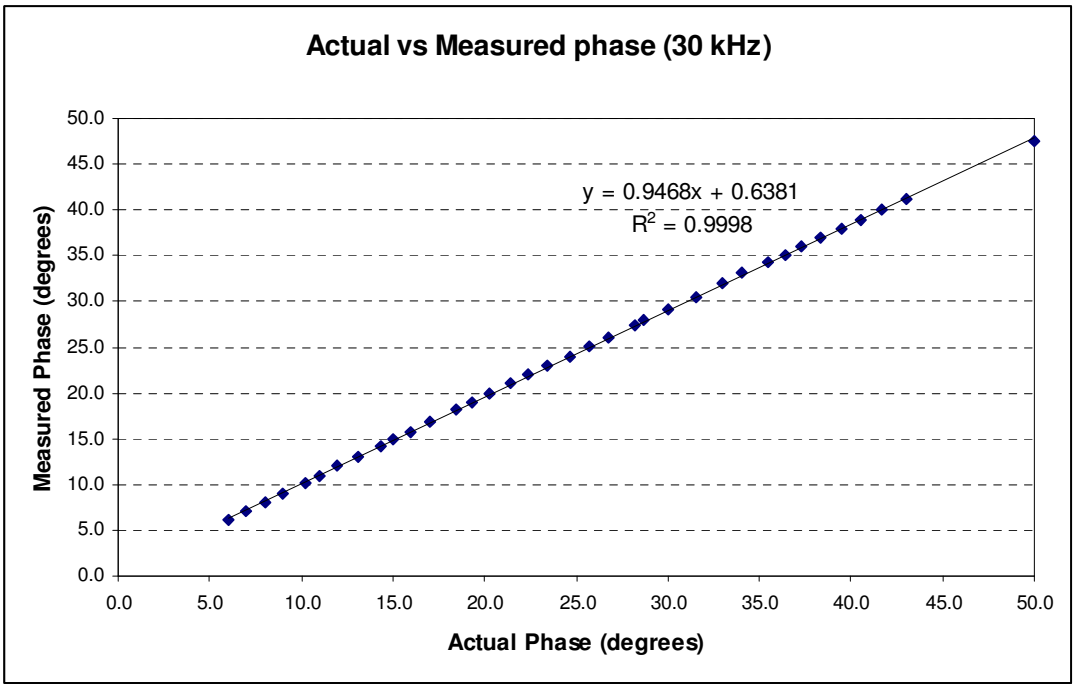

Figure 2-12: Actual phase vs. measured phase at 30 kHz

It is evident from the above graphs that the instrument is linear over all regions analyzed for both 2 kHz and 30 kHz signals. In both cases the correlation coefficient, R^2, is 0.9998. Absolute error was then calculated as the absolute value of the difference between the phase measured by the instrument and the actual phase.

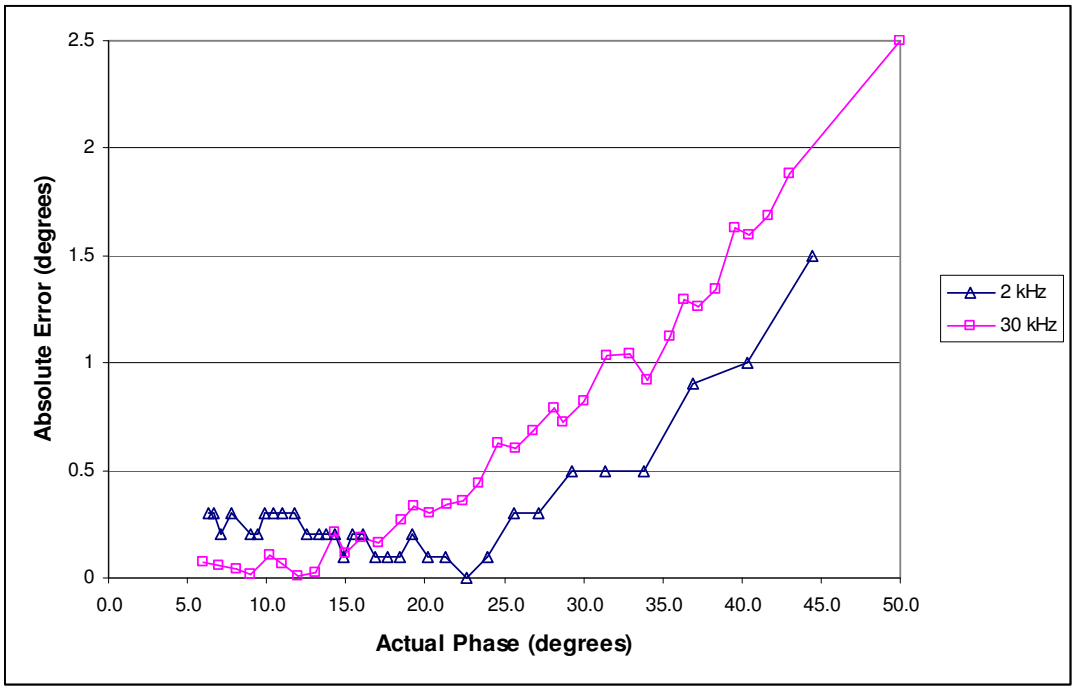

Figure 2-13: Actual phase vs. Error at 2 kHz and 30 kHz

It should be noted that this error is due to both error in the instrument and the error in the estimation of the actual input phase angle. Previous estimates of phase angle in the mouse myocardium using digital signal processing of the excitation and measured signals have shown phase angles between 5 and 30 degrees [29]. The instrumentation to measure admittance magnitude will induce a phase offset of about 10 degrees (at 30 kHz) from the band pass filters used in the circuit and the inter-wire capacitances in the surface probe.

2.3 REAL-TIME ADMITTANCE MEASUREMENT SYSTEM

The admittance magnitude and phase measurement systems described earlier are combined into a single integrated system. The block diagram of the new system is shown in Figure 2-14.

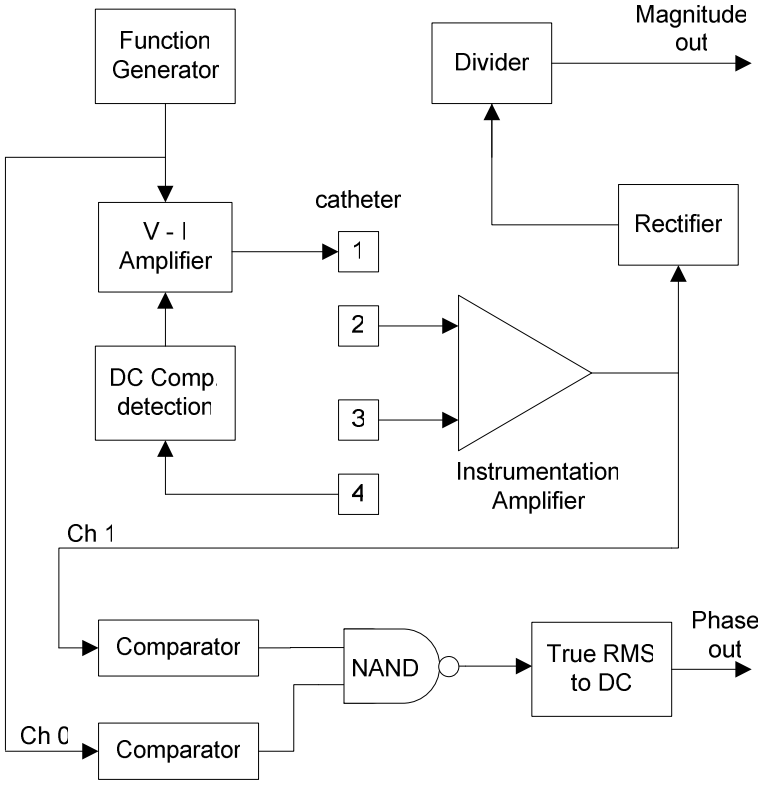

Figure 2-14: Instrument used to measure complex admittance

The RamsES I system has two BNC analog output channels, one each for the magnitude and the phase angle. These two parameters are also displayed on two LCD panel meters located on the front panel of the instrument. The system is designed to work over an admittance magnitude range of 500µS to 5000µS and phase angle range of -90° to +90°, which covers the range of values measured in the myocardium as well as in the

LV blood pool. A calibration switch is used to switch between the internal conductance calibrator and the external catheter. The catheter is plugged in via a six pin Redel™ connector (LEMO connectors). The system is powered using an external low-noise plug-in power supply manufactured by Stancor Electronic (Star-9007). The supply provides up to 1A at 5V and 300mA at ±12V. The RamsES I circuit draws approximately 100mA from the ±12V supply and about 20mA from the 5V supply, which is well within the limits of the power supply.

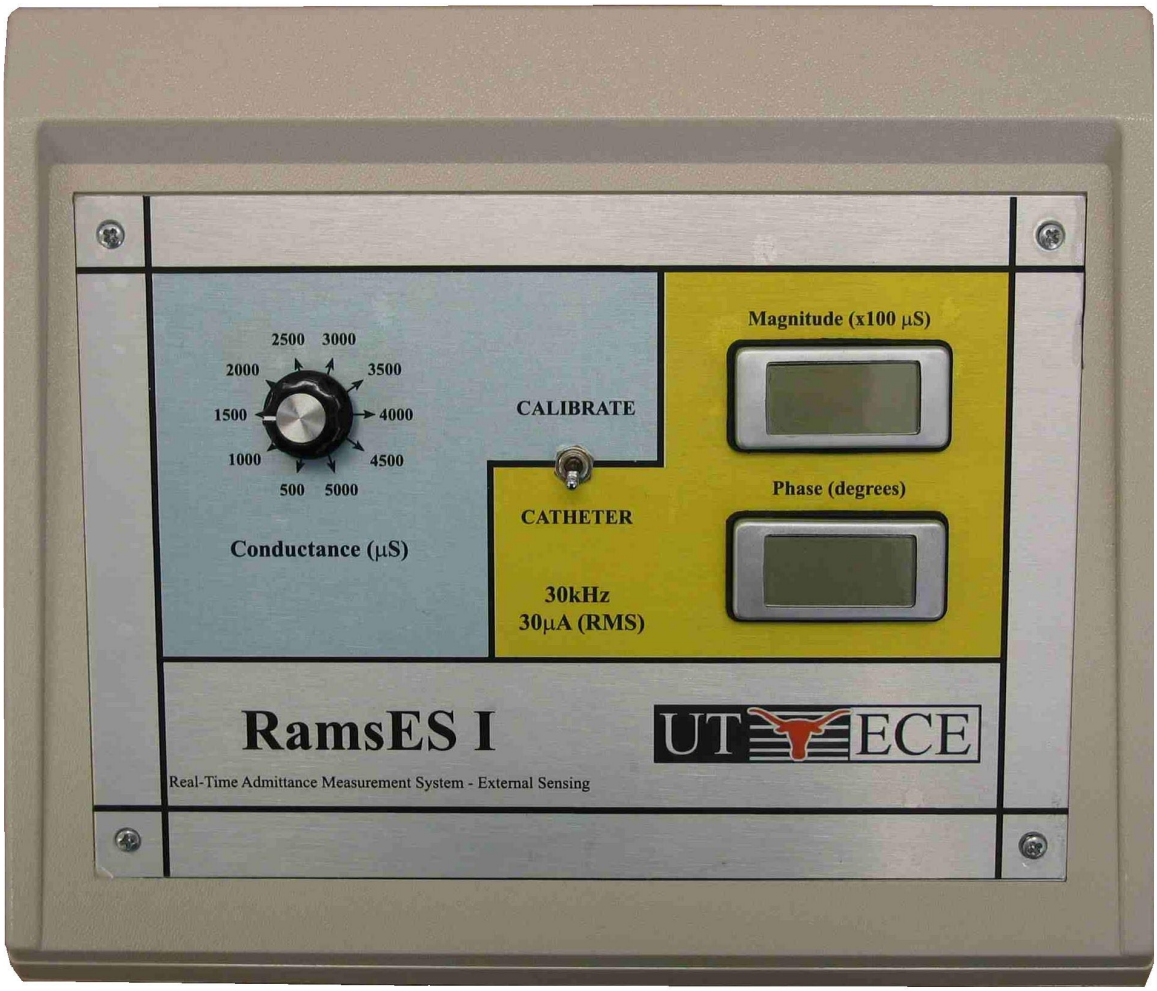

Figure 2-15: Front panel of the RamsES unit

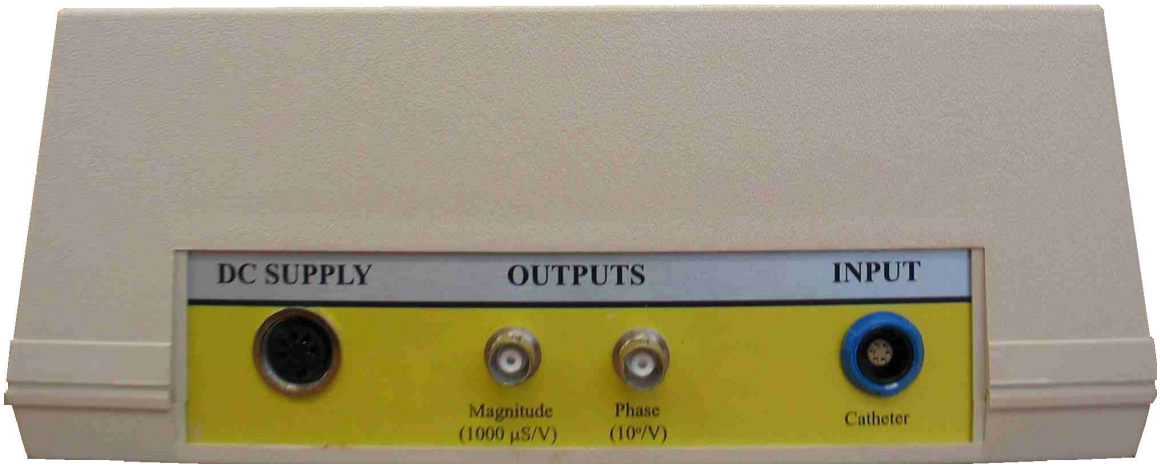

Figure 2-16: Back panel of the RamsES unit

CHAPTER 3

Design and Development of Tetrapolar Admittance Catheter

3.1 OVERVIEW

The use of tetrapolar electrode configuration for admittance measurements and its advantages over the bipolar electrode configuration have been described elsewhere [51, 54]. Briefly, the tetrapolar configuration is preferred since it compensates for the electrode-electrolyte interface impedances. In a linear tetrapolar electrode configuration, a constant current is injected through the outer electrode pair and the voltage difference between the inner electrode pair is measured. Since the current is kept constant, Ohms law dictates that any change in the measured voltage corresponds to a change in the admittance between the inner electrode pair.

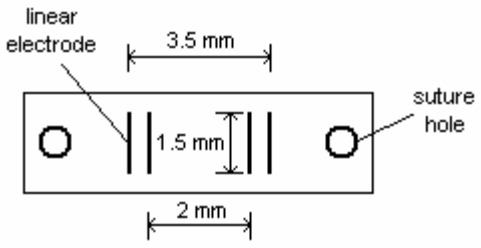

Figure 3-1: Surface probe used for admittance measurements

Myocardial tissue is highly anisotropic due to the complex structure of fiber orientation. There is a change in fiber orientation by over 120° between epicardium and endocardium. This anisotropy of the myocardial tissue makes it necessary to use a surface probe that has a depth of penetration approximately equal to the thickness of the

myocardium to ensure that the admittance measurements are isotropic. The field penetration depth is directly proportional to the electrode spacing on the probe.

3.2 ELECTRIC FIELD PENETRATION DEPTH

The experimental technique to determine the field penetration depth of tetrapolar surface admittance catheters is described by Kottam *et al.* [31]. Briefly, the experimental setup consists of a flat bottomed dish filled with saline with a movable plastic sheet at the bottom. The position of the movable sheet could be accurately adjusted by means of a micro manipulator with a resolution of 0.1 mm. The admittance catheter was placed on the saline surface and the plastic sheet was moved closer to the catheter. The admittance magnitude was monitored continuously and the depth of penetration was determined to be the spacing between the catheter and the plastic sheet that caused the admittance magnitude to drop to ninety percent of the magnitude when the plastic sheet is at the bottom of the dish (i.e. $|Y|_{inf}$). The experimental setup is shown in Figure 3-2.

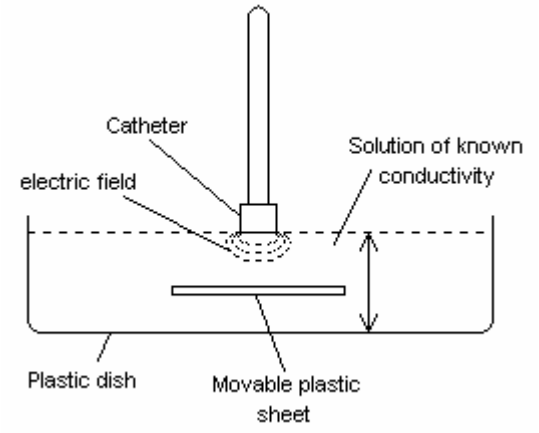

Figure 3-2: Experimental setup to measure field penetration depth of surface catheters

The measured depth of penetration was verified using finite element models developed using a commercially available software package (COMSOL). The simulation results were compared with the actual *in vitro* experimental results in saline of known conductivities. This also enabled the estimation of the probe constant K_p for the different catheter designs. The models indicate that the effective penetration depth increases as the spacing between the sensing electrodes (#2 and #3) is increased. If this spacing is kept constant, the effective penetration depth is affected by the spacing between the stimulation and the sense electrodes. This is because the field geometry is determined only by the spacing between the two outer stimulation electrodes (#1 and #4) and the penetration depth decreases as this spacing is decreased. The results are summarized in Table 3-1. The calculated penetration depths were also independent of the conductivity of the bulk medium in the models.

Electrode Spacing (mm)			**Calculated field**
1-2	**2-3**	**3-4**	**penetration depth (mm)**
0.75	1.6	0.75	1.73
0.75	2.2	0.75	1.93
0.75	2.0	0.75	1.87
0.5	2.0	0.5	1.41
0.5	1.8	0.5	1.33

Table 3-1: Electric field penetration for various electrode spacing (COMSOL results)

The current density over the electrode surface is not uniform, but is denser around the edges of the electrode. Using a constant current boundary condition at the electrodes will force the current density to be uniform over the entire electrode surface in the model.

To overcome this, I specified the stimulation electrodes as constant potential electrodes with an excitation voltage of ±1.5V at 31.25 kHz. The electric field distribution for a tetrapolar electrode configuration with constant voltages of ±1.5V applied between the outer electrodes is shown in Figure 3-3. In this case, the bulk medium is assumed to be isotropic with a conductivity of 2000 µS/cm.

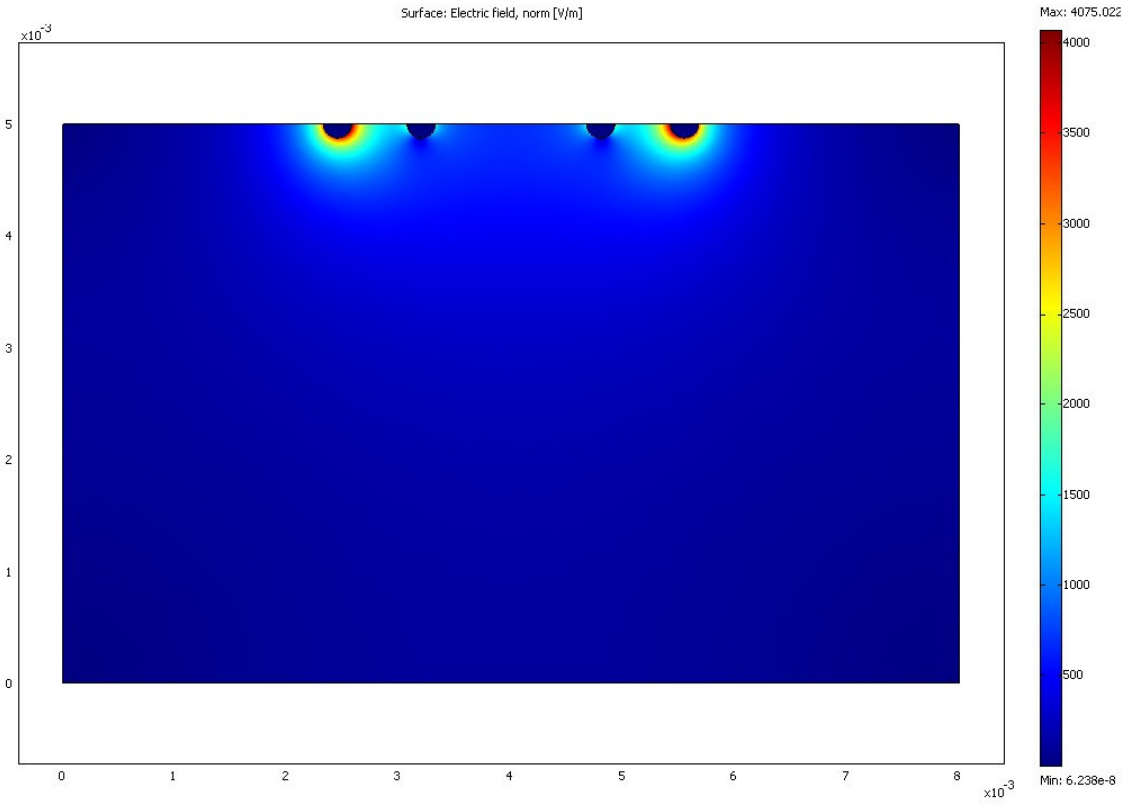

Figure 3-3: COMSOL simulation results for electric field distribution for tetrapolar electrode configuration

The admittance was measured between electrodes 2 and 3 for different distances of the bottom insulating layer from the tetrapolar electrode surface. The distance was decreased from 5mm down to 0.5mm and the distance at which the measured admittance dropped to 90% of the value at 5mm was considered as the effective penetration depth.

3.3 TETRAPOLAR SURFACE PROBE

I designed and built a tetrapolar admittance probe that can be sutured onto the epicardial surface of the left ventricle of rat hearts. This probe is used to measure localized myocardial admittance during baseline, varying durations of ischemia and reperfusion. The surface probe is comprised of four linear electrodes mounted on a polystyrene strip. The electrodes are made from 0.4 mm diameter solid gold wire (Cooner Wire, part no. CW 5263-26). The electrode spacing is illustrated in Figure 3-1.

The electrodes were attached to the polystyrene strip using fast acting cyanoacrylate glue. The other ends of the gold wires were connected to a four pin Molex header connector. The entire catheter and connector assembly is shown in Figure 3-5.

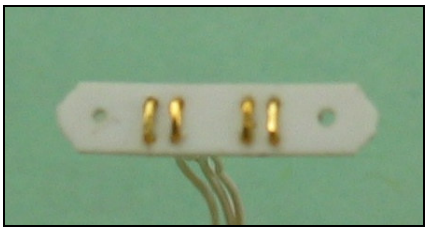

Figure 3-4: Epicardial surface probe used for admittance measurements

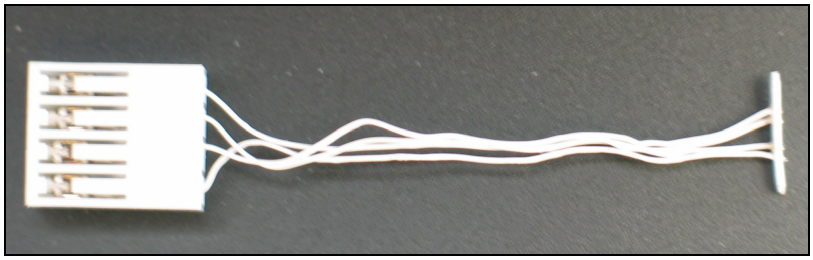

Figure 3-5: Epicardial surface probe and connector

The electric field penetration depth of this probe was determined experimentally using the technique described above. Two different saline solutions with conductivities of

10,500µS/cm and 1,850µS/cm were used to ensure that the measurement results were independent of the saline conductivity. The measurement results for one of the probes are shown in Figures 3-6 and 3-7. The field penetration depth was calculated to be 1.6mm in both cases. The COMSOL simulation results show a field penetration depth of 1.87mm for the same electrode spacing. This is because the COMSOL models are in 2D and assume an infinite electrode length along the third dimension. In reality, the finite electrode length causes the field lines to constrict around the ends of the electrode. Thus the model tends to overestimate the field penetration depths when compared with the experimental results.

The left ventricular wall thickness of rats ranges from 1.6 – 2.0 mm for body weights ranging from 200 to 300 grams [39]. I built and characterized a total of three surface probes with differing electrode spacing. The measured and calculated field penetration depths for all three probes are shown in Table 3-2.

Probe	**Electrode Spacing (mm)**			**Penetration Depth (mm)**	
#	**1-2**	**2-3**	**3-4**	**Experimental**	**Calculated**
6	0.75	2.0	0.75	1.60	1.87
7	0.50	1.8	0.50	1.15	1.33
8	0.75	1.6	0.75	1.47	1.73

Table 3-2: Measured vs. theoretical field penetration results for three surface probes

From the above table, it is evident that probe #6 the optimal choice for the myocardial properties measurement (field penetration depth almost equal to LV wall thickness). The length of the probe must also enable all four electrodes to be in contact with the tissue without having to bend the probe to conform to the curvature of the heart.

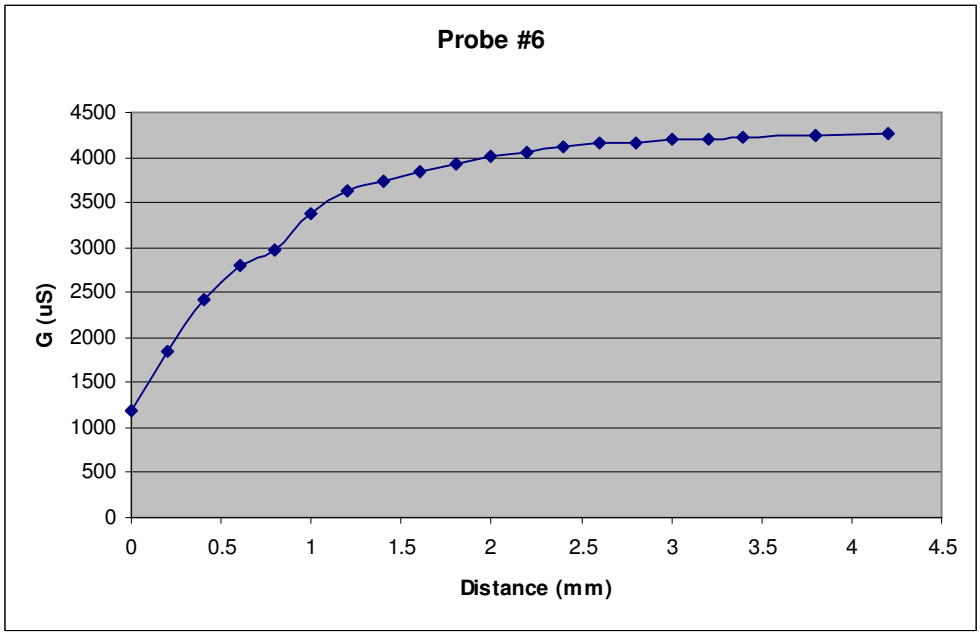

Figure 3-6: Field penetration results for σ = 10,500μS/cm

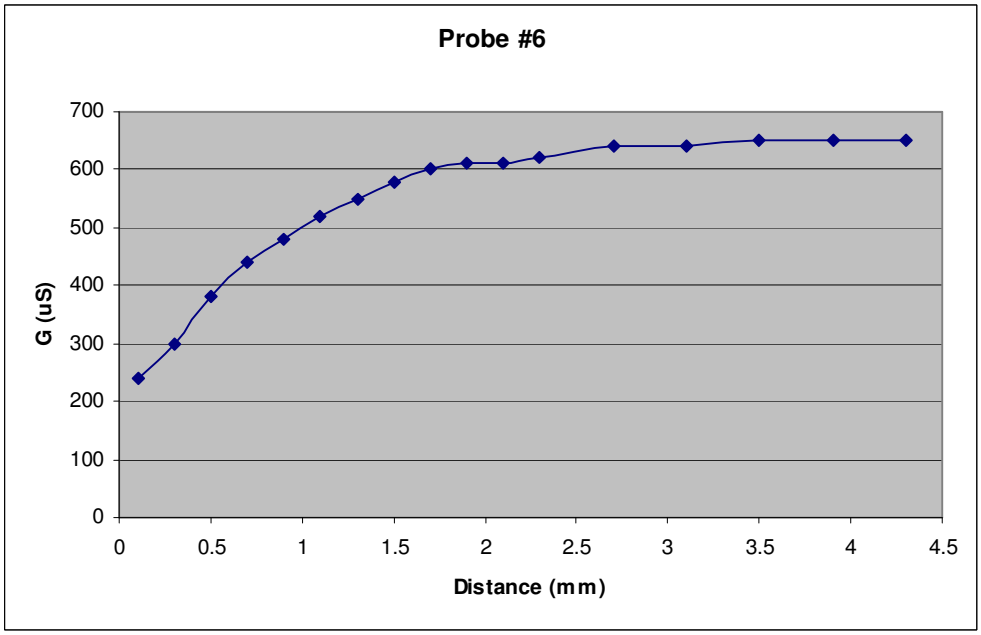

Figure 3-7: Field penetration results for σ = 1,850μS/cm

3.4 DETERMINATION OF PROBE CONSTANT

The probe constant K is defined as the ratio between the actual conductivity (σ) of the medium and the conductance (G) measured by the probe. Its value depends on the relative spacing of the electrodes on the probe which affect the field geometry.

$$\sigma = K \times G \tag{6}$$

In terms of the permittivity of the medium (ε_m) and the capacitance (C) measured by the probe,

$$\varepsilon_m = K \times C \tag{7}$$

From equation 3 described in chapter 1, the probe constant K can be related to the field form factor F as follows.

$$K = \frac{\sigma}{G} = \frac{\varepsilon_m}{C} = \frac{-\int_L E.dl}{\iint E.dA} = \frac{1}{F} \tag{8}$$

The probe constant was determined by making conductance measurements on saline of known conductivities. These calibration solutions were prepared by mixing calculated amounts of sodium chloride in distilled water. Six different calibration solutions with conductivities of 2000, 4000, 6000, 8000, 10000 and 12000μS/cm were prepared and the conductivities were verified using a commercially available conductivity meter (Hanna Instruments) with the temperature compensation turned off.

The known conductivities were plotted on the x axis and the measured admittance magnitudes were plotted on the y axis. This graph is shown in Figure 3-8. The probe constant K is calculated by taking the reciprocal of the slope of the line. For the probe shown above (probe #6), value of K is 2.35 cm^{-1}.

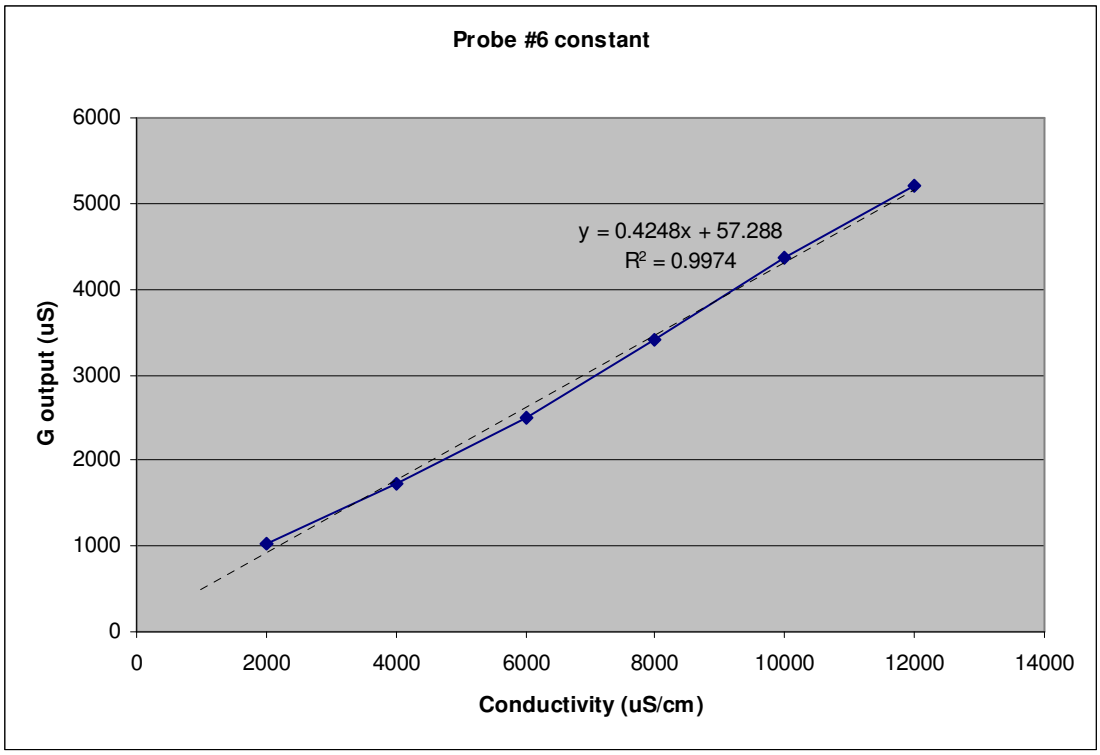

Figure 3-8: |Y| vs. σ for the surface probe

CHAPTER 4

Myocardial Ischemia and Stunning in the Isolated Rat Heart

4.1 OVERVIEW

The most prevalent experimental model to study myocardial ischemia and stunning is the Langendorff preparation of isolated perfused heart. The Langendorff model has been used in cardiovascular research for over 40 years [22] and provides a highly reproducible model that can be studied quickly and in large numbers at low cost. The effects of myocardial ischemia can be studied more easily under controlled conditions in isolated models.

The isolated heart can be perfused in either constant flow or constant pressure mode. Constant flow perfusion adds an additional element of constancy to the experiment and simplifies the analysis of experimental data. The disadvantage here is that unlike in a constant pressure system, autoregulatory mechanisms are overridden and the system does not automatically alter the amount of perfusate delivered to the whole heart when there are changes in heart rate or load or when regional ischemia is imposed [22]. In spite of this disadvantage, it is experimentally preferable to control flow rate and heart rate since these variables can influence other indices of mechanical function. I used a constant flow, non recirculating model (Radnoti Glass Technologies Inc.) for the ischemia/stunning studies. The system is shown in Figure 4-1.

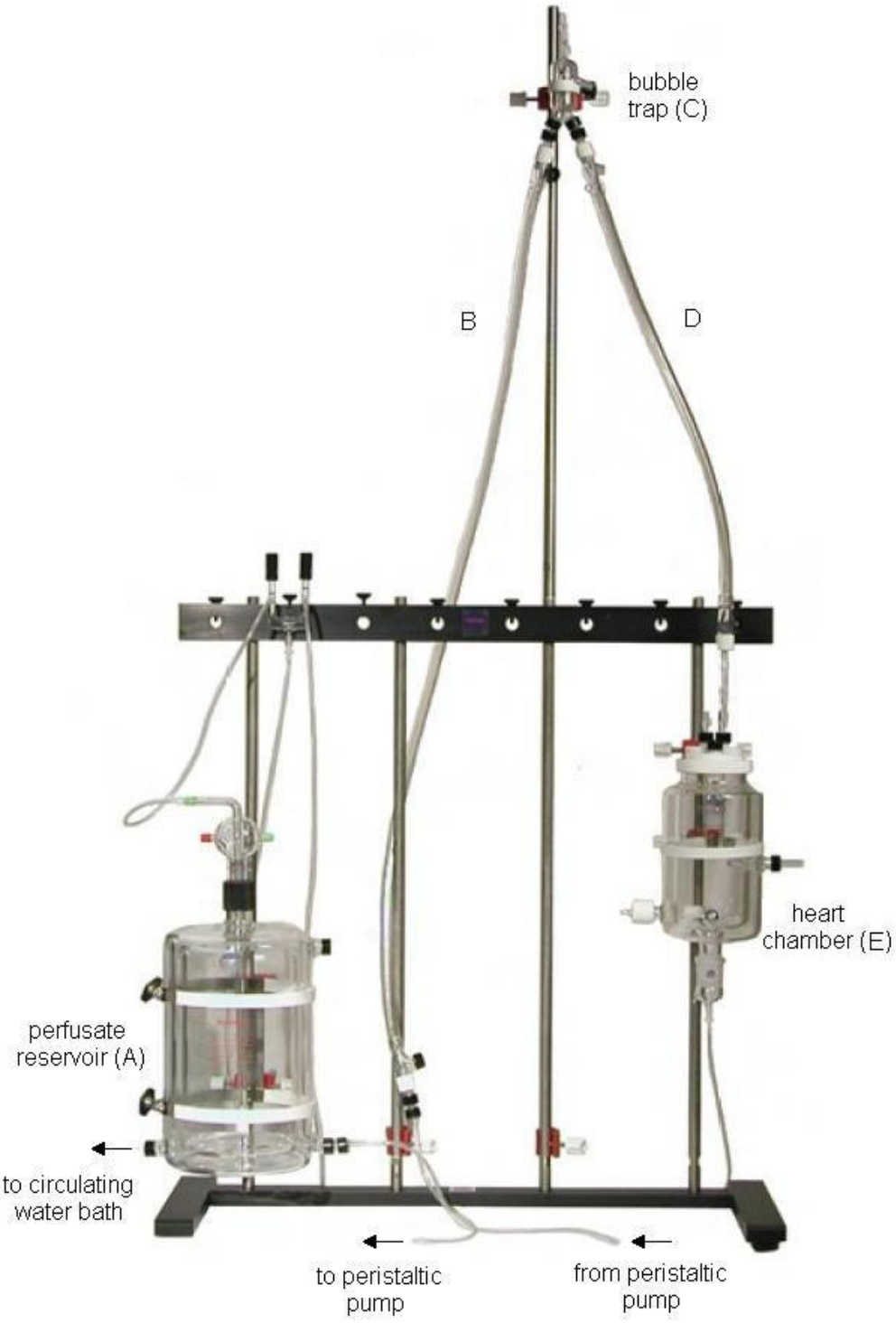

Figure 4-1: Constant flow, non recirculating Langendorff system

The system uses a water-jacketed 2-liter reservoir (A) to maintain and oxygenate the perfusate solution. A peristaltic pump draws perfusate from the reservoir and drives the solution up to a water-jacketed bubble trap (C) via a water jacketed flex tube assembly (B), where bubbles are removed from the flow, and then down to the aortic cannula into the heart chamber via a second water jacketed flex tube assembly (D). Effluent from the heart can be collected for evaluation. The constant flow peristaltic pump is adjustable with flow rates ranging from 1-10 ml/min. A pump-driven circulating water bath is used to circulate warm water through the water jackets on the tubes and glass reservoirs for excellent temperature control of the buffer. Myocardial stunning is induced in this model by 15 min of global no-flow ischemia.

The temperature of the myocardial surface must be monitored and regulated since conductance is a function of the temperature of the tissue. This was achieved by maintaining the perfusate at 36°C and placing the isolated heart in a water jacketed temperature regulated heart chamber (E). The relation between temperature and conductivity is given by

$$\sigma_t = \sigma_0 \exp[\alpha(t - t_0)] \tag{9}$$

where σ_t is the conductivity at temperature t, σ_0 is the conductivity at temperature t_0 and α is the temperature coefficient of conductivity (0.021 $^{\circ}C^{-1}$ for NaCl).

The perfusion fluid that is most commonly used in Langendorff studies is the Krebs-Henseleit bicarbonate buffer. This fluid mimics the key ionic content of blood and plasma and has a pH of 7.4 at 37°C. The effluent from the heart can be collected at regular intervals and analyzed for elevated LDH levels, which is an indicator of ischemic cell death.

4.2 LANGENDORFF SYSTEM SETUP

The various steps involved in setting up the constant flow, non recirculating Langendorff system are outlined below.

- Circulate distilled water through perfusate channels for 15 min to flush out the system.
- Insert Millar pressure transducer above the aortic cannula (pressure should be 50-100 mmHg).
- Run the water bath at ~42°C and circulate the warm water through the water jacket tubes. Verify that the temperature of liquid in perfusate channels is 37°C.
- Adjust perfusate flow rate to 10 ml/min.
- Attach LV balloon to the end of the fluid filled LV catheter, taking care to remove any trapped air bubbles.
- Prepare Krebs-Henseleit (KH) bicarbonate buffer by mixing the following amounts of salts in 1 litre of water. The calcium should be added at the very end after ensuring that the perfusion solution has a pH of 7.40.
    - NaCl (118.5mM) - 6.900 gms
    - $NaHCO_3$ (25mM) - 2.100 gms
    - KCl (4.7mM) - 0.350 gms
    - $MgSO_4$ (1.2mM) - 0.296 gms
    - KH_2PO_4 (1.2mM) - 0.163 gms
    - glucose (11.0mM) - 1.982 gms
    - $CaCl_2$ (1.4mM) - 0.155 gms

- If the pH is greater than 7.40, add a few drops of hydrochloric acid to reduce the pH.
- Pour into the buffer into the perfusate container of the Langendorff system.

- The buffer will be saturated with gas (95%O_2 / 5%CO_2) through a bubbler inserted into the perfusate container.

4.3 ISOLATED HEART PREPARATION

The isolated heart studies were done on adult male WKY rats weighing between 210 and 300gms. The protocol that was used for the ischemia and the stunning studies is outlined below.

- Weigh the rat after it is anesthetized using the standard rat cocktail.
- Rapidly excise the heart via anterior thoracotomy and place in ice-cold (4°C) beaker of Krebs-Henseleit (KH) bicarbonate buffer to arrest the heart.
- Perform aortic cannulation rapidly (within 60 seconds) and perfuse the hearts with KH buffer in Langendorff mode at a flow rate of 10 ml/min.
- Remove left atrial appendage to provide a clear field of view.
- Insert a deflated balloon into the LV via the mitral valve. This balloon is attached to a short rigid catheter and a Millar pressure transducer.
- Inflate the balloon with water from a micro syringe until an LVEDP of between 4 and 8 mmHg is obtained.
- Position the tetrapolar surface probe on the epicardial surface, above the LV. Monitor admittance magnitude and phase angle continuously using the RamsES I unit.
- Throughout the experiment the heart will be placed in a water-jacketed chamber (E) to maintain constant temperature during the ischemic period.
- Monitor aortic pressure throughout the working heart model perfusion periods in the aortic outflow line with a Millar transducer.
- Allow the isolated heart preparation to stabilize for about 10 min.
- Collect baseline perfusate samples.

4.3.1 Control Hearts Protocol

- The isolated heart system is setup as described above.
- Hang the heart and perfuse for 140 min.
- Draw perfusate samples at three, five and ten minute intervals during perfusion.
- Analyze the samples for markers of ischemia (LDH).
- Weigh the heart, make slices along the short axis and store the slices in formalin for histologic analysis.

4.3.2 Myocardial Ischemia Protocol

- The isolated heart system is setup as described above.
- Induce global no-flow ischemia by stopping aortic perfusion for 90 min.
- Reperfuse for 20 min by reestablishing aortic perfusion.
- Draw perfusate samples at five minute intervals.
- Analyze the samples for markers of ischemia (LDH).
- Weigh the heart, make slices along the short axis and store the slices in formalin for histologic analysis.

4.3.3 Myocardial Stunning Protocol

- The isolated heart system is setup as described above.
- Induce global no-flow ischemia by stopping aortic perfusion for 15 min.
- Reperfuse for 90 min by re-establishing aortic perfusion.
- Draw perfusate samples at three, five and ten minute intervals during reperfusion.
- Analyze the samples for markers of ischemia (LDH).

- Weigh the heart, make slices along the short axis and store the slices in formalin for histologic analysis.

4.4 CONTROL HEARTS RESULTS

Three adult male WKY rat hearts were perfused in constant flow Langendorff mode according to the protocol described in the earlier section. The measured admittance magnitude and phase angle was used to determine the relative permittivity and conductivity of the myocardial tissue over a perfusion duration of 140 min. LDH samples were also collected at regular intervals to determine the extent of myocardial cell damage, if any. These hearts served as controls and the results were compared with similar results from hearts subject to the stunning and ischemia protocols.

The LV pressure was monitored by inserting a fluid filled balloon into the LV. The pressure in the balloon was measured using a 1.4 Fr. Millar pressure sensor and was zeroed prior to insertion into the LV. After insertion, the balloon was inflated/deflated to obtain a left ventricular end diastolic pressure (LVEDP) between 4 and 8 mmHg. The LVEDP increased steadily from 2.7 to 20.6 mmHg within the first 15 minutes of hanging the heart and perfusing it. The diastolic pressure then gradually dropped to 19 mmHg over the next 45 minutes and then remained fairly constant over the remainder of the perfusion duration. This is illustrated in Figure 4-2. The error bars represent the standard deviation of the measurements over three different control hearts.

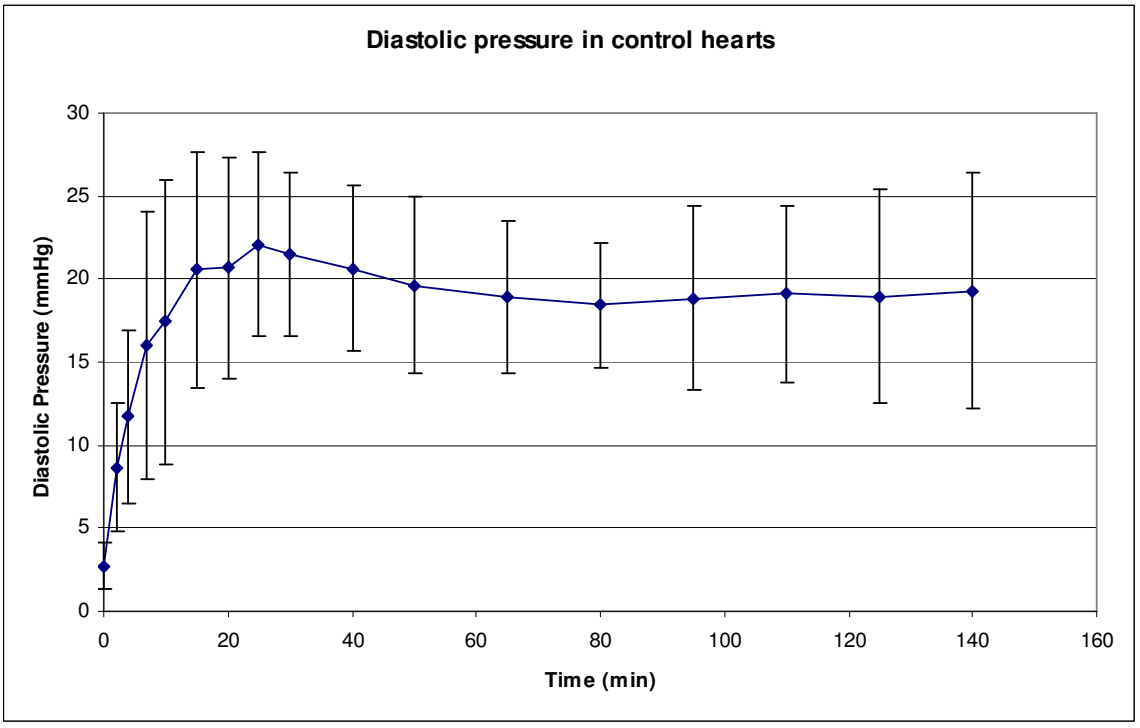

Figure 4-2: Measured LVEDP during 140 min of perfusion

The overall health of the heart was determined by monitoring the developed ventricular pressure. The developed pressure is defined as the difference between the systolic and diastolic pressure. The control hearts developed an average pressure of 77 mmHg during the initial period of perfusion. Thereafter, the average developed pressures started to drop gradually indicating that the hearts were slowly dying from the stress of being removed from the body and artificially perfused. At the end of the 140 minute perfusion period, the developed pressure had dropped from 77 to 30 mmHg. The temperature of the heart and the perfusate were measured at regular intervals using a thermistor based temperature probe (that was built and calibrated in Dr. Valvano's lab) and verified to be 37°C at all times during the experiment. The average developed

pressures in the control hearts are shown in Figure 4-3. The error bars represent the standard deviation of the measurements over three different hearts.

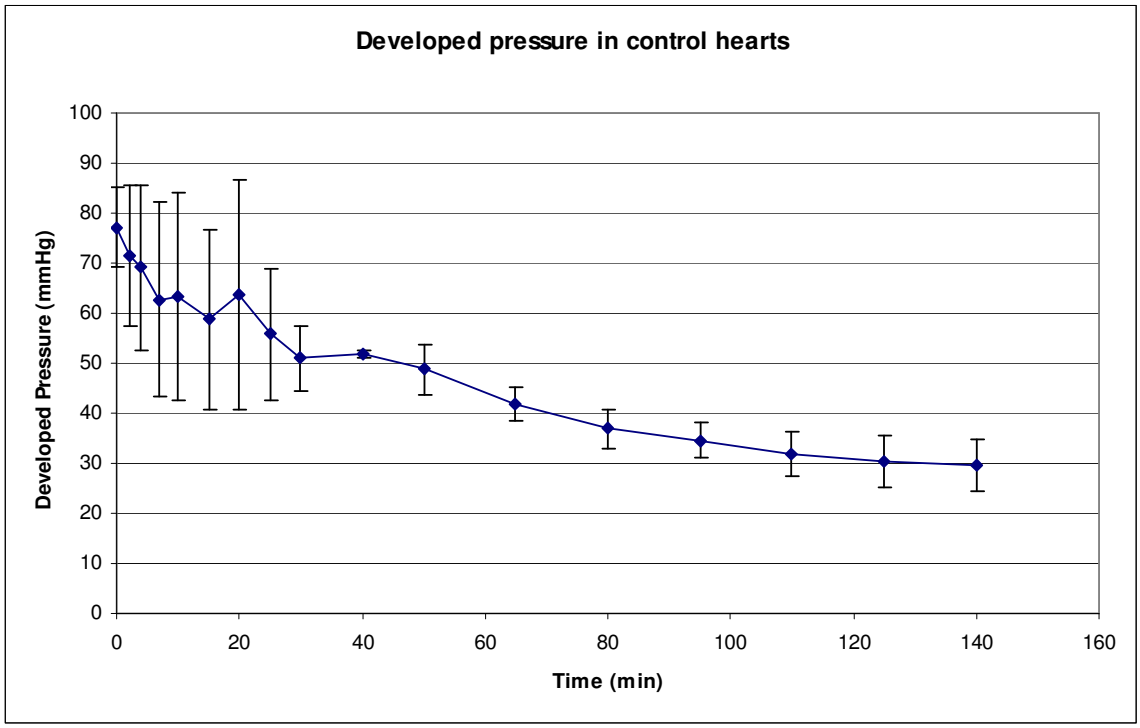

Figure 4-3: Developed pressure during 140 min of perfusion

The heart rate was calculated from the LV pressure measurements as an alternative indicator of the overall health of the heart. The control hearts start out with an average heart rate of 260 beats per minute and the rate gradually increases to over 300 beats per minute at the end of the perfusion duration. This instability in the heart rate is because *in vivo*, the atria and the SA node are not perfused by coronary vessels but by extracardiac vessels, which are severed when the heart is excised for perfusion [22]. Hence the affected tissue is dependent on superfusion by the coronary effluent flowing out of the right atrium for its oxygen, nutrients and temperature control. The variation of the heart rate with time is shown in Figure 4-4.

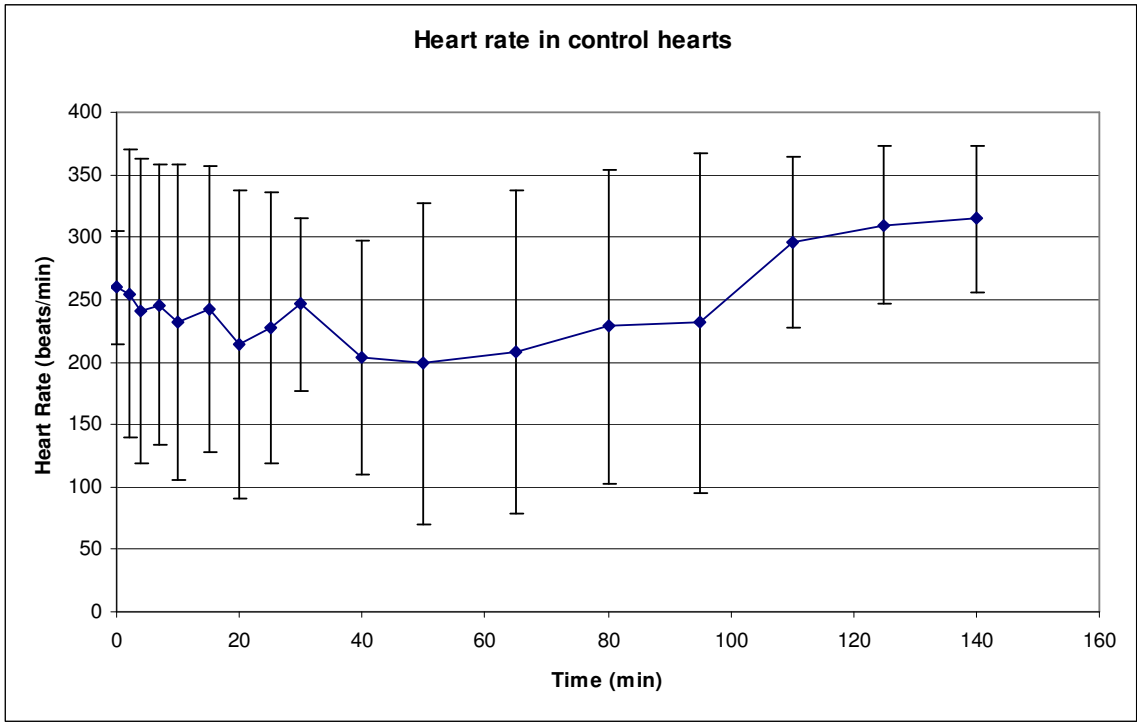

Figure 4-4: Average heart rate during 140 min of perfusion

The large standard deviations in the heart rate can be eliminated if the hearts are externally paced. However, external pacing would interfere with the electrical admittance measurements. On examining each of the hearts individually, it is seen that two of the three control hearts exhibit a marked increase in heart rate over the entire perfusion duration. The third heart exhibited an unusual drop in heart rate for 60 minutes during the perfusion interval, the cause of which is unknown. This is illustrated in Figure 4-5.

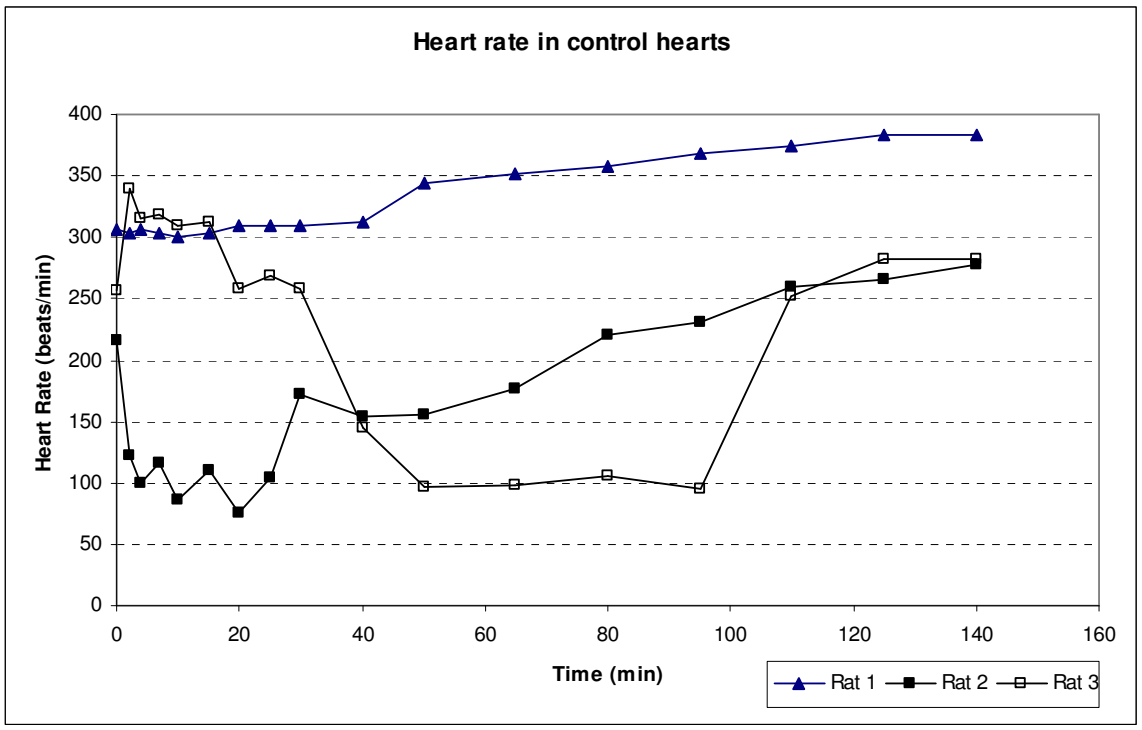

Figure 4-5: Heart rate of three control hearts during 140 min of perfusion

4.4.1 Relative Permittivity and Conductivity of Myocardium

The admittance magnitude |Y|, phase angle θ and left ventricular developed pressure were monitored in real time during the entire 140 minute perfusion duration. The values of |Y| and θ were used to calculate the relative permittivity (ε_r = K.C, after probe capacitance is removed) and conductivity (σ = K.G) of the myocardium based on the measured probe constant K (described by equations 6, 7 and 8 in section 3.4). These results are shown in Figures 4-6 and 4-7.

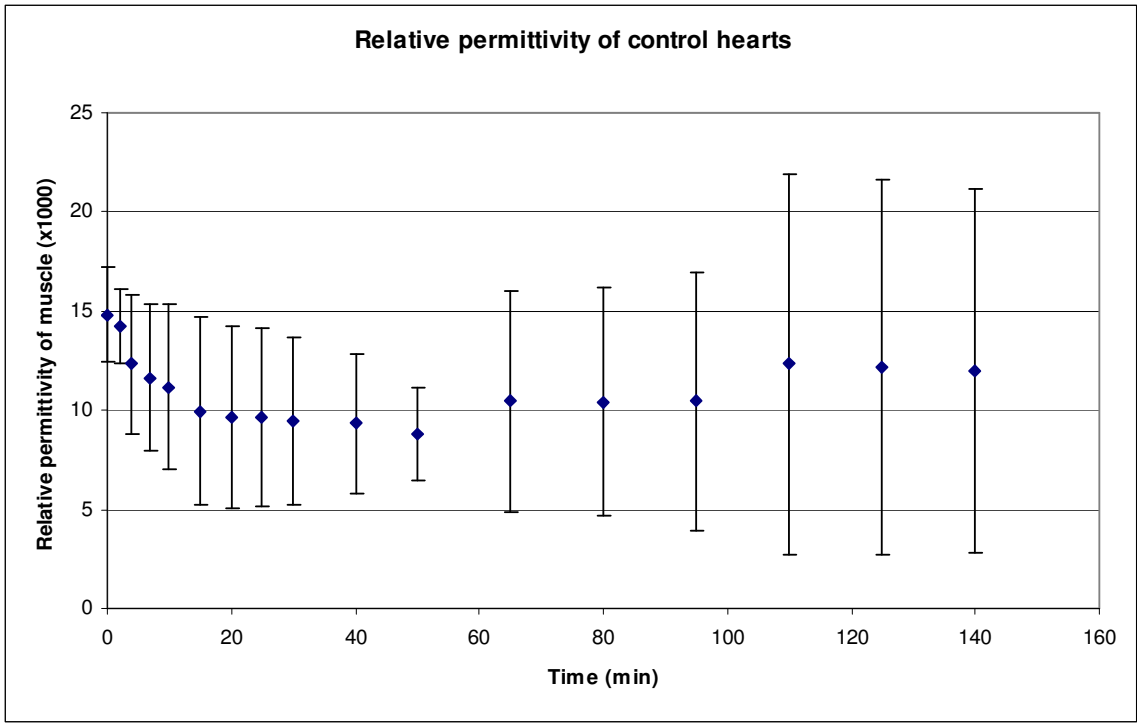

Figure 4-6: Relative permittivity of myocardium (at 30 kHz) in control hearts

The average permittivity starts out at 15,000 and decreases to 10,000 over the first 15 minutes after which it remains fairly constant over the next 80 minutes. The average permittivity then rises to 12,500 and remains at that value for the remainder of the perfusion duration.

The average value of myocardial conductivity is 0.75 S/m (7500 µS/cm) when the heart is initially perfused. The conductivity slowly rises to about 1.0 S/m (10000 µS/cm) during the first 50 minutes and remains at that value over the remainder of the perfusion duration. This trend along with the standard deviations is illustrated in Figure 4-7.

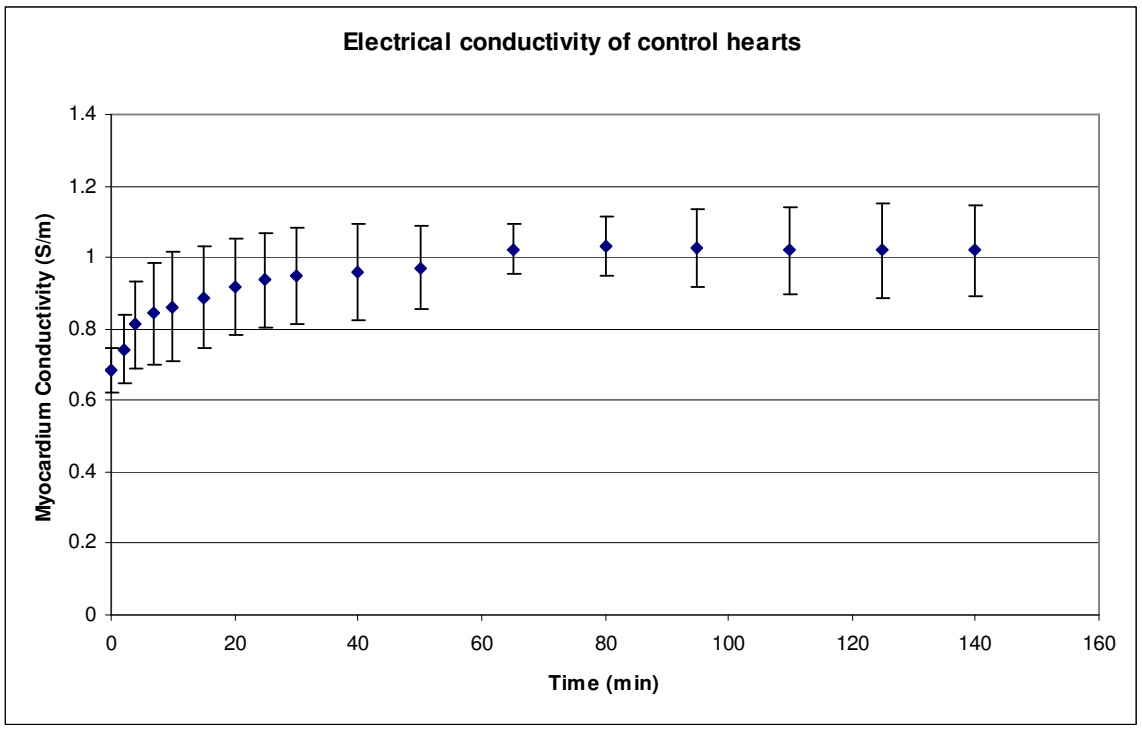

Figure 4-7: Electrical conductivity in control hearts

4.4.2 LDH Analysis of Coronary Effluent

Samples of the coronary effluent were collected during perfusion to determine the relative amount of LDH release. The samples were analyzed using a commercially available LDH cytotoxicity kit (Cayman Chemicals). The kit consisted of 100 µL each of NAD^+, Lactic Acid and INT (tetrazolium salt), 15 mL of assay buffer and one vial each of LDH standard and diaphorase. The diaphorase was reconstituted with 150 µL of the assay buffer. Following this, the reaction solution was prepared by mixing 100 µL each of NAD^+, Lactic Acid, INT and reconstituted diaphorase with 9.6 mL of assay buffer. When equal amounts of the reaction solution and the coronary effluent samples are mixed together, the following coupled two-step reaction occurs. In the first step, LDH catalyzes

the reduction of NAD^+ to NADH and H^+ by oxidation of lactate to pyruvate. In the second step of the reaction, diaphorase uses the newly formed NADH and H^+ to catalyze the reduction of INT to highly colored formazan, which absorbs light of wavelength 490-520 nm. The amount of formazan formed is proportional to the amount of LDH present in the coronary effluent. LDH standard solutions were prepared by adding 1.8 mL of the assay buffer to the vial containing the LDH standard. The concentration of this standard is 200 mU/mL. One unit (U) is the amount of enzyme that catalyzes the reaction of 1 µmol of substrate per minute. This standard solution can be diluted in differing amounts of the assay buffer to obtain desired concentrations of standard solutions. A spectrophotometer was used to determine the absorbance of the effluent samples and the standards at 490 nm. The LDH level in the sample was determined by comparing the absorbance of the sample with the absorbance of the known standards.

The results show that the highest concentration of LDH is present in the samples collected within the first 10 minutes. This is to be expected, since the process of removing the heart from the animal, cannulating the aorta and inserting the ventricular balloon all cause some tissue death. The subsequent samples contain decreasing amounts of this intracellular protein, as seen in Tables 4-1 and 4-2. The concentration of LDH in the sample is expressed in terms of µU/ml.

Rat #	Time (minutes)										
	0	5	10	15	20	25	30	35	40	45	50
1	400	138	325	342	396	413	200	129	0	83	46
2	2208	1308	1300	1317	1275	733	717	550	429	308	283
3	2367	5967	7267	4408	4033	3567	2925	2958	2329	1700	1829

Table 4-1: LDH concentration in control hearts (0 min to 50 min)

Rat #	Time (minutes)									
	59	64	74	84	94	104	114	124	134	144
1	33	8	13	13	8	17	4	0	0	4
2	258	238	217	175	133	163	192	171	150	400
3	1958	1642	1325	1117	908	775	642	542	442	425

Table 4-2: LDH concentration in control hearts (59 min to 144 min)

The LDH analysis of the control hearts shows that rat 1 exhibits the least amount of LDH release and should therefore be considered the best control. Rat 3 has a high and sustained LDH release for over 85 minutes and is the worst of the three controls. Rat 3 also exhibited an unusual drop in heart rate for 60 minutes during the perfusion interval, which was illustrated in Figure 4-5. The average change in LDH release from baseline (time = 0) for the three control hearts is shown in Figure 4-8.

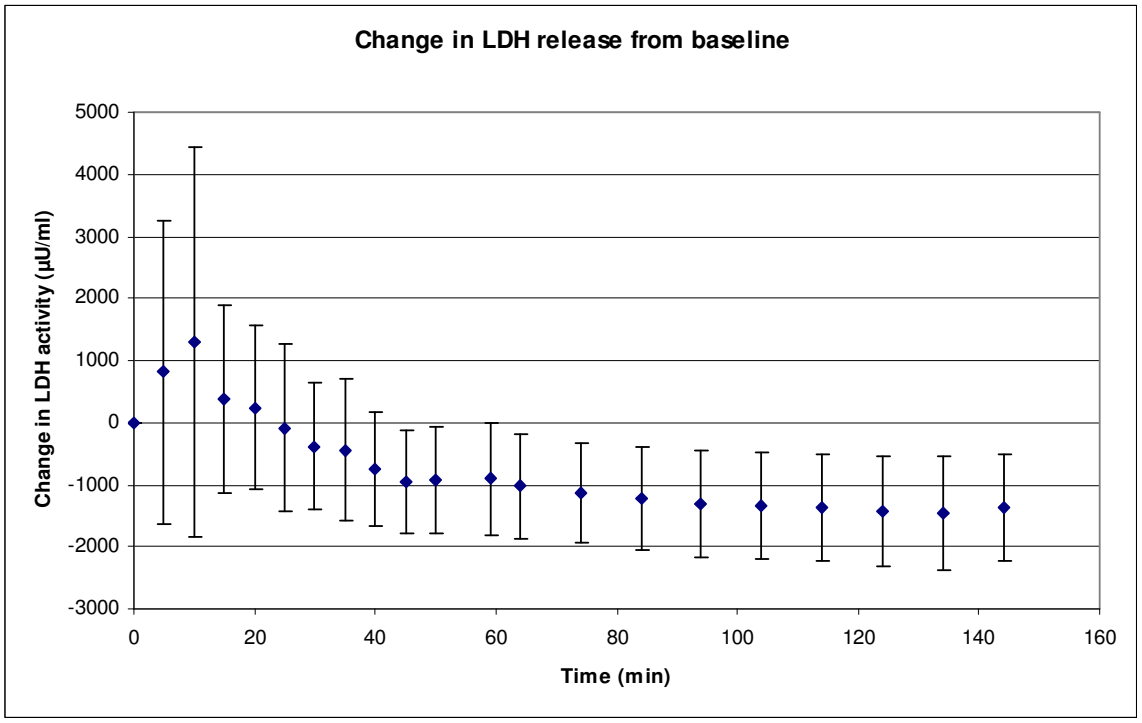

Figure 4-8: Average change in LDH release for the control hearts

4.5 MYOCARDIAL ISCHEMIA RESULTS

Eight adult male WKY rat hearts were subject to 90 min of global no-flow ischemia according to the protocol described in the earlier section. The measured admittance magnitude and phase angle were used to determine the relative permittivity and conductivity of the myocardial tissue during baseline, ischemia and reperfusion. LDH samples were collected during baseline and reperfusion to investigate the incidence of the cell plasma membrane damage due to ischemia.

The LV pressure was monitored in the same manner as in the control heart protocol, by inserting a balloon into the LV. The LVEDP dropped to zero within the first minute of occlusion and then gradually increased to about 5 mmHg over the next 30 min of occlusion. This was followed by a 10-15 min period where the LVEDP increased rapidly from 5 to 15 mmHg, indicating diastolic dysfunction as a result of calcium overload within the cells. The pressure then gradually drops by about 2 mmHg over the next 30 min. On reperfusion, the LVEDP increases to nearly 100 mmHg indicating total diastolic failure.

The measured LVEDP during baseline and the 90 min occlusion period is shown in Figure 4-9. The error bars represent the standard deviation of the measurements over seven different hearts.

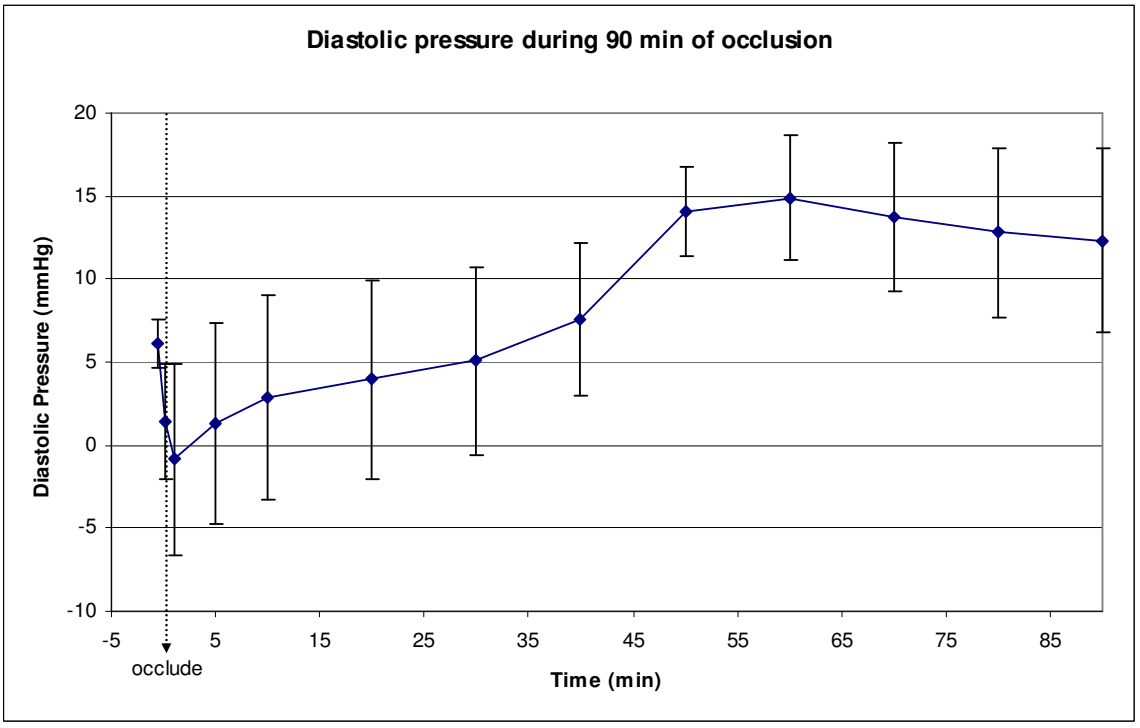

Figure 4-9: Measured LVEDP during 90 min of occlusion

4.5.1 Relative Permittivity and Conductivity of Myocardium

The admittance magnitude, phase angle and left ventricular developed pressure were monitored in real time during baseline, occlusion and reperfusion. The measured admittance magnitude and phase angles were then used to calculate the relative permittivity (ε_r) and conductivity (σ) of the myocardium. These results are summarized in Tables 4-3 and 4-4 for baseline and at specific times during occlusion. The occlusion was performed at time = 0 min and all other times on the table are relative to the occlusion time.

Rat #	Time (minutes)						
	-0.6	0.1	1.1	5	10	20	30
1	13587	12555	10183	10498	9396	8344	8595
2	12263	12840	13329	12950	12686	12095	12102
3	9670	9616	11461	11710	11304	10943	11491
4	3942	4047	3423	4528	4849	5240	6620
5	17317	17219	14869	13621	13169	12333	11627
6	7818	6470	6068	9204	8943	8450	8871
7	11633	11374	11295	9746	8751	7914	7498
Mean	10890	10589	10090	10322	9871	9331	9543
Std. Dev	4286	4363	4027	3025	2841	2574	2189

Rat #	Time (minutes)						
	40	50	60	70	80	90	
1	10804	13003	14229	14285	13606	13061	
2	11557	13838	15543	13059	11400	15409	
3	14690	13929	12393	11961	12347	12103	
4	8885	10622	12974	14009	14164	13908	
5	10847	11619	12445	15300	16925	16468	
6	9596	11361	13182	13870	13812	13634	
7	9230	12940	12765	12398	12145	11599	
Mean	10801	12473	13362	13555	13486	13740	
Std. Dev	1970	1283	1142	1155	1819	1732	

Table 4-3: Relative permittivity of myocardium during baseline and 90 min of occlusion

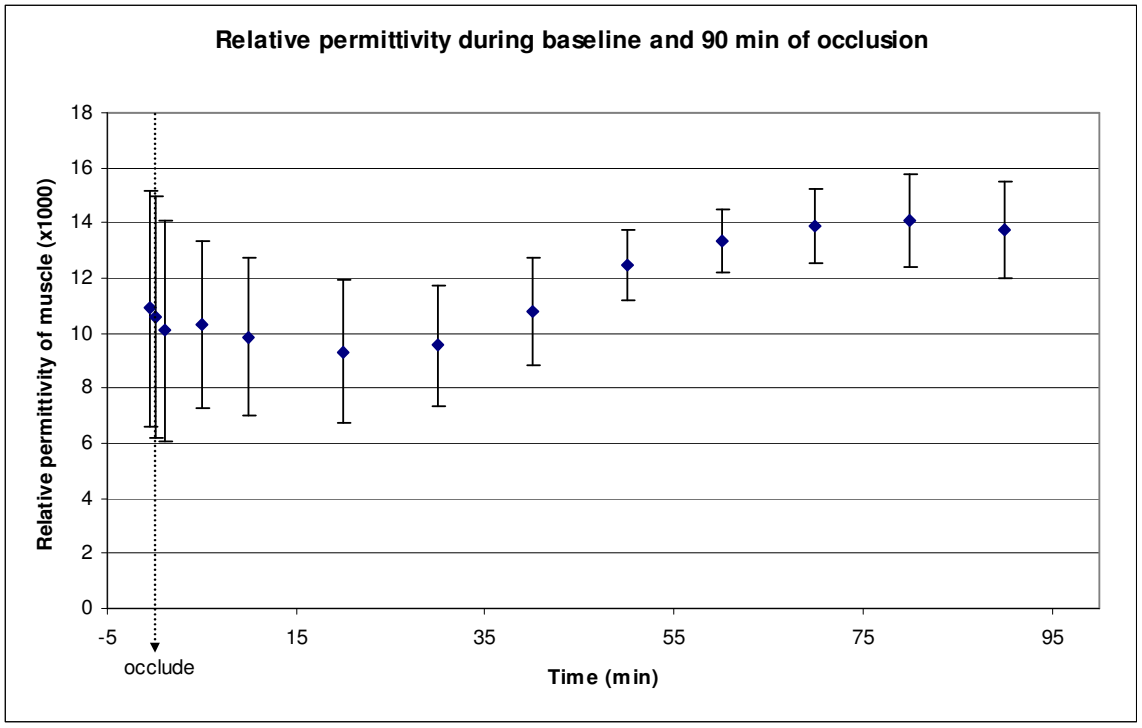

Figure 4-10: Relative permittivity of myocardium during baseline and 90 min of occlusion

It is seen that the average ε_r is about 11,000 during baseline. After occlusion, ε_r drops gradually by about 15% for the first 20 minutes. This is followed by a 10 minute period where ε_r gradually increases by about 2% following which there is a 30 minute period where ε_r increases rapidly by nearly 40% to a value of 13,400. After this, the relative permittivity remains fairly constant until reperfusion. This trend along with the standard deviations is illustrated in Figure 4-10.

Rat #	Time (minutes)						
	-0.6	0.1	1.1	5	10	20	30
1	0.488	0.448	0.490	0.447	0.264	0.231	0.221
2	0.558	0.520	0.438	0.372	0.344	0.308	0.272
3	0.552	0.491	0.366	0.292	0.269	0.246	0.223
4	0.711	0.667	0.623	0.509	0.470	0.451	0.441
5	0.394	0.404	0.396	0.396	0.379	0.382	0.382
6	0.608	0.656	0.222	0.307	0.293	0.291	0.289
7	0.348	0.435	0.256	0.190	0.173	0.159	0.153
Mean	0.523	0.517	0.399	0.359	0.313	0.296	0.283
Std. Dev	0.125	0.105	0.137	0.106	0.095	0.097	0.099

Rat #	Time (minutes)						
	40	50	60	70	80	90	
1	0.217	0.222	0.227	0.233	0.228	0.224	
2	0.246	0.238	0.235	0.265	0.313	0.235	
3	0.194	0.198	0.228	0.271	0.256	0.245	
4	0.231	0.228	0.284	0.312	0.321	0.323	
5	0.367	0.275	0.288	0.423	0.479	0.531	
6	0.240	0.224	0.226	0.227	0.228	0.232	
7	0.151	0.190	0.205	0.213	0.213	0.205	
Mean	0.235	0.225	0.242	0.278	0.291	0.285	
Std. Dev	0.067	0.028	0.032	0.072	0.093	0.115	

Table 4-4: Electrical conductivity of myocardium during baseline and 90 min of occlusion

The average value of myocardial conductivity is 0.52 S/m during baseline. The conductivity drops rapidly to 0.4 S/m during the first minute of occlusion and then reduces further to 0.3 S/m over the next 10 minutes. Following this, the conductivity drop is more gradual and falls to 0.23 S/m over the next 40 minutes and then slowly increases to 0.29 S/m during the remainder of the occlusion period. This trend along with the standard deviations is illustrated in Figure 4-11.

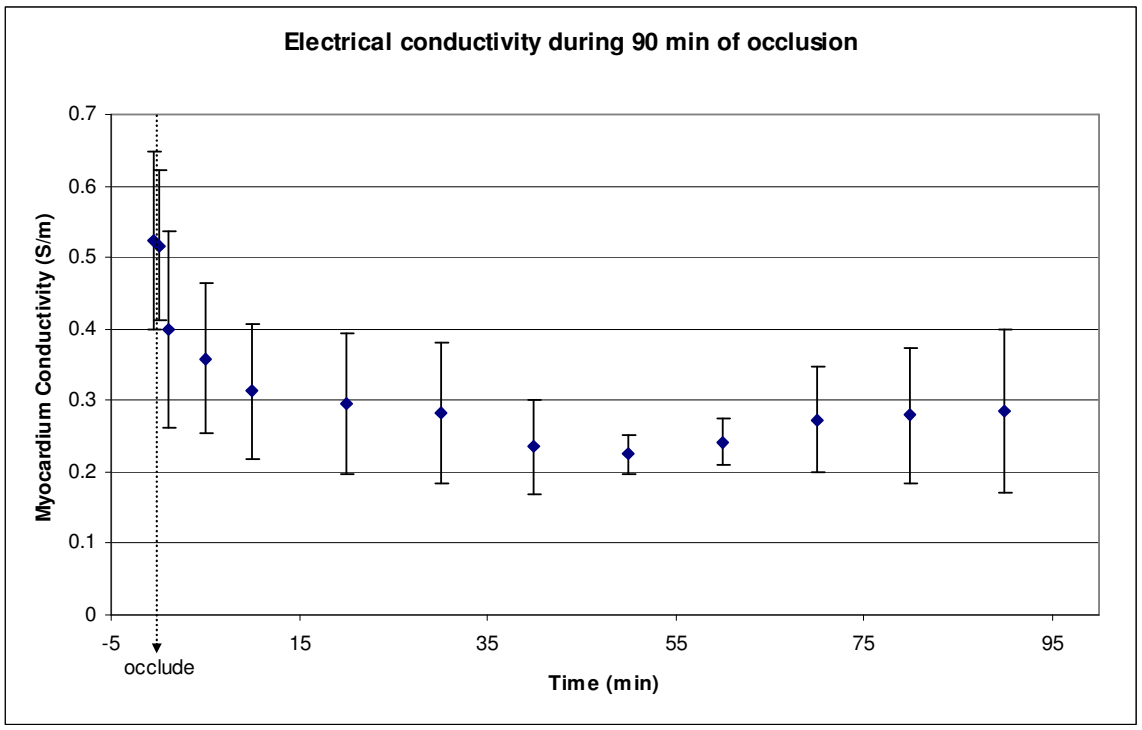

Figure 4-11: Electrical conductivity of myocardium during baseline and 90 min of occlusion

The reduction in myocardial conductivity during occlusion is due to the absence of the high conductivity perfusate in the myocardium. On reperfusion, the conductivity increases almost instantaneously to 0.7 S/m and remains elevated during the entire 20 min reperfusion period. This elevated conductivity value was seen in the three control hearts as well and was shown in Figure 4-7. The conductivity of the perfusate was measured to be 1.2 S/m.

4.5.2 LDH Analysis of Coronary Effluent

Samples of the coronary effluent were collected during baseline and reperfusion to determine the amount of LDH release. The samples were analyzed as described in section 4.4.2. The results show that the highest concentration of LDH is present in the sample collected immediately after reperfusion. This is to be expected, since almost all the LDH released during the 90 min occlusion period remains in the extracellular space and will be washed out all at once when reperfusion begins. The subsequent samples contain decreasing amounts of this intracellular protein, as is evident from Table 4-5. The concentration of LDH in the sample is expressed in terms of μU/ml. One unit (U) is the amount of enzyme that catalyzes the reaction of 1 μmol of substrate per minute.

Rat #	Sample #				
	1	2	3	4	5
1	4300	1633	21600	6033	4983
2	550	23733	12417	8767	5367
3	2483	22967	5167	2400	1250
4	2017	26017	10767	7017	5983
5	2500	28950	10150	6717	6233
6	6783	39317	16300	12167	10250
7	12717	50800	17733	16100	14483

Table 4-5: LDH concentration in hearts subject to 90 min of ischemia

Sample 1 is taken at baseline and sample 2 is taken immediately upon reperfusion. Samples 3, 4 and 5 are taken after subsequent 5 min intervals. The average increase in LDH release from baseline for all seven hearts is plotted in Figure 4-12. The error bars represent the standard deviation of the measurements.

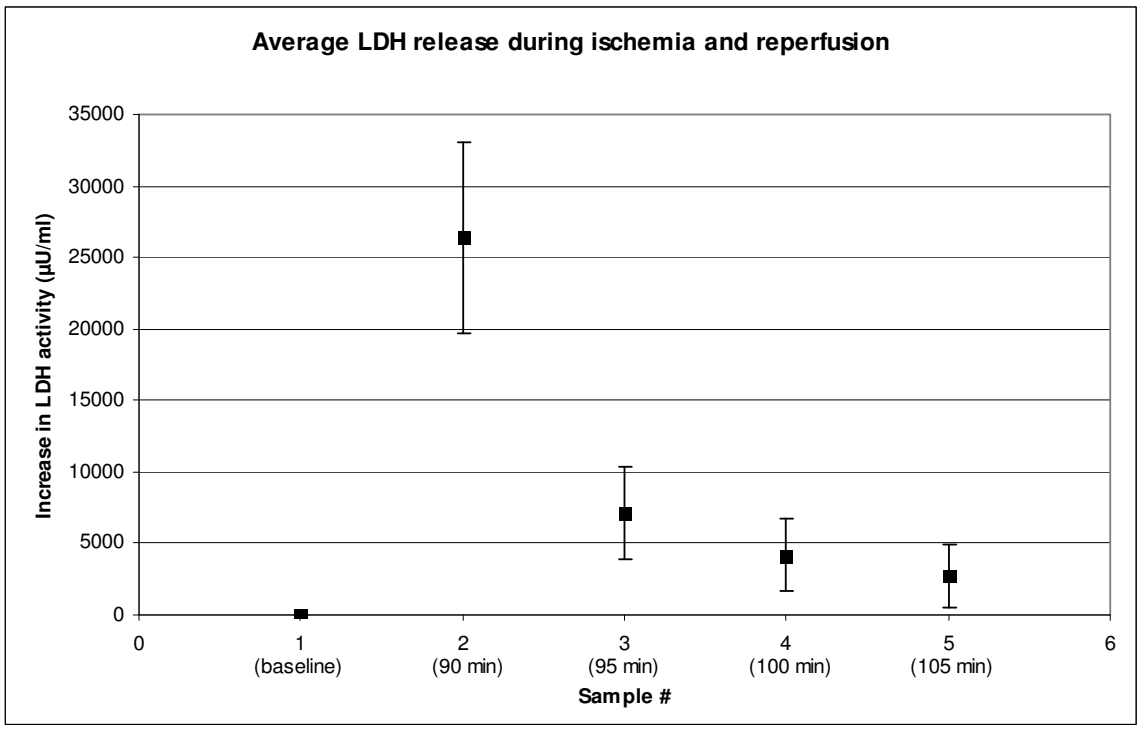

Figure 4-12: Average increase in LDH release from baseline after 90 min occlusion

4.6 MYOCARDIAL STUNNING RESULTS

Eight adult male WKY rat hearts were subject to 15 min of global no-flow ischemia followed by 95 min of reperfusion according to the protocol described in the earlier section. The measured admittance magnitude and phase angle were used to determine the relative permittivity and conductivity of the myocardial tissue during baseline, ischemia and reperfusion. LDH samples were collected during baseline and reperfusion to investigate the incidence of the cell plasma membrane damage due to ischemia. Out of the eight rat hearts subject to this protocol, two hearts did not recover from the occlusion and did not develop measurable ventricular pressures over the entire reperfusion period. Data from these two hearts were excluded from the data analysis.

The LV pressure was monitored in the same manner as in the control hearts protocol, by inserting a balloon into the LV. The LVEDP dropped rapidly within the first minute of occlusion and remained at -10 mmHg over the entire 15 min occlusion period. On reperfusion, the LVEDP increased to 35 mmHg within a minute and then gradually dropped to 16 mmHg over the entire 95 min reperfusion period. This is illustrated in Figure 4-13. The error bars represent the standard deviation of the measurements over six different hearts.

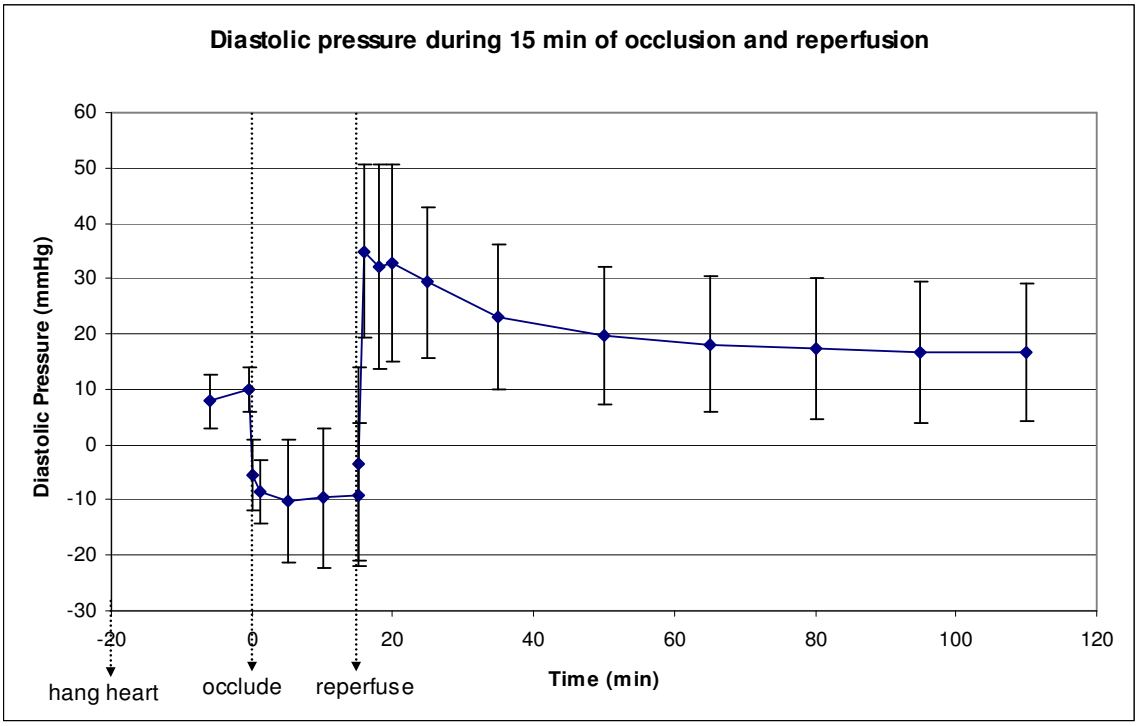

Figure 4-13: Measured LVEDP during 15 min of occlusion and 95 min of reperfusion

On reperfusion, six of the eight hearts recovered and were able to achieve developed pressures of 45 mmHg after 20 minutes of reperfusion. Thereafter, the developed pressures started to drop gradually indicating that the hearts were slowly dying. At the end of the 95 min reperfusion period, the developed pressure had dropped

to 31 mmHg. This is illustrated in Figure 4-14. The error bars represent the standard deviation of the measurements over six different hearts.

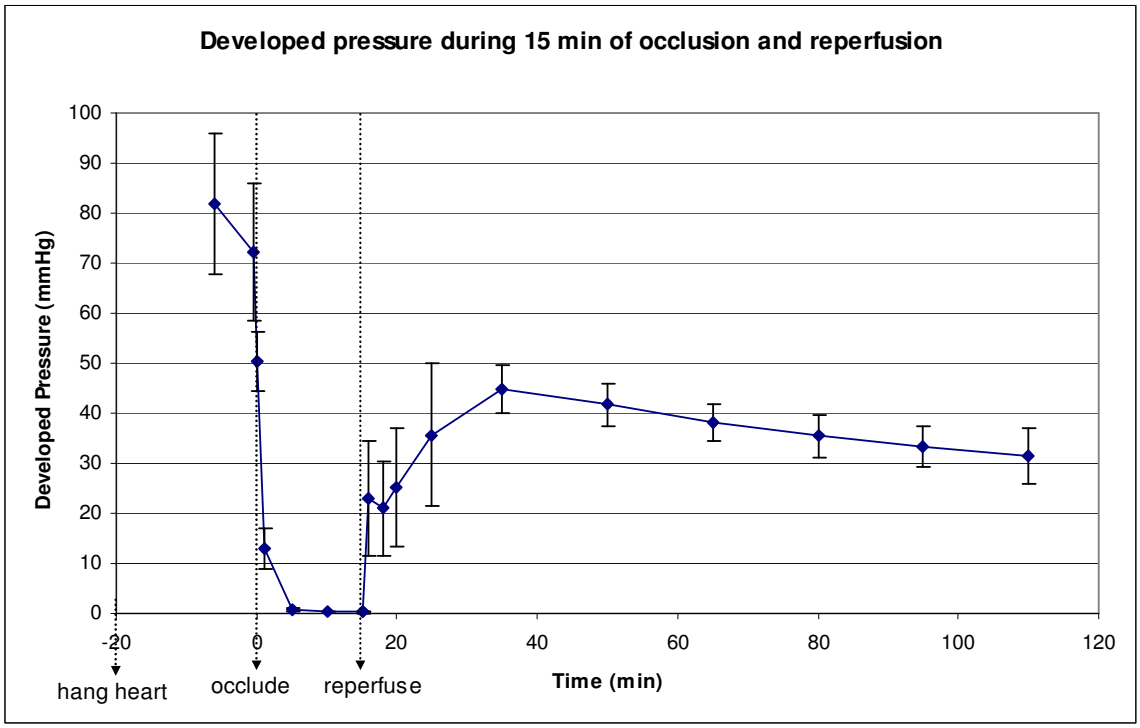

Figure 4-14: Developed pressure during 15 min of occlusion and 95 min of reperfusion

The heart rate was calculated from the LV pressure measurements to further ensure that the hearts had recovered from ischemia during the reperfusion period. It is seen that the heart stops beating completely during occlusion. Although there is a large standard deviation in the measured heart rate within the first 10 minutes of reperfusion, the rate stabilizes to about 275 beats per minute after 35 minutes of reperfusion. This is shown in Figure 4-15.

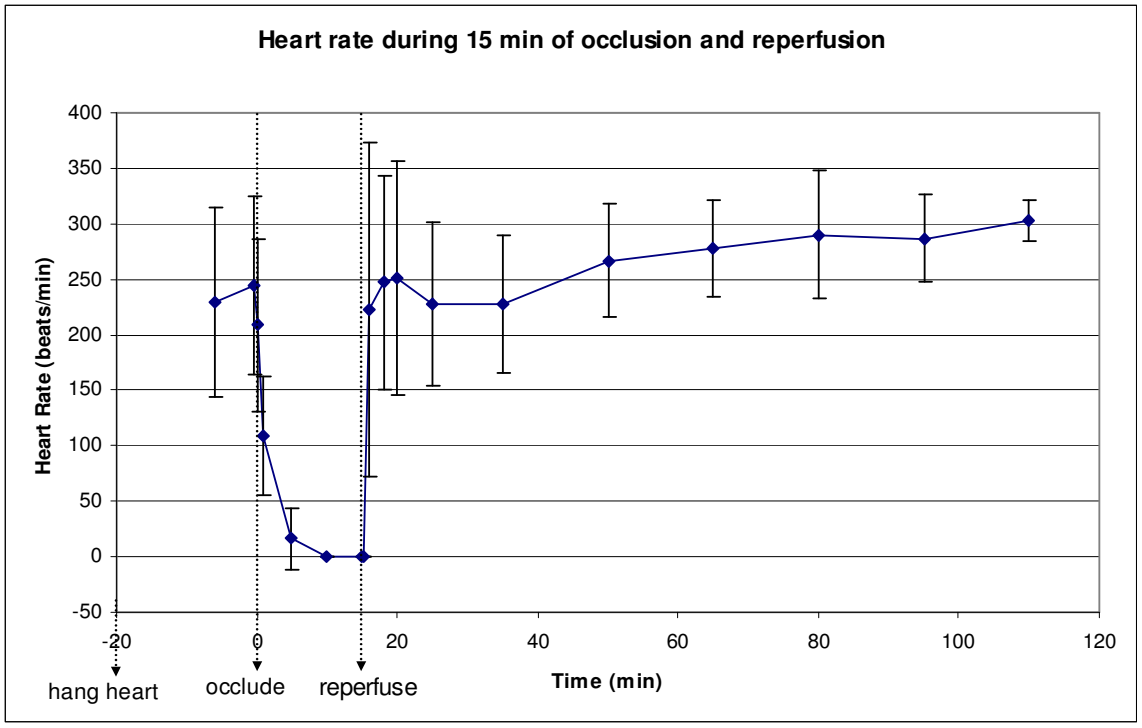

Figure 4-15: Heart rate during 15 min of occlusion and 95 min of reperfusion

4.6.1 Confirmation of Stunning

As previously described, stunning is the mechanical dysfunction that persists after reperfusion despite the absence of irreversible damage and despite restoration of normal coronary flow. The developed ventricular pressures in these six hearts were compared with the pressures developed in the controls to verify that true stunning had occurred. The left ventricular end diastolic pressures (LVEDP) of the stunned hearts were also compared with the controls. These are shown in Figures 4-16 and 4-17, which confirm that the hearts subject to 15 minutes of occlusion eventually recover and attain diastolic and developed pressures identical to the controls. It is also evident from these Figures that the stunned hearts recover within 35 min of reperfusion.

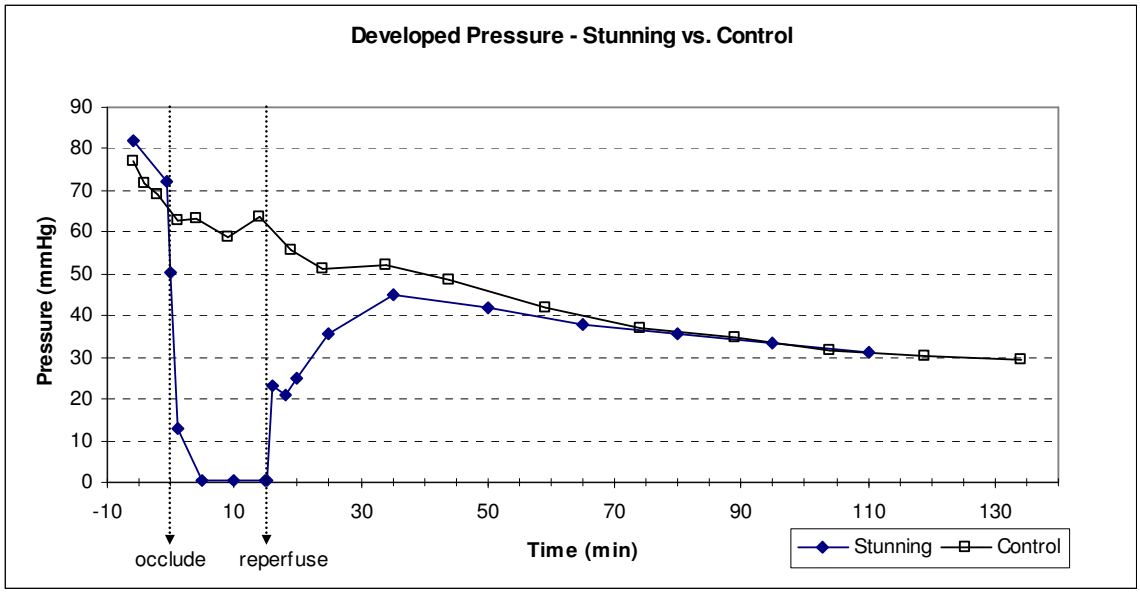

Figure 4-16: Developed LV pressure in stunned vs. control hearts

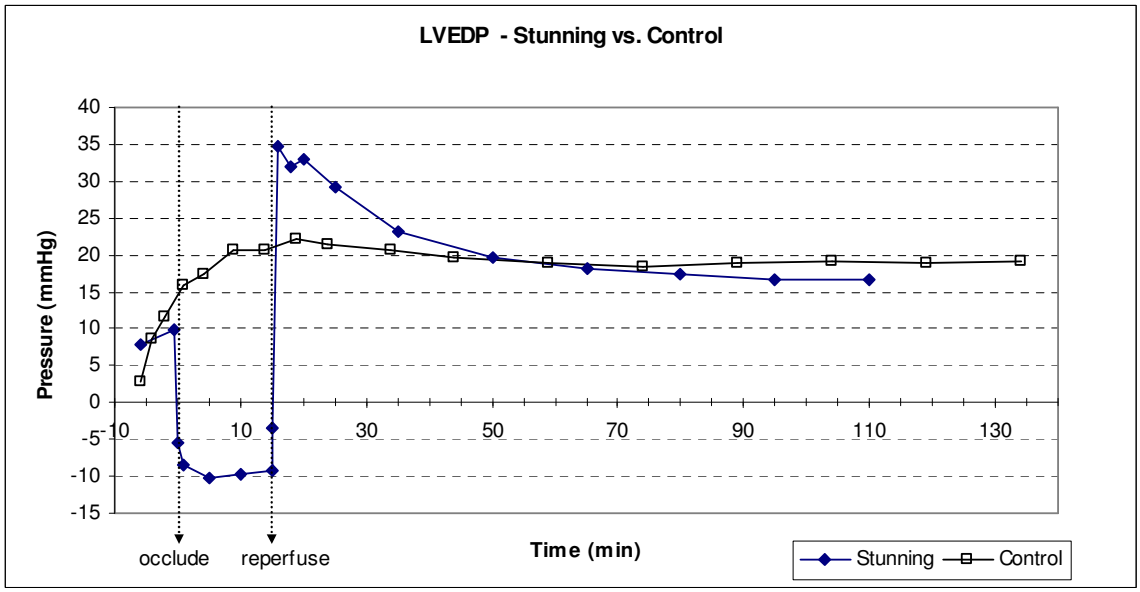

Figure 4-17: LVEDP in stunned vs. control hearts

4.6.2 Relative Permittivity and Conductivity of Myocardium

As in the ischemia protocol, the admittance magnitude, phase angle and left ventricular developed pressure were monitored in real time during baseline, occlusion and reperfusion and used to calculate the relative permittivity (ε_r) and conductivity (σ) of the myocardium. These results are shown in Figures 4-18, 4-19 and 4-20 for baseline and at specific times during occlusion and reperfusion. The occlusion was performed at time = 0 min and all other times on the graph are relative to the occlusion time.

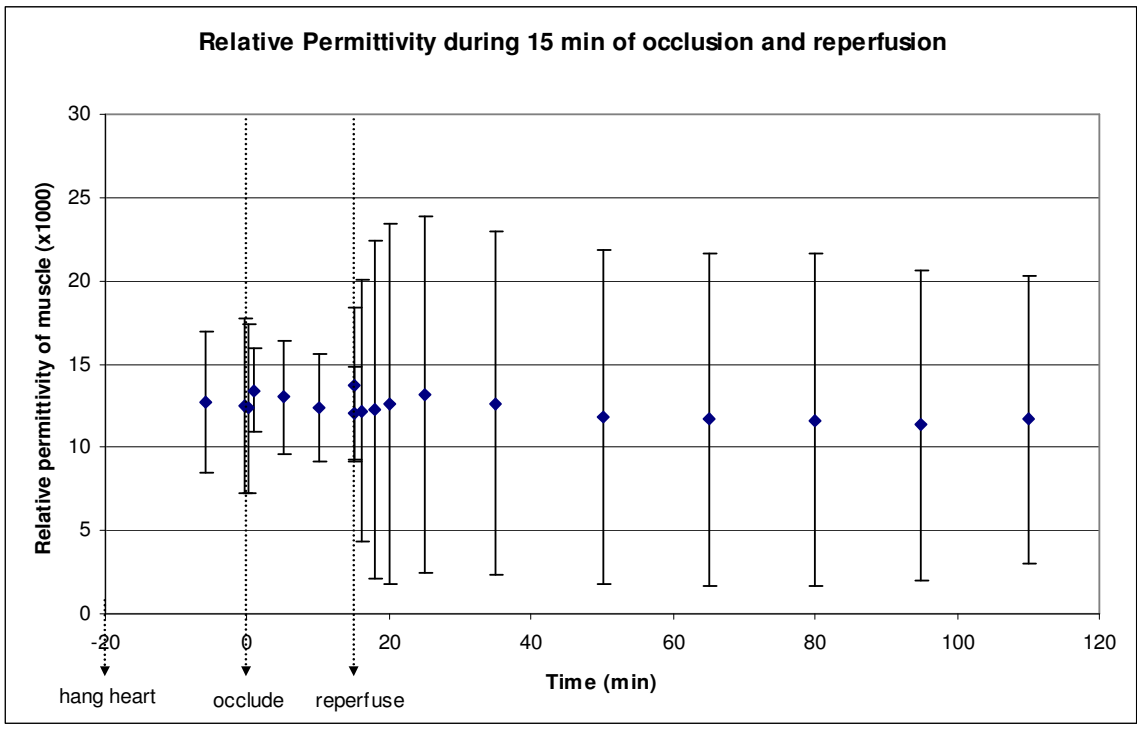

Figure 4-18: Relative permittivity of myocardium during baseline, 15 min of occlusion and 95 min of reperfusion

The error bars represent the standard deviation of the measurements over six different hearts. The permittivity data do not show any statistically significant changes during baseline, occlusion and subsequent reperfusion. The normalized permittivity

values do not show any statistically significant trends either (Figure 4-19). This indicates that the relative permittivity of the myocardium may not be a good indicator of myocardial stunning, and is more useful as an indicator of ischemia and diastolic dysfunction.

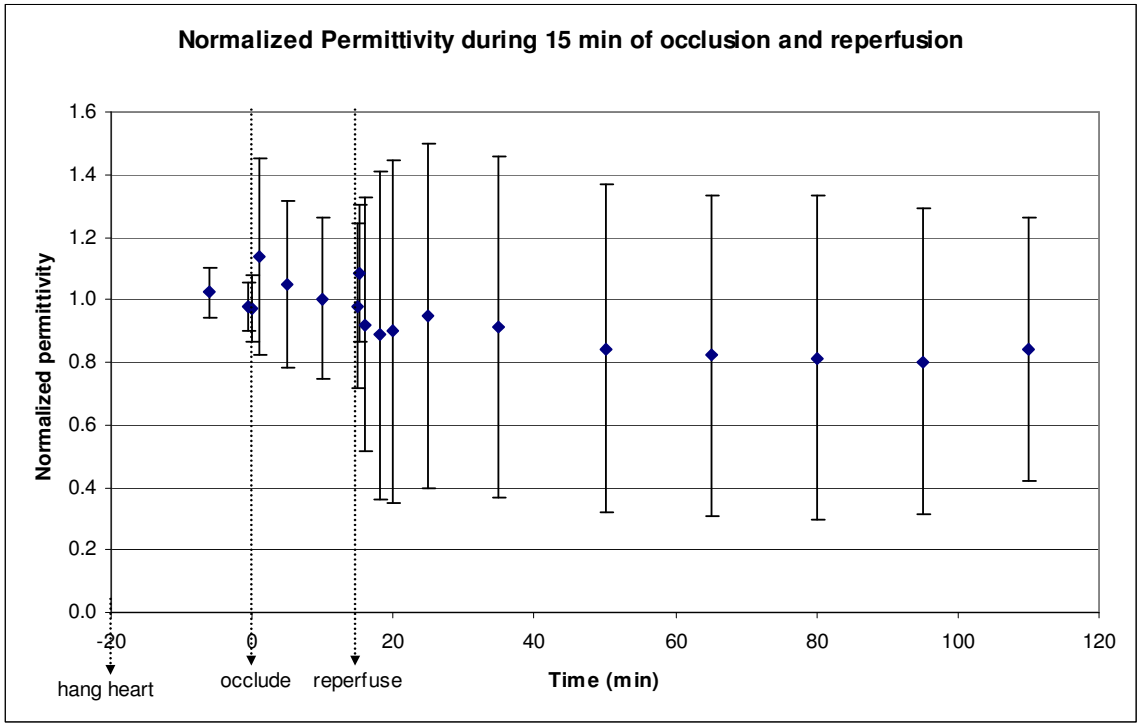

Figure 4-19: Normalized permittivity of myocardium during baseline, 15 min of occlusion and 95 min of reperfusion

The average value of myocardial conductivity is 0.67 S/m during baseline. The conductivity drops rapidly to 0.54 S/m during the first minute of occlusion and then reduces further to 0.33 S/m over the next 14 minutes. On reperfusion, the conductivity increases almost instantaneously to 0.84 S/m and remains elevated during the entire 95 min reperfusion period. This trend along with the standard deviations is illustrated in Figure 4-20.

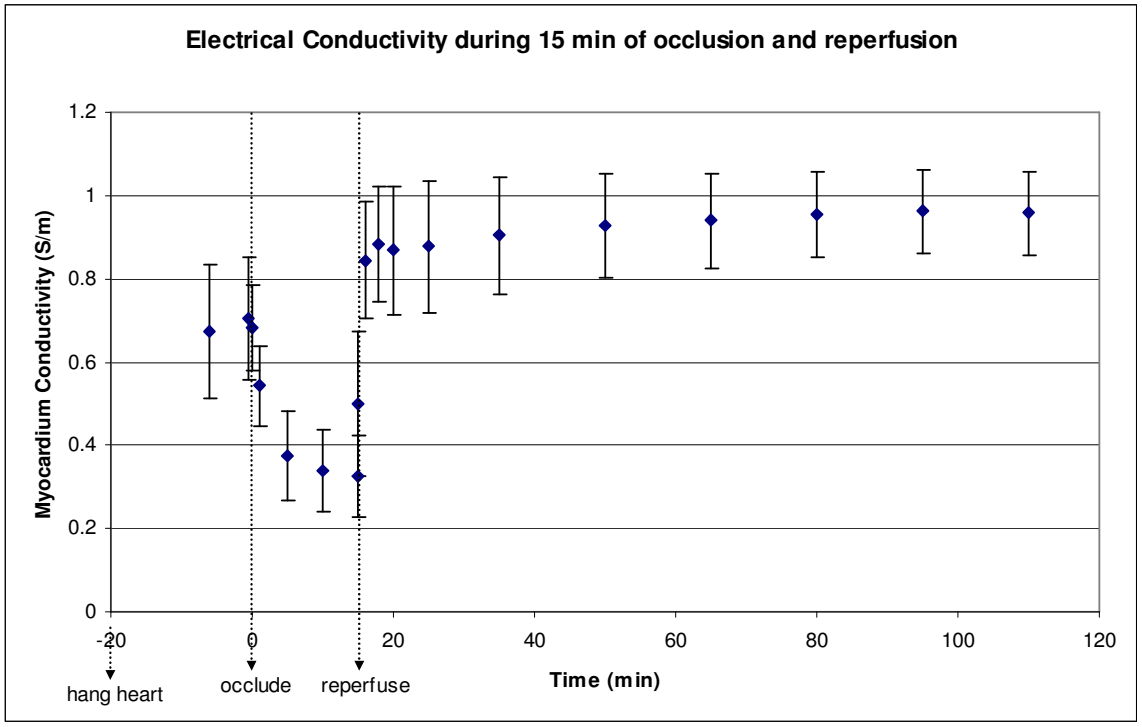

Figure 4-20: Electrical conductivity of myocardium during baseline, 15 min of occlusion and 95 min of reperfusion

The reduction in myocardial conductivity during occlusion is due to the absence of the high conductivity perfusate in the myocardium. This trend is similar to that observed in hearts subject to the 90 min ischemia protocol. On reperfusion, the conductivity increases almost instantaneously and reaches a maximum value of 0.96 S/m during the reperfusion period. This elevated conductivity value was seen in the three control hearts as well, and has been shown in Figure 4-7.

4.6.3 LDH analysis of Coronary Effluent

Samples of the coronary effluent were collected during baseline and reperfusion to determine the amount of LDH release. Two samples were collected at baseline; one immediately after the heart was hung on the system and instrumented and the second one after ten minutes of stabilization. The heart was then subjected to 15 min of global no-flow ischemia, followed by 95 min of reperfusion. The third sample was collected immediately upon reperfusion and three more samples were collected at 3 min intervals. Seven subsequent samples were collected at 5 min intervals and the last five samples were collected at 10 min intervals. The samples were analyzed using the Cayman LDH cytotoxicity kit. The results indicate the highest concentration of LDH in the sample collected immediately after reperfusion, since almost all the LDH released during the 15 min occlusion period remains in the extracellular space and will be washed out all at once when reperfusion begins. This LDH concentration is lower than that obtained after 90 min of occlusion, which implies that there is substantially less changes in cell membrane permeability for shorter occlusion periods. The subsequent samples contain reducing amounts of this intracellular protein, as is evident from Tables 4-6 and 4-7.

Rat #	Time (min)								
	-10	-1	15	18	21	24	29	34	39
1	533	770	12870	2708	2333	1183	795	395	270
2	1445	908	26565	2745	1083	933	1008	445	345
3	1118	883	15675	1703	893	403	538	363	63
4	558	783	10895	1508	1320	1045	1126	1208	908
5	420	445	7070	695	658	2045	1501	958	801
6	1070	1008	4420	3083	5108	5520	4453	3387	2320
7	1683	1758	9820	3858	2533	1458	1224	991	758
8	942	525	4550	2450	2142	1683	1125	567	500

Table 4-6: LDH concentration in hearts subject to 15 min of ischemia (baseline and partial reperfusion)

Rat #	Time (min)								
	44	49	54	59	69	79	89	99	109
1	201	133	66	0	0	0	0	0	0
2	133	183	20	8	45	0	0	0	0
3	113	0	13	53	3	0	0	0	0
4	608	641	674	708	683	658	633	608	583
5	645	595	545	495	445	391	337	283	229
6	2337	2353	2370	2245	2120	1995	1799	1603	1408
7	658	558	458	424	391	358	374	391	408
8	433	358	283	208	133	100	67	33	0

Table 4-7: LDH concentration in hearts subject to 15 min of ischemia (remainder of reperfusion)

The concentration of LDH in the sample is expressed in terms of μU/ml. One unit (U) is the amount of enzyme that catalyzes the reaction of 1 μmol of substrate per minute. The times represented in Tables 4-6 and 4-7 correspond to the time following the start of occlusion. Thus, the occlusion is started at time = 0 min and reperfusion begins at time = 15 min. The two baseline values are represented by time = -10 min and -1 min.

Rat #4 and #5 did not recover from the 15 min occlusion and were excluded from the analysis. An abnormally high level of LDH release was observed in rat 2 immediately upon reperfusion, indicating a high degree of cell necrosis. The average increase in LDH release from baseline for the remaining five hearts is plotted in Figure 4-21. The error bars represent the standard deviation of the measurements over five different hearts.

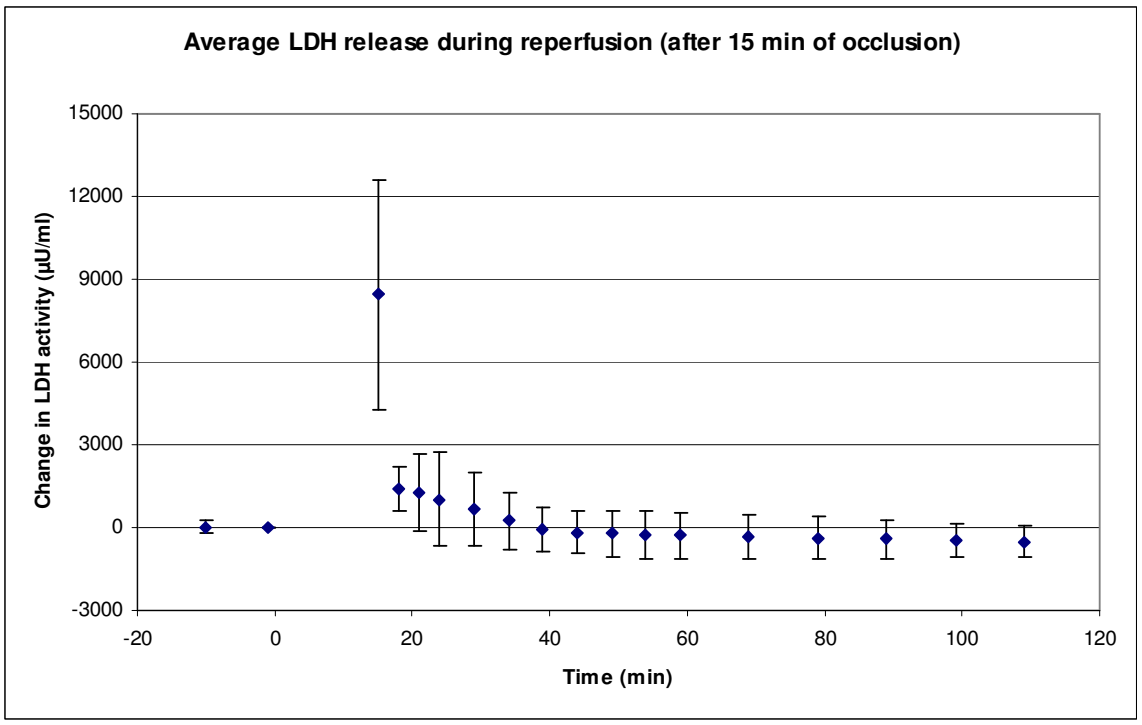

Figure 4-21: Average change in LDH release from baseline after 15 min occlusion

All the LDH release occurred within 20 minutes reperfusion, indicating that cell necrosis only occurred during the occlusion period and no further cell necrosis occurs during the recovery period.

4.7 CONCLUSIONS

4.7.1 Myocardial Ischemia

The myocardial ischemia studies confirm the occurrence of diastolic dysfunction during a prolonged period of no-flow ischemia. This is characterized by a rapid increase in diastolic pressure within the left ventricle and occurs about 30 minutes after the onset of ischemia. An interesting observation here is the behavior of the myocardial permittivity during this period. The permittivity reduces during the first 20 min following occlusion and then starts to increase. This inflection point is observed prior to the onset of diastolic dysfunction and precedes it by 15 minutes. This is illustrated in Figure 4-22.

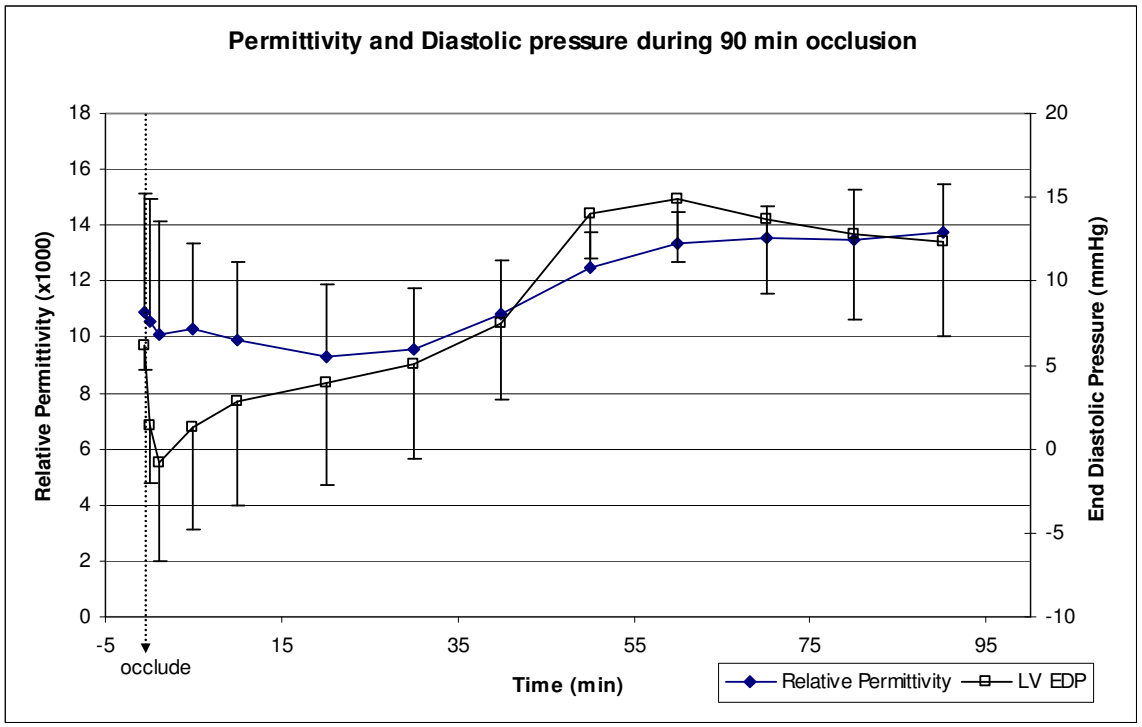

Figure 4-22: Comparison between myocardial permittivity and diastolic pressure during baseline and 90 min of occlusion

Intracellular calcium levels have been reported to be elevated during ischemia [32, 36, 53] and remain elevated until reperfusion. The elevated calcium levels are due to the reduced rate of calcium uptake by the sarcoplasmic reticulum. This excess calcium binds Troponin I to actin in thin myofilaments to hold the troponin-tropomyosin complex in place. This prevents ventricular relaxation and results in stiffening of the ventricular muscle. As a result, diastolic pressure increases leading to diastolic dysfunction. Diastolic dysfunction is hence caused by calcium overload in the cytoplasm due to a breakdown of the functioning of the sarcoplasmic reticulum. This alteration of the intracellular electrolyte composition increases the trans-membrane charge distribution across the cell membrane and causes a sudden increase in permittivity. The myocardial conductivity, however, exhibits no such trends and exhibits no correlation with diastolic dysfunction.

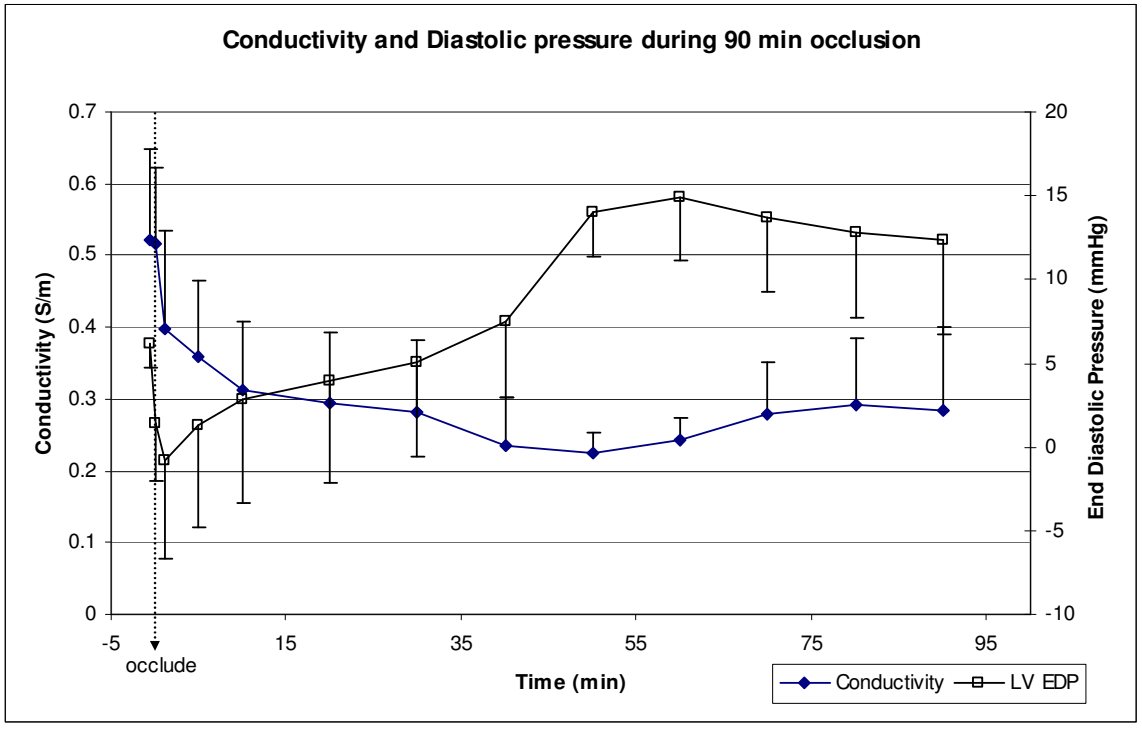

Figure 4-23: Comparison between myocardial conductivity and diastolic pressure during baseline and 90 min of occlusion

4.7.2 Myocardial Stunning

Eight rats were subject to the myocardial stunning protocol. Only six of the eight hearts recovered on reperfusion and these hearts were analyzed for trends in permittivity and conductivity during occlusion and reperfusion. The permittivity results did not show any statistically significant trends during baseline, occlusion and subsequent reperfusion. Out of these six hearts, one of the hearts exhibited abnormally high LDH levels and another heart had permittivity values gradually reduce to zero on reperfusion. These two hearts were also excluded from the analysis and the average relative permittivity of the four remaining hearts is plotted in Figure 4-24.

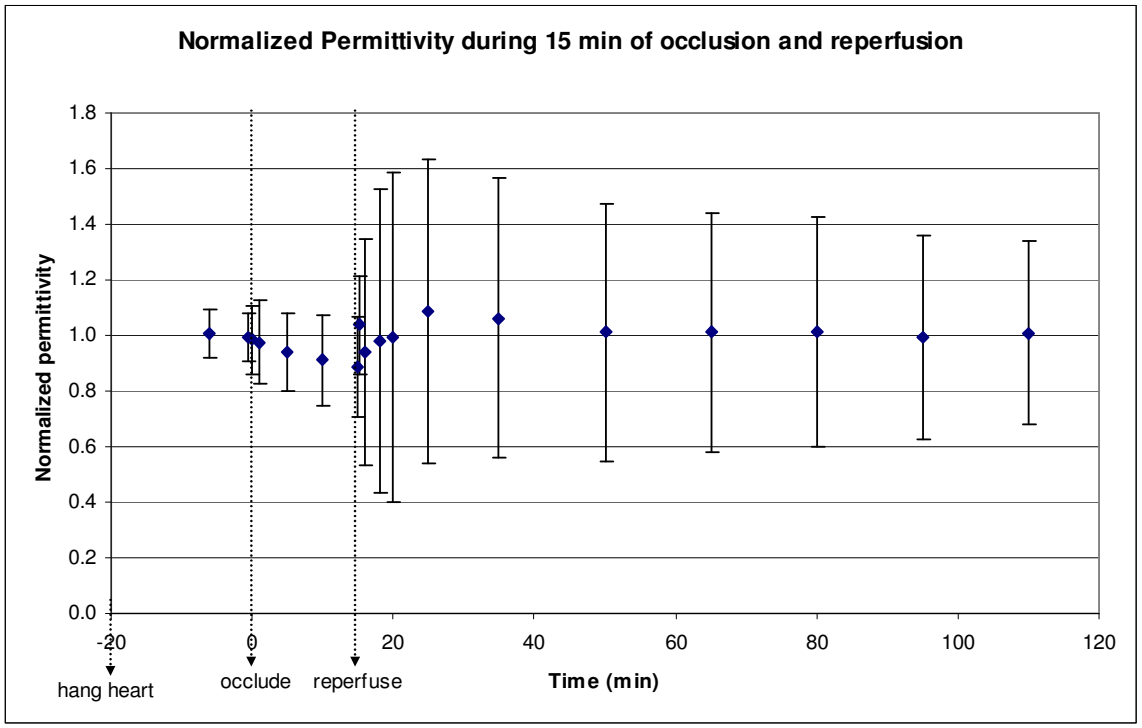

Figure 4-24: Normalized permittivity of myocardium during baseline, 15 min of occlusion and 95 min of reperfusion (n = 4)

The normalized permittivity results indicate a gradual decrease in permittivity from baseline during the 15 min occlusion period. The elevated LDH activity that has been observed during this period indicates increasing plasma membrane permeability due to necrosis. As a result, the membrane becomes more permeable to Na^+, K^+, Ca^{2+} and other ion species. This affects the trans-membrane charge distribution that is responsible for the physical origin of permittivity. Since the permittivity is seen to gradually decrease, it can be concluded that the trans-membrane charge density decreases during the initial 15 min of ischemia. The permittivity increases rapidly upon reperfusion and remains elevated above baseline values for about 35 min following reperfusion. The elevated permittivity could be an indicator of stunned myocardium, since it was shown in section 4.6.1 that the stunned hearts recover after 35 min of reperfusion.

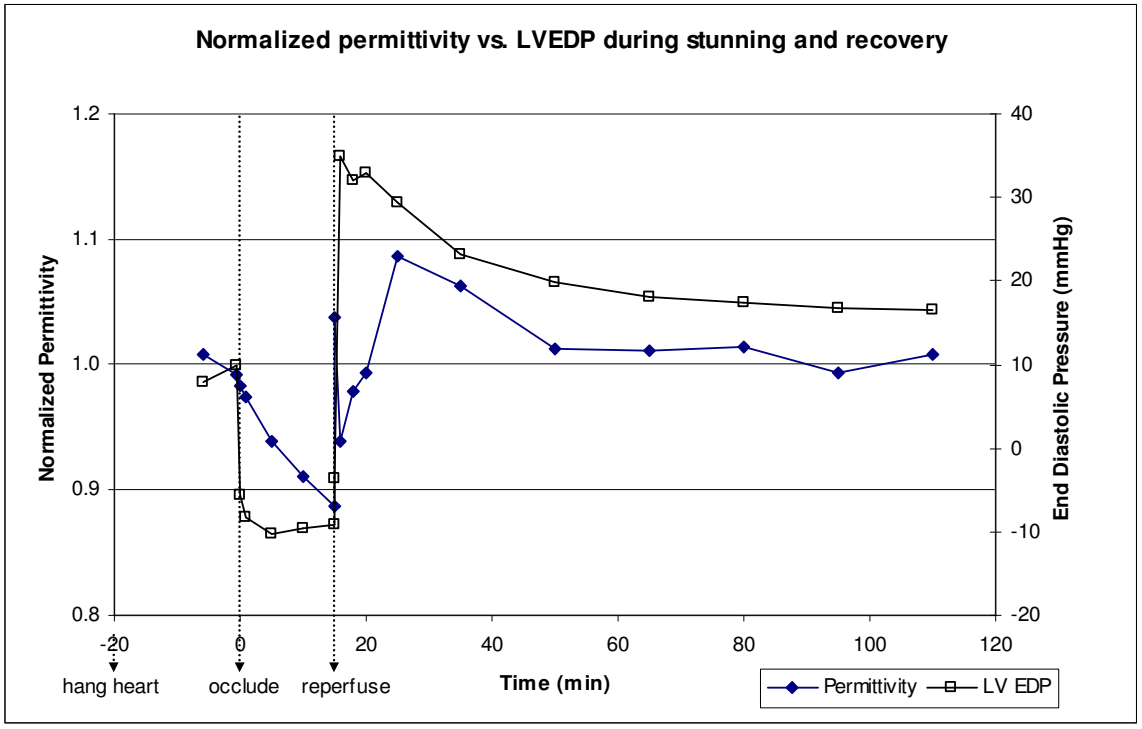

Figure 4-25: Comparison between normalized mean permittivity and LVEDP during baseline, 15 min of occlusion and 95 min of reperfusion (n = 4)

Stunning is characterized by an elevation in end diastolic pressure, possibly due to an overload of Ca^{2+} ions in the cytoplasm. The Ca^{2+} levels remain elevated during the early phase of reperfusion. A specific hypothesis regarding this has been suggested by Grinwald [21]. There is an accumulation of intracellular sodium during ischemia due to the inhibition of Na^{+}/K^{+} - ATPase. The Na^{+}/Ca^{2+} exchanger also remains suppressed by acidosis. Increased Na^{+}/H^{+} exchange due to accumulation of H^{+} during ischemia also favors sodium overload. On reperfusion, the rapid reversal of acidosis allows the reactivation of the Na^{+}/Ca^{2+} exchanger when sodium overload has not been resolved. The enhanced sodium efflux causes movement of calcium into the cells, causing the Ca^{2+} levels to remain elevated during the early phase of reperfusion.

This elevation in intracellular Ca^{2+} along with a gradual restoration of membrane permeability to normal levels could cause an increase in myocardial permittivity (similar to that observed during the 90 min ischemia protocol). Once the functioning of the sarcoplasmic reticulum and other calcium transport pumps is restored, the Ca^{2+} levels in the cells return to normal and the diastolic pressures reduce to normal values. The permittivity should hence return to baseline, thereby indicating recovery from stunning. This is in contrast with the ischemic hearts where the hearts do not recover once diastolic dysfunction has set in.

The myocardial conductivity in the four selected stunned hearts was compared with the controls and is shown in Figure 4-26. The occlusion causes a sudden drop in myocardial conductivity due to the absence of the high conductivity perfusion fluid. On reperfusion, the conductivity returns to normal value almost instantly and is not affected by the stunned state of the myocardium.

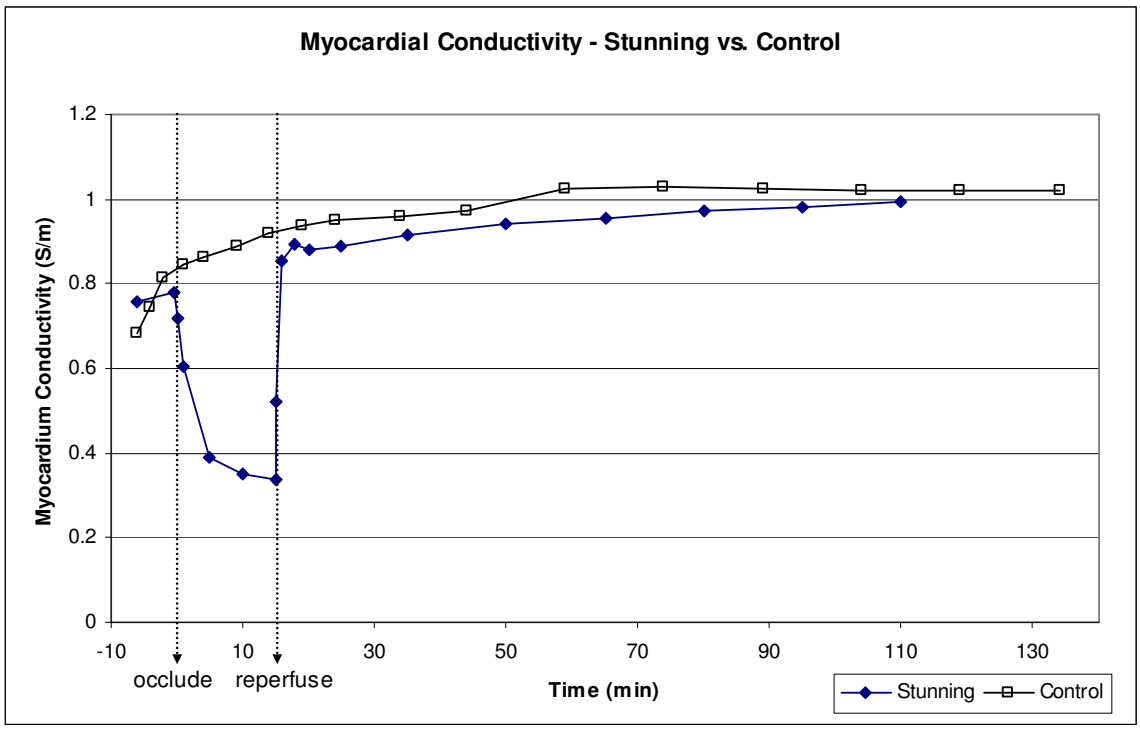

Figure 4-26: Myocardial conductivity in stunned vs. control hearts (n = 4)

From the above graph, it is evident that myocardial conductivity cannot be used as an indicator of stunning in the myocardium. It may be useful in the detection of no-flow ischemia, since the cessation of blood flow will cause a rapid decrease in the conductivity of the tissue.

4.7.3 Comparison between Ischemia and Stunning

The measured permittivity and conductivity during ischemia and stunning has been described in detail in the previous sections. The permittivity and conductivity values were normalized with respect to baseline values to enable comparison their comparison between ischemia and stunning. Normalizing with respect to baseline also causes each heart to serve as its own control, thereby eliminating differences that arise among different hearts as a result of baseline variations.

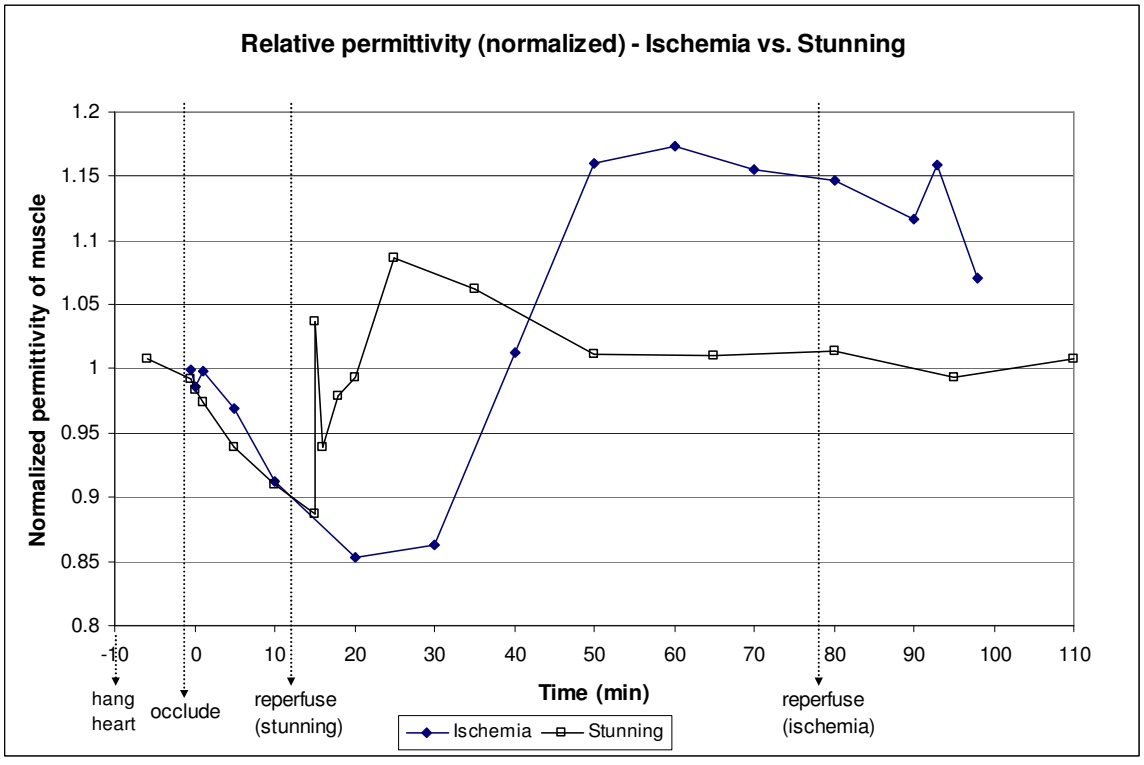

Figure 4-27: Normalized relative permittivity – ischemia vs. stunning

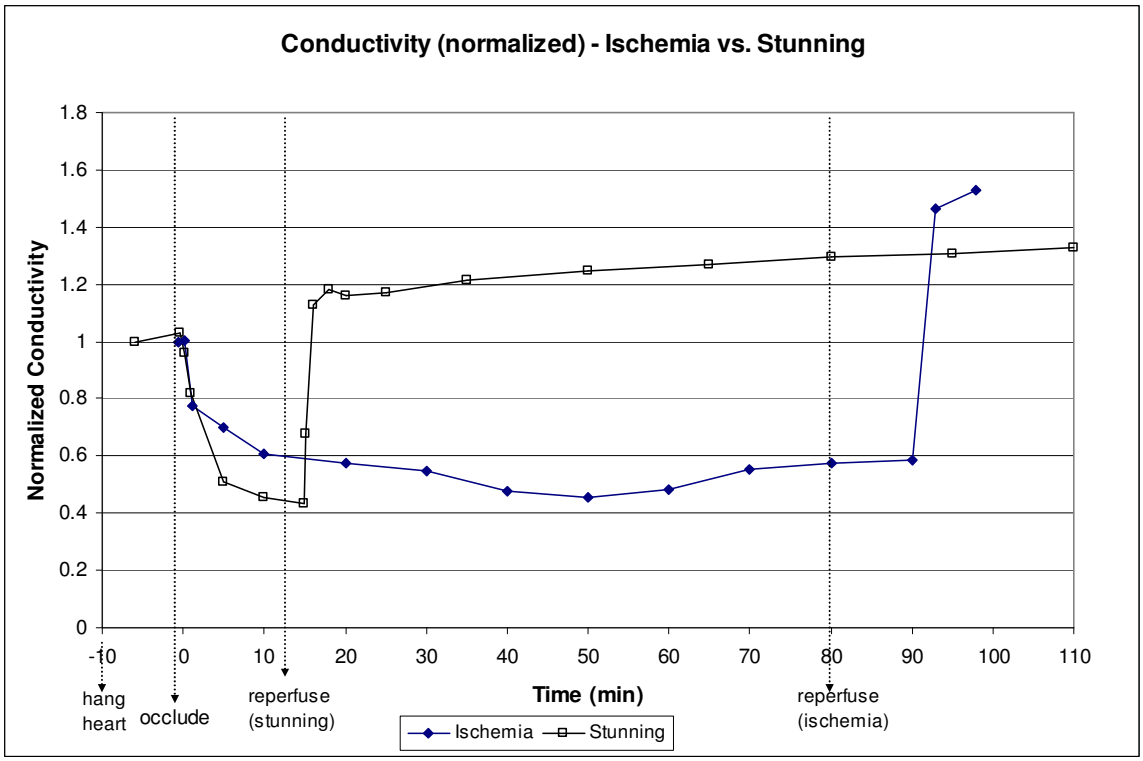

Figure 4-28: Normalized conductivity – ischemia vs. stunning

CHAPTER 5

Discussion

5.1 SUMMARY OF FINDINGS

A novel instrument (RamsES I) was designed and developed to determine the magnitude and phase angle of the electrical admittance of tissue in real time. The system was tested on isolated rat heart models of stunning and ischemia. The key findings have been listed below and summarized in Table 5-1.

- Myocardial permittivity decreases during the first 20 min of global no flow ischemia.
- Prolonged ischemia (30 min in the isolated rat heart) eventually causes diastolic dysfunction, verified by an increase in LVEDP.
- The permittivity increases prior to the onset of diastolic dysfunction in the left ventricle.
- Reperfusion after 15 min of occlusion results in myocardial stunning, with the tissue recovering after 35 min of reperfusion.
- The permittivity is temporarily elevated in the stunned myocardium and returns to baseline on recovery from stunning.
- The myocardial conductivity decreases drastically during occlusion and returns back to baseline almost instantaneously upon reperfusion.
- The conductivity measurements are dominated by the high conductivity perfusate in the myocardium and are not affected by the state of the myocardium.
- Increase in myocardial permittivity is as good an indicator of diastolic dysfunction as an increase in diastolic pressure.

The effects of myocardial ischemia, stunning and diastolic dysfunction on the permittivity, conductivity and LVEDP are summarized in Figures 5-1 and 5-2 as well as in Table 5-1. The relative permittivity of the myocardium is seen to decrease by 15% from baseline during 20 min of global no flow ischemia until the onset of diastolic dysfunction. The conductivity is also decreased due to the absence of the high conductivity perfusate (blood) in the myocardium. The onset of diastolic dysfunction is seen to increase the permittivity to 18% above the baseline values. Reperfusion before the onset of diastolic dysfunction causes the permittivity to rise to 10% above baseline (stunned myocardium) and gradually decrease towards baseline as the heart recovers from stunning. The conductivity returns to baseline almost instantaneously upon reperfusion.

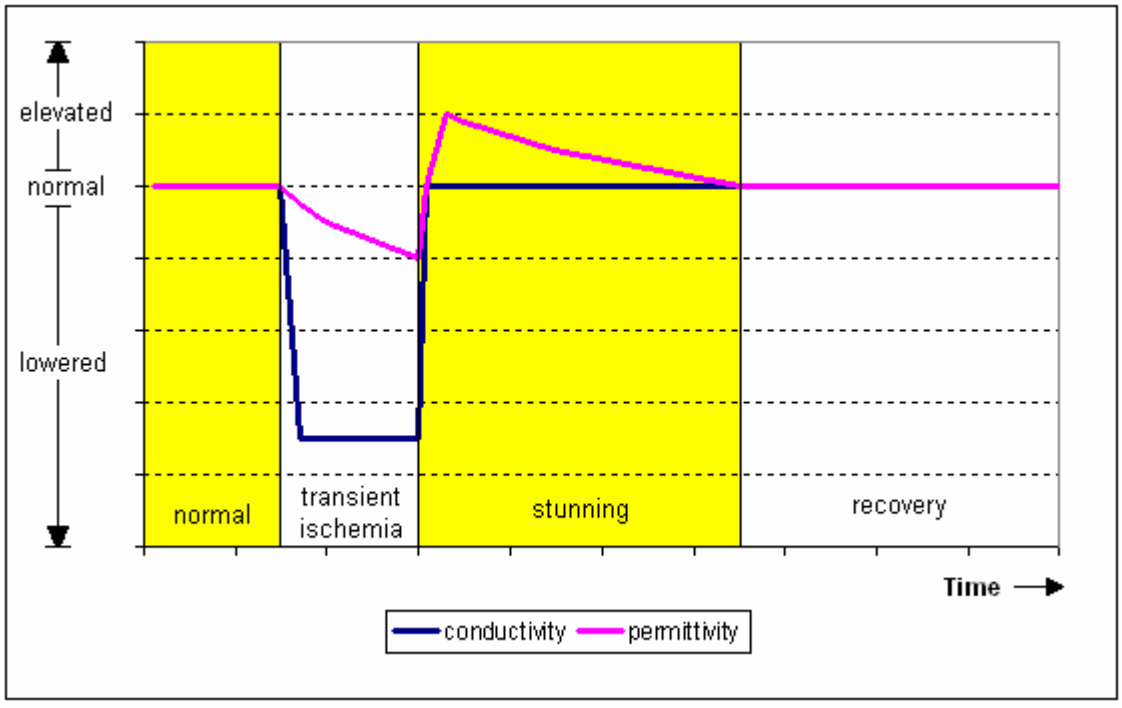

Figure 5-1: Trends in myocardial permittivity and conductivity in normal, transient ischemic, stunned and recovered myocardium

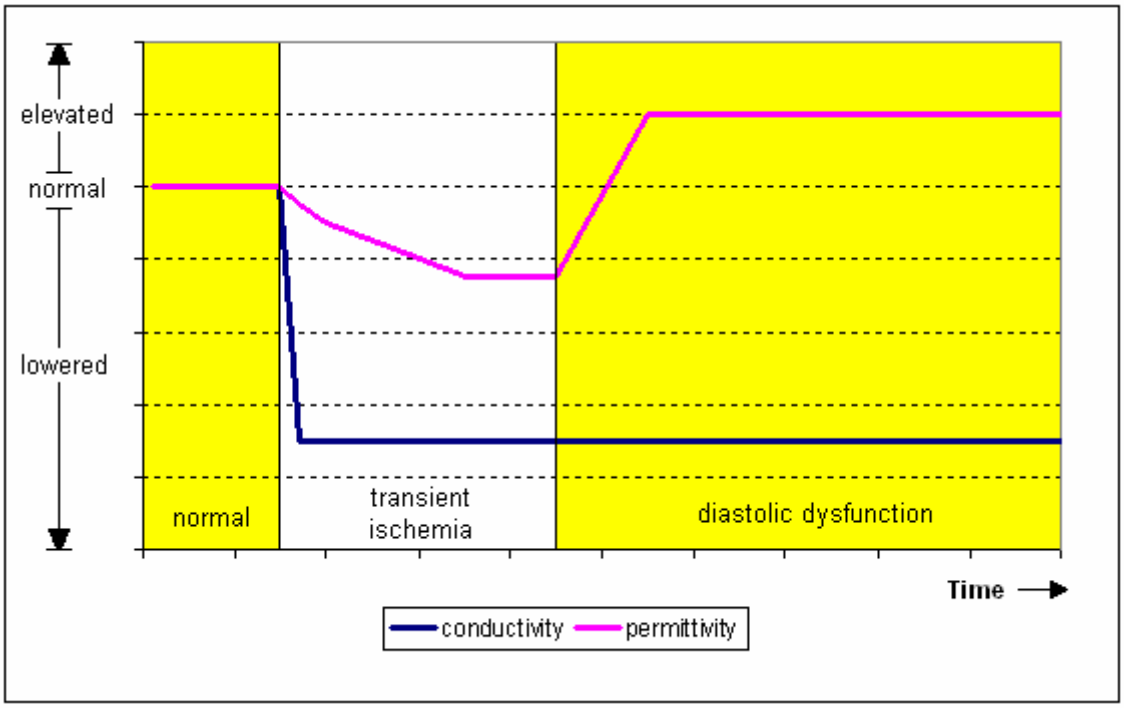

Figure 5-2: Trends in myocardial permittivity and conductivity during baseline, transient ischemia and diastolic dysfunction

	Permittivity	**Conductivity**	**LVEDP**
Ischemia	decreases	decreases	decreases
Stunning	increases	unchanged	increases
Diastolic dysfunction	increases	decreases	increases

Table 5-1: Summary of electrical properties and LV pressure during ischemia and stunning

The trans-membrane charge density is responsible for the physical origin of myocardial permittivity. During global no flow ischemia, cell necrosis occurs and is accompanied by mitochondrial swelling and increased plasma membrane permeability [6, 7, 52, 59]. This is manifested by elevated levels of LDH in the extracellular space. As a

result, the membrane may become more permeable to several ion species like Na^+, K^+ and Ca^{2+}. This would reduce the trans-membrane charge distribution, thereby lowering the measured tissue permittivity. Diastolic dysfunction is characterized by a rapid increase in LVEDP due to calcium overload in the cytoplasm (due to breakdown in the functioning of the sarcoplasmic reticulum [6, 7, 52]). This alteration of the intracellular electrolyte composition increases the trans-membrane charge distribution across the cell membrane and would explain the sudden increase in permittivity. Myocardial stunning also causes an intracellular calcium overload, primarily due to the reactivation of the Na^+/Ca^{2+} exchanger when the intracellular sodium overload has not been resolved. Since coronary perfusion has been restored in stunned myocardium, the functioning of voltage gated membrane ion channels is restored and membrane permeability gradually returns to normal. All these mechanisms cause rapid changes in the intracellular and extracellular ion concentrations and affect the charge distribution across the cell membranes. This could explain the increased myocardial permittivity during stunning.

5.2 FUTURE WORK

The effect of diastolic dysfunction on myocardial permittivity has been established with a high level of certainty. However, determination of the exact effect of myocardial stunning on the permittivity requires extensive further research. The degree of stunning and the recovery duration are highly dependent on baseline pressures and heart rates, making it necessary to perform the studies on a large number of hearts and divide the hearts into various groups depending on baseline parameters. Repeated experiments of the stunning protocol on a large number of hearts may also help identify subtle trends in the permittivity values during stunning and recovery.

The extent of tissue necrosis was verified by measuring the amount of LDH release. This is a fairly straightforward process and was accomplished using commercially available kits. However, other biomarkers like troponin I are highly specific to cardiac tissue and could have been used instead of LDH as a more accurate indicator of cardiac cell death. The hearts could also be fixed in neutral buffered formalin and examined using various histological techniques (Hematoxylin and Eosin staining for necrosis and TUNEL assays for apoptosis) for additional information on the extent of cell death.

The use of the patch clamp technique to study individual ion channels in myocardial cells will enable better understanding of the changes in the intracellular ion compositions that occur during ischemia, reperfusion and stunning. This would help identify intracellular and extracellular mechanisms responsible for the measured changes in permittivity and conductivity of the myocardium.

The RamsES I system can be upgraded to calculate the conductivity and permittivity in real time from the admittance magnitude and phase measurements. This would enable real time monitoring of hearts for calcium overload or myocardial stiffening during vascular surgery or other cardiopulmonary bypass procedures. The system can also be used to search for necrotic areas on the heart during cardiac bypass surgery. Another application would be to monitor the health of donor hearts during transport prior to implantation. The system may also be extended to monitor ischemia in other organs like liver and kidneys.

References

1. Arthur, W. and Kaye, G. C. *Clinical use of intracardiac impedance: current applications and future perspectives*. PACE 24[Pt. I]:500-506, 2001.

2. Bolli, R. *Mechanism of myocardial "stunning"*. Circulation. 82:723-738, 1990.

3. Bolli, R. and Marban, E. *Molecular and cellular mechanisms of myocardial stunning*. Physiol. Rev. 79:609-634, 1999.

4. Cascio, W. E., Yan, G. X. and Kleber, A.G. *Passive electrical properties, mechanical activity, and extracellular potassium in arterially perfused and ischemic rabbit ventricular muscle*. Circ. Res. 66:1461-1473, 1990.

5. Cinca, J., Warren, M., Carreno, A., Tresanchez, M., Armadans, L., Gomez, P. and Soler-Soler, J. *Changes in myocardial electrical impedance induced by coronary artery occlusion in pigs with and without preconditioning*. Circulation. 96:3079-3086, 1997.

6. Cinca, J., Warren, M., Rodriguez-Sinovas, A., Tresanchez, M., Carreno, A., Bragos, R., Casas, O., Domingo, A. and Soler-Soler, J. *Passive transmission of ST segment changes in low electrical resistance myocardial infarct scar in the pig*. Cardiovasc. Res. 40:103-112, 1998.

7. Dekker, L. R., Fiolet, J. W., VanBavel, E., Coronel, R., Opthof, T., Spaan, J. A. and Janse, M. J. *Intracellular Ca^{2+}, intercellular electrical coupling, and mechanical activity in ischemic rabbit papillary muscle. Effects of preconditioning and metabolic blockade*. Circ. Res. 79:237-246, 1996.

8. del Rio, C. L., McConnell, P. I., Clymer, B. D., Dzwonczyk, R., Michler, R. E., Billman, G. E. and Howie, M. B. *Early time course of myocardial electrical impedance during acute coronary artery occlusion in pigs, dogs, and humans*. J. Appl. Physiol. 99(4):1576-1581, 2005.

9. Ellenby, M. I., Small, K. W., Wells, R. M., Hoyt, D. J. and Lowe, J. E. *On-line detection of reversible myocardial ischemic injury by measurement of myocardial electrical impedance*. Ann. Thorac. Surg. 44:587-597, 1987.

10. Fallert, M. A., Mirotznik, M. S., Downing, S. W., Savage, E. B., Foster, K. R., Josephson, M. E. and Bogen, D. K. *Myocardial electrical impedance mapping of ischemic sheep hearts and healing aneurysms*. Circulation. 87:199-207, 1993.

11. Feldman, M. D., Yi Mao, Valvano, J. W., Pearce, J. A. and Freeman, G, L. *Development of a multi frequency conductance catheter based system to determine LV function in mice*. Am. J. Physiol. Heart. Circ. Physiol. 279:H1411-H1420, 2000.

12. Fernandez, D. J. *Frequency scalable left ventricular admittance measuring instrument for determining cardiac function*. Thesis (M.S. in Engineering) – University of Texas at Austin, 2006.

13. Flores, J., DiBona, D. R., Beck, C. H. and Leaf, A. *The role of cell swelling in ischemic renal damage and the protective effect of hypertonic solute*. J. Clin. Invest. 51:118-126, 1972.

14. Foster, K. S., Petit, R. L., Pearce, J. A., Bourland, J. D. and Geddes, L. A. *Tissue resistivity measurement using an annular tetrapolar electrode*. J. Clin. Eng. 6:208-212, 1981.

15. Frank, A., Rauen, U. and de Groot, H. *Protection by glycine against hypoxic injury of rat hepatocytes: inhibition of ion fluxes through non-specific leaks*. J. Hepatol. 32:58-66, 2000.

16. Gabriel, C., Gabriel, S. and Corthout, E. *The dielectric properties of biological tissues: I. Literature survey*. Phys. Med. Biol. 41:2231-2250, 1996.

17. Gabriel, S., Lau, R. W. and Gabriel, C. *The dielectric properties of biological tissues: II. Measurements in the frequency range 10 Hz to 20 GHz*. Phys. Med. Biol. 41:2251-2269, 1996.

18. Gabriel, S., Lau, R. W. and Gabriel, C. *The dielectric properties of biological tissues: III. Parametric models for the dielectric spectrum of tissues*. Phys. Med. Biol. 41:2270-2282, 1996.

19. Gebhard, M. M., Gersing, E., Brockhoff, C. J., Schnabel, P. A. and Bretschneider, H. J. *Impedance spectroscopy: A method for surveillance of ischemic tolerance of the heart*. Thorac. Cardiovasc. Surg. 35:26-32, 1987.

20. Gores, G. J., Nieminen, A. L., Wray, B. E., Herman, B. and Lemasters, J. J. *Intracellular pH during "chemical hypoxia" in cultured rat hepatocytes*. J. Clin. Invest. 83:386-396, 1989.

21. Grinwald, P. M. *Calcium uptake during post ischemic reperfusion in the isolated rat heart: influence of extracellular sodium*. J. Mol. Cell. Cardiol. 14:359-365, 1982.

22. Hearse, D. J. and Sutherland, F. J. *The isolated blood and perfusion fluid perfused heart*. Pharmacol. Res. 41(6):613-627, 2000.

23. Herman, B., Nieminen, A. L., Gores, G. J. and Lemasters, J. J. *Irreversible injury in anoxic hepatocytes precipitated by an abrupt increase in plasma membrane permeability*. FASEB J. 2:146-151, 1988.

24. Hoffstein, S., Gennaro, D. E., Fox, A. C., Hirsch, J., Streuli, F. and Weissman, G. *Colloidal lanthanum as a marker for impaired plasma membrane permeability in ischemic dog myocardium*. Am. J. Pathol. 79:207-218, 1975.

25. Howie, M. B., Dzwonczyk, R. and McSweeney, T. D. *An evaluation of a new two-electrode myocardial electrical impedance monitor for detecting myocardial ischemia.* Anesth. Analg. 92:12-18, 2001.

26. Ivorra, A., Gomez, R., Noguera, N., Villa, R., Sola, A., Palacios, L., Hotter, G. and Aguilo, J. *Minimally invasive silicon probe for electrical impedance measurements in small animals*. Biosensors Bioelectron. 391:391-399, 2003.

27. Jain, S. K., Schuessler, R. B. and Saffitz, J. E. *Mechanisms of delayed electrical uncoupling induced by ischemic preconditioning*. Circ. Res. 92:1138-1144, 2003.

28. Kleber, A. G., Riegger, C. B. and Janse, M. J. *Electrical uncoupling and increase of extracellular resistance after induction of ischemia in isolated, arterially perfused rabbit papillary muscle*. Circ. Res. 61:271-279, 1987.

29. Karthik Raghavan. *A real-time approach in in-vivo phase measurements for the determination of volume in the murine heart*. Thesis (M.S. in Engineering) – University of Texas at Austin, 2004.

30. Kottam, A. *Determination of parasitic circuit elements in cardiac conductance catheters*. Thesis (M.S. in Engineering) – University of Texas at Austin, 2003.

31. Kottam, A. and Pearce, J. A. *Electric field penetration depth of myocardial surface catheters and the measurement of myocardial resistivity*. Biomedical Sciences Instrumentation. 40:155-160, 2004.

32. Lee, H. C., Smith, N., Mohabir, R. and Clusin, W. T. *Cytosolic calcium transients from the beating mammalian heart*. Proc. Natl. Acad. Sci. USA. 84:7793-7797, 1987.

33. Lofgren, B. *The electrical impedance of a complex tissue and its relation to changes in volume and fluid distribution; a study on rat kidneys*. Acta. Physiol. Scand. Suppl. 81:1-51, 1951.

34. Lüss, H., Schäfers, M., Neumann, J., Hammel, D., Vahlhaus, C., Baba, H. A., Janssen, F., Scheld, H. H., Schober, O., Breithardt, G., Schmitz, W. and Wichter, T. *Biochemical mechanisms of hibernation and stunning in the human heart*. Cardiovasc. Res. 56:411-421, 2002.

35. Mangano, D. T. *Perioperative cardiac morbidity*. Anesthesiology. 72:153-184, 1990.

36. Marban, E., Koretsune, Y., Corretti, M., Chacko, V. P. and Kusuoka, H. *Calcium and its role in myocardial cell injury during ischemia and reperfusion*. Circulation. 80:IV17-IV22, 1989.

37. Nieminen, A. L., Gores, G. J., Wray, B. E., Tanaka, Y., Herman, B. and Lemasters, J. J. *Calcium dependence of bleb formation and cell death in hepatocytes*. Cell Calcium. 9:237-246, 1988.

38. Nishimura, Y. and Lemasters, J. J. *Glycine blocks opening of a death channel in cultured hepatic sinusoidal endothelial cells during chemical hypoxia*. Cell Death Differ. 8:850-858, 2001.

39. Olivetti, G., Lagrasta, C., Quaini, F., Ricci, R., Moccia, G., Capasso, J. M. and Anversa, P. *Capillary growth in anemia-induced ventricular wall remodeling in the heart*. Circ. Res. 65:1182-1192, 1989.

40. Owens, L. M., Fralix, T. A., Murphy, E., Cascio, W. E. and Gettes, L. S. *Correlation of ischemia-induced extracellular and intracellular ion changes to cell-to-cell electrical uncoupling in isolated blood-perfused rabbit hearts*. Circulation. 94:10-13, 1996.

41. Padilla, F., Garcia-Dorado, D., Rodriguez-Sinovas, A., Ruiz-Meana, M., Inserte, J. and Soler-Soler, J. *Protection afforded by ischemic preconditioning is not mediated by effects on cell-to-cell electrical coupling during myocardial ischemia-reperfusion*. Am. J. Physiol. Heart. Circ. Physiol. 285:H1909-H1916, 2003.

42. Panteghini, M. *Acute coronary syndrome: biochemical strategies in the troponin era*. Chest. 122:1428-1435, 2002.

43. Raby, K. E., Barry, J., Creager, M. A., Cook, E. F., Weisberg, M. C. and Goldman, L. *Detection and significance of intraoperative and postoperative myocardial ischemia in peripheral vascular surgery*. JAMA 268:222-227, 1992.

44. Raby, K. E., Brull, S. J., Timimi, F., Akhtar, S., Rosenbaum, S., Naimi, C. and Whittemore, A. D. *The effect of heart rate control on myocardial ischemia among high-risk patients after vascular surgery*. Anesth. Analg. 88:477-482, 1999.

45. Ramos, A., Raizer, A. and Marques, J. L. B. *A new computational approach for electrical analysis of biological tissues*. Bioelectrochemistry. 59:73-84, Jan. 2003.

46. Rodriguez-Sinovas, A., Garcia-Dorado, D., Padilla, F., Inserte, J., Barrabes, J. A., Ruiz-Meana, M., Agullo, L. and Soler-Soler, J. *Pre-treatment with the Na^+/H^+*

exchange inhibitor cariporide delays cell-to-cell electrical uncoupling during myocardial ischemia. Cardiovasc. Res. 58:109-117, 2003.

47. Rodriguez-Sinovas, A., Garcia-Dorado, D., Pina, P., Ruiz-Meana, M. and Soler-Soler, J. *Effect of sarcolemmal rupture on myocardial electrical impedance during oxygen deprivation*. Am. J. Physiol. Heart. Circ. Physiol. 288:H1396-H1403, 2005.

48. Rodriguez-Sinovas, A., Garcia-Dorado, D., Ruiz-Meana, M. and Soler-Soler, J. *Protective effect of gap junction uncouplers given during hypoxia against reoxygenation injury in isolated rat hearts*. Am. J. Physiol. Heart. Circ. Physiol. 290:H648-H656, 2006.

49. Salazar, Y., et al., *Transmural versus nontransmural in situ electrical impedance spectrum for healthy, ischemic, and healed myocardium*. IEEE Trans. Biomed. Eng. 51:1421-1427, Aug. 2004.

50. Schaefer, M., Gross, W., Ackemann, J. and Gebhard, M. M. *The complex dielectric spectrum of heart tissue during ischemia*. Bioelectrochemistry. 58:171-180, Mar. 2002.

51. Schwan, H. P. Physical techniques in biological research. *Electrophysiological Methods*. vol. 6, pt. B, W. L. Nastuk, Ed., 1963, ch. 6.

52. Schwartzman, D., Chang, I., Michele, J. J., Mirotznik, M. S. and Foster, K. R. *Electrical impedance properties of normal and chronically infarcted left ventricular myocardium*. J. Interv. Card. Electrophysiol. 3:213-224, Oct. 1999.

53. Steenbergen, C., Murphy, E., Levy, L. and London, R. E. *Elevation in cytosolic free calcium concentration early in myocardial ischemia in perfused rat heart*. Circ. Res. 60:700-707, 1987.

54. Steendijk, P., Mur, G., Van Der Velde, E. T. and Baan, J. *The four electrode resistivity technique in anisotropic media: theoretical analysis and application of myocardial tissue in vivo.* IEEE Trans. Biomed. Eng. 40:1138-1148, 1993.

55. Sugiura, H., Toyama, J., Tsuboi, N., Kamiya, K. and Kodama, I. *ATP directly affects junctional conductance between paired ventricular myocytes isolated from guinea pig heart*. Circ. Res. 66:1095-1102, 1990.

56. Surowiec, A., Stuchly, S. S. and Swarup, A. *Postmortem changes of the dielectric properties of bovine brain tissues at low radiofrequencies*. Bioelectromagnetics. 7:31-43, 1986.

57. Surowiec, A., Stuchly, S. S. and Swarup, A. *Radiofrequency dielectric properties of animal tissues as a function of time following death*. Phys. Med. Biol. 30:1131-1141, 1985.

58. Thom, T., Haase, N., Rosamond, W., Howard, V. J., Rumsfeld, J., Manolio, T., Zheng, Z., Flegal, K., O'Donnell, C., Kittner, S., Lloyd-Jones, D., Goff, D. and Hong, Y. *Heart Disease and Stroke Statistics-2006 Update: A Report From the American Heart Association Statistics Committee and Stroke Statistics Subcommittee*. Circulation. 113(6):E85-E151, 2006.

59. Urban, M. K., Gordon, M. A., Harris, S. N., O'Connor, T. and Barash, P. G. *Intraoperative hemodynamic changes are not good indicators of myocardial ischemia*. Anesth. Analg. 76:942-949, 1993.

60. van Oosterom, A., de Boer, R. W. and van Dam, R. T. *Intramural resistivity of cardiac tissue*. Med. Biol. Eng. Comput. 17:337-343, 1979.

61. Wtorek, J., et al., *An averaging two electrode probe for monitoring changes in myocardial conductivity evoked by ischemia*. IEEE Trans. Biomed. Eng. 49:240-246, Mar. 2002.

62. Wu, J., McHowat, J., Saffitz, J. E., Yamada, K. A. and Corr, P. B. *Inhibition of gap junctional conductance by long-chain acylcarnitines and their preferential accumulation in junctional sarcolemma during hypoxia*. Circ. Res. 72:879-889, 1993.

63. Zahrebelski, G., Nieminen, A. L., Al-Ghoul, K., Qian, T., Herman, B. and Lemasters, J. J. *Progression of subcellular changes during chemical hypoxia to cultured rat hepatocytes: a laser scanning confocal microscopic study*. Hepatology 21:1361-1372, 1995.

Vita

Anil George Kottam was born in Secunderabad, India on the 20th of September, 1979. He is the son of Dr. George J. Kottam and Mrs. Laila George Kottam. After completing his primary schooling at the Indian School in the Sultanate of Oman, his higher secondary education was completed at Toc-H Public School, India. Following this, he obtained a bachelors degree in biomedical engineering from the Cochin University of Science and Technology in India in July, 2001. Immediately afterwards, he entered the graduate school at the University of Texas at Austin in the Fall of 2001, where he received his masters degree in 2003 and doctoral degree in 2007.

Permanent address: 30/118, Pettah
Poonithura P.O.
Kochi – 682317
Kerala, INDIA

This dissertation was typed by Anil George Kottam.